EGG-2097
Distribution Categeory: UC-78

AN ADVANCED DIGITAL PWR PLANT PROTECTION SYSTEM BASED ON OPTIMAL ESTIMATION THEORY

J. Louis Tylee

Published April 1981

EG&G Idaho, Inc.
Idaho Falls, Idaho 83415

Prepared for the
U.S. Department of Energy
Idaho Operations Office
Under DOE Contract No. DE-AC07-76IDO1570

ABSTRACT

An advanced plant protection system for the Loss-of-Fluid Test (LOFT) reactor plant is described and evaluated. The system, based on a Kalman filter estimator, is capable of providing on-line estimates of such critical variables as fuel and cladding temperature, departure from nucleate boiling ratio, and maximum linear heat generation rate. The Kalman filter equations are presented, as is a description of the LOFT plant dynamic model inherent in the filter. Simulation results demonstrate the performance of the advanced system.

CONTENTS

ABSTRACT ii

NOMENCLATURE vi

INTRODUCTION 1

THE ADVANCED PLANT PROTECTION SYSTEM 3

KALMAN FILTER ESTIMATOR 6

LOFT PLANT MODEL 9

Nonlinear LOFT Model 9

Model Linearization and Discretization 38

THE DNBR AND LHGR CALCULATION 43

SIMULATION RESULTS 45

CONCLUSIONS 64

REFERENCES 65

FIGURES

1. LOFT reactor plant schematic diagram 2

2. Advanced LOFT plant protection system 4

3. Discrete Kalman filter information flow 7

4. ANS decay heat curve 11

5. Core thermal model 12

6. Primary loop nodalization 14

7. Pressurizer schematic 17

8. Pressurizer spray logic 21

9. Pressurizer relief valve logic 21

10. Pressurizer heater logic 22

11. Steam generator model 23

12. Main steam control valve throttling logic 27

13. Steam generator relief valve logic 28

14. Steam generator water level controller 29
15. Air-cooled condenser model schematic 31
16. Condensate receiver model 34
17. Condensate receiver relief valve logic 35
18. Condensate receiver pressure control system 36
19. Feedwater system model 37
20. Sensor model 37
21. Rod withdrawal accident, core power response 45
22. Rod withdrawal accident, hot leg temperature response 46
23. Rod withdrawal accident, pressurizer pressure response 46
24. Rod withdrawal accident, pressurizer level response 47
25. Rod withdrawal accident, secondary pressure response 47
26. Rod withdrawal accident, steam generator level response 48
27. Rod withdrawal accident, steam flow response 48
28. Rod withdrawal accident, feed flow response 49
29. Rod withdrawal accident, fuel temperature estimate 49
30. Rod withdrawal accident, clad temperature estimate 50
31. Rod withdrawal accident, minimum DNBR estimate 50
32. Rod withdrawal accident, maximum LHGR estimate 51
33. Primary flow reduction, core power response 52
34. Primary flow reduction, hot leg temperature response 52
35. Primary flow reduction, pressurizer pressure response 53
36. Primary flow reduction, pressurizer level response 53
37. Primary flow reduction, secondary pressure response 54
38. Primary flow reduction, steam generator level response 54
39. Primary flow reduction, steam flow response 55
40. Primary flow reduction, feed flow response 55
41. Primary flow reduction, fuel temperature estimate 56

42. Primary flow reduction, clad temperature estimate 56
43. Primary flow reduction, minimum DNBR estimate 57
44. Primary flow reduction, maximum LHGR estimate 57
45. MSCV opening, core power response 58
46. MSCV opening, hot leg temperature response 58
47. MSCV opening, pressurizer pressure response 59
48. MSCV opening, pressurizer level response 59
49. MSCV opening, secondary pressure response 60
50. MSCV opening, steam generator level response 60
51. MSCV opening, steam flow response 61
52. MSCV opening feed flow response 61
53. MSCV opening, fuel temperature estimate 62
54. MSCV opening, clad temperature estimate 62
55. MSCV opening, minimum DNBR estimate 63
56. MSCV opening, maximum LHGR estimate 63

TABLES

1. Linear LOFT model state vector 40
2. Linear LOFT model input vector 41
3. Linear LOFT model output vector 42

NOMENCLATURE

a	constant use to define control rod scram reactivity ($/sec^3)
A	linearized model system matrix as defined in Equation (145)
A_{clad}	outside surface area of fuel cladding (ft^2)
A_{core}	cross-sectional flow area of core (ft^2)
A_f	external condenser tube fin area (ft^2/ft)
(A_f/l_f)	fuel area-to-length ratio (ft)
A_{fan}	cross-sectional flow area for condenser fans (ft^2)
A_o	base condenser tube area (ft^2/ft)
A_{pri}	inside surface area of steam generator tubes (ft^2)
A_{sec}	outside surface area of steam generator tubes (ft^2)
B	linearized model input matrix as defined in Equation (146)
B_{ave}	average boron concentration in reactor core (ppm)
B_{aveo}	reference average boron concentration in reactor core used to initialize net reactivity (ppm)
B_{rsp}	pressurizer backup heater resetpoint (psia)
B_{sp}	pressurizer backup heater setpoint (psia)
c_p	subcooled liquid specific heat (Btu/lbm-°F)
c_{pa}	specific heat of air (Btu/lbm-°F)
c_{pbp}	specific heat of water in core bypass (Btu/lbm-°F)
c_{pc}	specific heat of fuel cladding (MW-sec/lbm-°F)
c_{pcore}	specific heat of water in core (Btu/lbm-°F)
c_{pf}	specific heat of fuel (MW-sec/lbm-°F)
c_{psg}	specific heat of water in primary side of steam generator (Btu/lbm-°F)
c_{ptsg}	specific heat of steam generator tubes (Btu/lbm-°F)
c_{ptube}	specific heat of condenser tubes (Btu/lbm-°F)
C	linearized model output matrix as defined in Equation (147)
C_{rsp}	pressurizer safety relief valve resetpoint (psia)

C_{sp}	pressurizer safety relief valve setpoint (psia)
C_{vfwv}	feedwater valve flow coefficient as defined in Equation (135)
C_{vmscv}	main steam control valve flow coefficient as defined in Equation (88) (lbm/sec-psi)
d_{cltsg}	diameter to the centerline of steam generator tubes (in.)
d_{in}	inside diameter of condenser tubes (ft)
d_{itsg}	inside diameter of steam generator tubes (in.)
d_{otsg}	outside diameter of steam generator tubes (in.)
d_{out}	outside diameter of condenser tubes (ft)
D	linearized model matrix as defined in Equation (148)
D_{eq}	equivalent diameter for condenser fan air flow (ft)
D_{eqcor}	equivalent diameter for flow through core (ft)
D_{eqpri}	equivalent diameter for flow through steam generator tubes (ft)
DNBR	departure from nucleate boiling ratio
f	nonlinear model state function vector
f_{dhbp}	fraction of total reactor power deposited directly to core bypass coolant
f_{dhc}	fraction of total reactor power deposited to core coolant
f_1	first delayed neutron group fraction
f_2	second delayed neutron group fraction
F_{bp}	fraction of total primary loop flow to core bypass
F_h	condenser tube fin heat transfer parameter defined by Equation (121)
g	nonlinear model output function vector
G	core flow mass flux (lbm/hr-ft^2)
h_{cl}	enthalpy of water in cold leg (Btu/lbm)
h_{clad}	convective heat transfer coefficient for fuel cladding (Btu/ft^2-hr-°F)
h_{cr}	enthalpy of fluid mixture in condensate receiver (Btu/lbm)
h_d	enthalpy of steam generator downcomer flow (Btu/lbm)
h_{dc}	enthalpy of steam generator downcomer water (Btu/lbm)
h_f	saturated liquid enthalpy (Btu/lbm)

h_{fg}	heat of vaporization (Btu/lbm)
h_{fin}	convective heat transfer coefficient for condenser tube fins (Btu/ft^2-hr-°F)
h_{fw}	enthalpy of feedwater flow (Btu/lbm)
h_{fwp}	head generated by feedwater pump (psi)
h_g	saturated vapor enthalpy (Btu/lbm)
h_{local}	local enthalpy of core coolant (Btu/lbm)
h_p	enthalpy of fluid mixture in pressurizer (Btu/lbm)
h_{pri}	convective heat transfer coefficient for primary side of steam generator tubes (Btu/ft^2-hr-°F)
h_{sg}	enthalpy of fluid mixture in steam generator (Btu/lbm)
h_{spray}	enthalpy of pressurizer spray flow (Btu/lbm)
h_{surge}	enthalpy of pressurizer surge flow (Btu/lbm)
H_{rsp}	pressurizer cycling heater resetpoint (psia)
H_{sp}	pressurizer cycling heater setpoint (psia)
j_H	Sieder-Tate heat transfer factor defined by Equation (117)
J	units conversion factor (ft^3-psia/Btu)
k	subcooled liquid thermal conductivity (Btu/ft-hr-°F)
k_a	thermal conductivity of air (Btu/ft-hr-°F)
k_c	thermal conductivity of fuel cladding (MW/ft-°F)
k_{core}	thermal conductivity of water in core (Btu/ft-hr-°F)
k_f	thermal conductivity of fuel (MW/ft-°F)
k_g	thermal conductivity of gas in gas gap of fuel rod (MW/ft-°F)
k_{sg}	thermal conductivity of water in primary side of steam generator (Btu/ft-hr-°F)
k_{tsg}	thermal conductivity of steam generator tubes (Btu/ft-hr-°F)
K	Kalman gain matrix
K_{cl}	Conductance of fuel cladding from inner surface to centerline (MW/°F)
K_{c2}	conductance of fuel cladding from centerline to outer surface (MW/°F)
K_f	conductance of fuel (MW/°F)
K_g	conductance of gas gap (MW/°F)

K_{surge}	flow coefficient for pressurizer surge flow as defined by Equation (70)
K_{t1}	conductance of steam generator tubes from inner surface to centerline (Btu/hr-°F)
K_{t2}	conductance of steam generator tubes from centerline to outer surface (Btu/hr-°F)
K_A	condensate receiver pressure control system averager gain as used in Equation (133)
K_{IP}	condensate receiver pressure control system transducer gain as used in Equation (133)
K_{PA}	condensate receiver pressure control system pressure amplifier gain as used in Equation (133)
K_{POS}	condensate receiver pressure control system blade position gain as used in Equation (133)
K_{PX}	condensate receiver pressure control system position transmitter gain as used in Equation (133)
K_1	steam generator water level controller steam flow amplifier gain as used in Equation (93)
K_2	steam generator water level controller error amplifier gain as used in Equation (93)
K_3	steam generator water level controller valve position amplifier gain as used in Equation (92)
K_4	steam generator water level controller valve position feedback amplifier gain as used in Equation (92)
ℓ	prompt neutron generation time (sec)
L_{cr}	water level in condensate receiver (in.)
L_{drum}	length of steam generator drum (ft)
L_o	zero power steam generator water level (in.)
L_p	pressurizer water level (in.)
L_{riser}	length of steam generator riser (ft)
L_{rod}	length of fuel rod (ft)
L_s	water level in steam generator shroud (in.)
L_{sg}	water level in steam generator downcomer (in.)
L_t	length of condenser tubes (ft)
L_{tsg}	length of steam generator tubes (ft)
LHGR	linear heat generation rate (kW/ft)
LOFT	Loss-of-Fluid Test
M_{bp}	mass of water in core bypass (lbm)
M_c	mass of fuel cladding (lbm)

M_{core}	mass of water in core (lbm)
M_{cr}	mass of fluid mixture in condensate receiver (lbm)
M_{dc}	mass of water in steam generator downcomer (lbm)
M_{dome}	mass of fluid in steam generator dome (lbm)
M_f	mass of fuel (lbm)
M_{loop}	mass of water in primary loop (lbm)
M_p	mass of fluid mixture in pressurizer (lbm)
M_{sg}	mass of water in steam generator primary side (lbm)
M_{sgs}	mass of fluid mixture in steam generator secondary (lbm)
M_{shd}	mass of fluid in steam generator shroud (lbm)
M_{tsg}	mass of steam generator tubes (lbm)
M_{tube}	mass of condenser tubes (lbm)
MSCV	main steam control valve
N	number of delayed neutron groups
N_{rod}	number of fuel rods in core
N_t	number of condenser tubes
N_{tsg}	number of steam generator tubes
P	estimate error covariance matrix
P	reactor power generated in fuel (MW)
$\bar{P}$	average pressure across main steam control valve (psia)
ΔP	pressure drop across main steam control valve (psi)
P_{air}	ambient air pressure (psia)
P_{cr}	condensate receiver pressure (psia)
P_{crsp}	condensate receiver pressure control system setpoint (psia)
P_f	condenser fan blade pitch angle (degrees)
ΔP_{fw}	pressure drop across feedwater valve (psi)
P_{loop}	primary loop pressure (psia)
P_P	pressurizer pressure (psia)

P_{rsp}	pressurizer power-operated relief valve resetpoint (psia)
P_{sg}	steam generator secondary pressure (psia)
P_{sp}	pressurizer power-operated relief valve setpoint (psia)
P_T	total reactor power (MW)
$(Pr)_{core}$	Prandtl number of flow through core
$(Pr)_{pri}$	Prandtl number of flow through steam generator tubes
PPS	Plant Protection System
q_{air}	heat flow to air from condenser tubes (Btu/hr-ft)
q_{cond}	heat flow to condenser tubes from condensing fluid (Btu/hr-ft)
q_{dnb}	critical heat flux in hot fuel rod (Btu/hr-ft^2)
q_{hot}	actual heat flux in hot fuel rod (Btu/hr-ft^2)
Q	process noise covariance matrix
Q_{bp}	heat removed by core bypass flow (Btu/sec)
Q_{bup}	capacity of pressurizer backup heaters (Btu/sec)
Q_{core}	heat removed by core flow (Btu/sec)
Q_{cp}	heat transferred to core flow from fuel cladding (Btu/sec)
Q_{cyc}	capacity of pressurizer cycling heaters (Btu/sec)
Q_{dhbp}	direct heat deposited to core bypass coolant (Btu/sec)
Q_{dhc}	direct heat deposited to core coolant (Btu/sec)
Q_{htr}	total pressurizer heating (Btu/sec)
Q_{sg}	heat transferred to steam generator tubes by primary coolant (Btu/sec)
Q_{sgout}	heat removed from steam generator primary coolant flow (Btu/sec)
Q_{stm}	heat transferred from steam generator tubes to secondary fluid (Btu/sec)
r_c	fuel cladding outer radius, unexpanded (in.)
$\Delta r_c/r_c$	fuel cladding expansion (in./in.)
r_{cl}	radius to clad centerline, expanded (in.)
r_f	fuel radius, unexpanded (in.)
$\Delta r_f/r_f$	fuel expansion (in./in.)

r_{oc}	fuel cladding outer radius, expanded (in.)
r_{lg}	radius to inner edge of gas gap, expanded (in.)
r_{2g}	radius to outer edge of gas gap, expanded (in.)
R	measurement noise covariance matrix
R_{crrsp}	condensate receiver relief valve resetpoint (psia)
R_{crsp}	condensate receiver relief valve setpoint (psia)
R_{film}	condenser tube film heat resistance (ft-hr-°F/Btu)
R_{fin}	condenser tube fin heat resistance (ft-hr-°F/Btu)
R_{int}	condenser tube internal heat resistance (ft-hr-°F/Btu)
R_{wall}	condenser tube wall heat resistance (ft-hr-°F/Btu)
R_{1rsp}	steam generator relief valve 1 resetpoint (psia)
R_{1sp}	steam generator relief valve 1 setpoint (psia)
R_{2rsp}	steam generator relief valve 2 resetpoint (psia)
R_{2sp}	steam generator relief valve 2 setpoint (psia)
$(Re)_a$	Reynolds number of condenser fan air flow
$(Re)_{core}$	Reynolds number of flow through core
$(Re)_{pri}$	Reynolds number of flow through steam generator tubes
s	Laplace operator
S_{rate}	main steam control valve motion rate (%/sec)
S_{rsp}	pressurizer spray flow resetpoint (psia)
S_{sp}	pressurizer spray flow setpoint (psia)
t	time (sec)
t	fuel cladding thickness (in.)
t_d	scram delay time (sec)
t_e	duration of scram (sec)
t_s	start time of scram (sec)
T_{air}	average air temperature surrounding condenser tubes (°F)
T_{amb}	ambient air temperature (°F)

T_{ave}	average temperature of core coolant (°F)
T_{bpa}	average temperature of core bypass coolant (°F)
T_c	fuel cladding temperature at centerline (°F)
T_{cond}	temperature of fluid in condenser tubes (°F)
T_f	average fuel temperature (°F)
T_{fo}	reference average fuel temperature used to initialize net reactivity (°F)
T_{fw}	temperature of feedwater (°F)
ΔT_{fw}	degrees of feedwater subcooling (°F)
T_{hla}	average temperature of hot leg coolant (°F)
T_{hlm}	measured average hot leg coolant temperature (°F)
T_{hot}	reactor vessel outlet coolant temperature (°F)
T_{in}	reactor vessel inlet coolant temperature (°F)
T_{lpzr}	temperature of water in pressurizer (°F)
T_{out}	temperature of coolant at core outlet (°F)
T_{sga}	average temperature of primary coolant in steam generator (°F)
T_{sgi}	temperature of primary coolant at inlet to steam generator (°F)
T_{sgo}	temperature of primary coolant at outlet of steam generator (°F)
T_{stm}	temperature of secondary steam (°F)
T_{surge}	temperature of pressurizer surge flow (°F)
T_{tsg}	temperature at centerline of steam generator tubes (°F)
T_{tube}	temperature at outer surface of condenser tubes (°F)
u	linearized model input vector
u^o	optimal input vector
$\tilde{u}$	value of u at linearized model operating point
U_{cp}	overall heat transfer coefficient from cladding centerline to core coolant (Btu/sec-°F)
U_{fc}	overall heat transfer coefficient from fuel to cladding centerline (MW/°F)
U_{pri}	overall heat transfer coefficient from primary coolant to steam generator tube centerline (Btu/sec-°F)

U_{sec}	overall heat transfer coefficient from steam generator tube centerline to secondary fluid (Btu/sec-°F)
v	measurement white noise vector
v_{cr}	specific volume of fluid mixture in condensate receiver (ft^3/lbm)
v_{drum}	specific volume of fluid mixture in steam generator drum (ft^3/lbm)
v_f	saturated liquid specific volume (ft^3/lbm)
v_g	saturated vapor specific volume (ft^3/lbm)
v_p	specific volume of fluid mixture in pressurizer (ft^3/lbm)
v_{riser}	specific volume of fluid mixture in steam generator riser (ft^3/lbm)
v_{sg}	specific volume of fluid mixture in steam generator secondary (ft^3/lbm)
v_{shd}	specific volume of fluid mixture in steam generator shroud (ft^3/lbm)
V_a	volumetric flow of air from condenser fans (ft^3/hr)
V_{core}	volumetric flow of core coolant (ft^3/hr)
V_{crsp}	main steam control valve throttling closing resetpoint (psia)
V_{csp}	main steam control valve throttling closing setpoint (psia)
V_{loop}	volumetric flow of primary coolant (ft^3/sec)
V_{orsp}	main steam control valve throttling opening resetpoint (psia)
V_{osp}	main steam control valve throttling opening setpoint (psia)
V_{spray}	pressurizer spray flow capacity (ft^3/sec)
V_{surge}	pressurizer surge volumetric flow (ft^3/sec)
V_{bp}	volume of core bypass (ft^3)
V_{cl}	volume of cold leg (ft^3)
V_{cr}	volume of condensate receiver (ft^3)
V_{core}	volume of core (ft^3)
V_{dc}	volume of water in steam generator downcomer (ft^3)
V_{hl}	volume of hot leg (ft^3)
V_l	volume of liquid in pressurizer (ft^3)
V_p	volume of pressurizer (ft^3)

V_{sgp}	volume of steam generator primary side (ft^3)
V_{sg}	volume of steam generator secondary side (ft^3)
V_{sgs}	volume of steam generator secondary fluid (dome and shroud) (ft^3)
V_{shd}	volume of fluid mixture in steam generator shroud (ft^3)
w	process white noise vector
W_d	steam generator downcomer flow (lbm/sec)
W_{fw}	feedwater flow (lbm/sec)
W_l	liquid flow into condensate receiver (lbm/sec)
W_{loop}	primary loop flow (lbm/sec)
W_{lout}	liquid flow out of condenser (lbm/sec)
W_{por}	capacity of pressurizer power-operated relief valve (lbm/sec)
W_r	steam generator recirculation flow (lbm/sec)
W_{crlf}	capacity of condensate receiver relief valve (lbm/sec)
W_{rcr}	condensate receiver relief valve flow (lbm/sec)
W_{rv}	pressurizer total relief valve flow (lbm/sec)
W_s	steam flow into condensate receiver (lbm/sec)
W_s	normalized secondary steam flow
W_{saf}	capacity of pressurizer safety relief valves (lbm/sec)
W_{sgrv}	steam generator total relief valve flow (lbm/sec)
W_{sgrl}	capacity of steam generator relief valve 1 (lbm/sec)
W_{sgr2}	capacity of steam generator relief valve 2 (lbm/sec)
W_{sout}	steam flow out of condenser (lbm/sec)
W_{spray}	pressurizer spray flow (lbm/sec)
W_{sref}	reference secondary steam flow (lbm/sec)
W_{stm}	secondary steam flow (lbm/sec)
W_{surge}	pressurizer surge flow (lbm/sec)
x	linearized model state vector
$\hat{x}$	estimated value of x

$\bar{x}$	value of x at linearized model operating point
X_{cr}	quality of fluid mixture in condensate receiver
X_{fwv}	feedwater valve stem position
X_{fwvd}	demanded feedwater valve stem position (%)
X_{local}	local quality of core coolant
X_{mscv}	main steam control valve stem position
X_{mscvd}	desired main steam control valve stem position
X_p	quality of fluid mixture in pressurizer
X_{riser}	quality of fluid mixture in steam generator riser
X_{sg}	quality of secondary fluid mixture in steam generator
X_{shd}	quality of fluid mixture in steam generator shroud
X_A	actual variable value
X_M	measured variable value
y	linearized model output vector
$\hat{y}$	estimated value of y
$\bar{y}$	value of y at linearized model operating point
α	steam generator recirculation flow coefficient as defined in Equation (99)
α_b	boron concentration reactivity coefficient ($/ppm)
α_f	fuel temperature reactivity coefficient ($/°F)
α_m	core coolant density reactivity coefficient [$/(lbm/ft^3)]
β	effective delayed neutron fraction
γ_{local}	peaking factor on core coolant local heating
γ_{peak}	peaking factor on hot fuel rod heat flux
Γ	denominator term in steam generator state equations (Btu-ft^3/lbm^2-psi)
η_c	condenser tube fin effectiveness defined by Equation (120)
θ	air temperature coefficient defined by Equation (126)
Θ	linear discrete model input matrix
λ_l	first delayed neutron group decay constant (sec^{-1})

λ_2	second delayed neutron group decay constant (sec^{-1})
Λ	empirical correlation coefficient for condenser tube heat resistance defined in Equation (113)
μ	subcooled liquid viscosity (lbm/ft-hr)
μ_a	viscosity of air (lbm/ft-hr)
ρ	subcooled liquid density (lbm/ft^3)
ρ	net reactivity ($)
ρ_a	air density (lbm/ft^3)
ρ_b	net boron reactivity ($)
ρ_{bp}	density of core bypass coolant (lbm/ft^3)
ρ_{bpo}	density of coolant at outlet of core bypass (lbm/ft^3)
ρ_{cl}	density of coolant in cold leg (lbm/ft^3)
ρ_{core}	density of core coolant (lbm/ft^3)
ρ_f	net reactivity due to fuel temperature ($)
ρ_{fw}	density of feedwater flow (lbm/ft^3)
ρ_{hl}	density of coolant in hot leg (lbm/ft^3)
ρ_m	net reactivity due to core coolant moderator density ($)
ρ_{out}	density of coolant at outlet of core (lbm/ft^3)
ρ_{rod}	control rod reactivity ($)
ρ_{sg}	density of coolant in steam generator primary (lbm/ft^3)
ρ_{tsg}	density of steam generator tubes (lbm/ft^3)
$\bar{\rho}_m$	average core coolant density (lbm/ft^3)
$\bar{\rho}_{mo}$	reference average core coolant density used to initialize net reactivity (lbm/ft^3)
Σ	denominator term in pressurizer state equations ($Btu\text{-}ft^3/lbm^2\text{-}psi$)
τ	measurement sensor time constant (sec)
τ_{cr}	condensate receiver pressure control system blade positioner time constant (sec)
τ_{hl}	hot leg temperature sensor time constant (sec)
τ_{mscv}	main steam control valve motion time constant (sec)
ϕ	denominator term in condensate receiver state equations ($Btu\text{-}ft^3/lbm^2\text{-}psi$)

Φ	linear model state transition matrix
Ψ	fraction of total power remaining in fuel
Ψ_1	first delayed neutron group precursor concentration (MW-sec)
Ψ_2	second delayed neutron group precursor concentration (MW-sec)
Ω	units conversion constant (Btu/MW-sec)

AN ADVANCED DIGITAL PWR PLANT PROTECTION SYSTEM BASED ON OPTIMAL ESTIMATION THEORY

INTRODUCTION

The accident at Three Mile Island has restimulated interest in the protection and control of nuclear power plants. An active area of research is the application of optimal estimation and control theories to the development of protection and control strategies for these plants. To date, the research and implementation indicate that on-line, digital, optimal estimation and prediction of plant variables and unmeasured parameters, coupled with optimal control algorithms, offer increased plant safety and efficiency over current, conventional controls.

Under a project sponsored by the Department of Energy, the preliminary design of an advanced plant protection system has been developed for the Loss-of-Fluid Test (LOFT) reactor plant, a 50-MW(t) test facility used to analyze both operational transients and loss-of-coolant accidents in pressurized water reactors (shown schematically in Figure 1). The advanced plant protection system developed for LOFT incorporates a Kalman filter estimator to provide optimal estimates of unmeasurable variables, such as clad temperature and DNBR (departure from nucleate boiling ratio), which are critical to overall plant integrity. This advanced protection system is described and evaluated in this report.

Need for an advanced plant protection system is discussed, and the equations involved in the Kalman filter estimator are presented. An important aspect of the Kalman filter design is that it be provided with a relatively low-order, accurate model of the dynamics of the system to which it is applied; such a model of the LOFT plant is described, as is the correlation used in the DNBR calculation. Finally, using several sets of simulated transient data, the performance of the advanced plant protection system is evaluated.

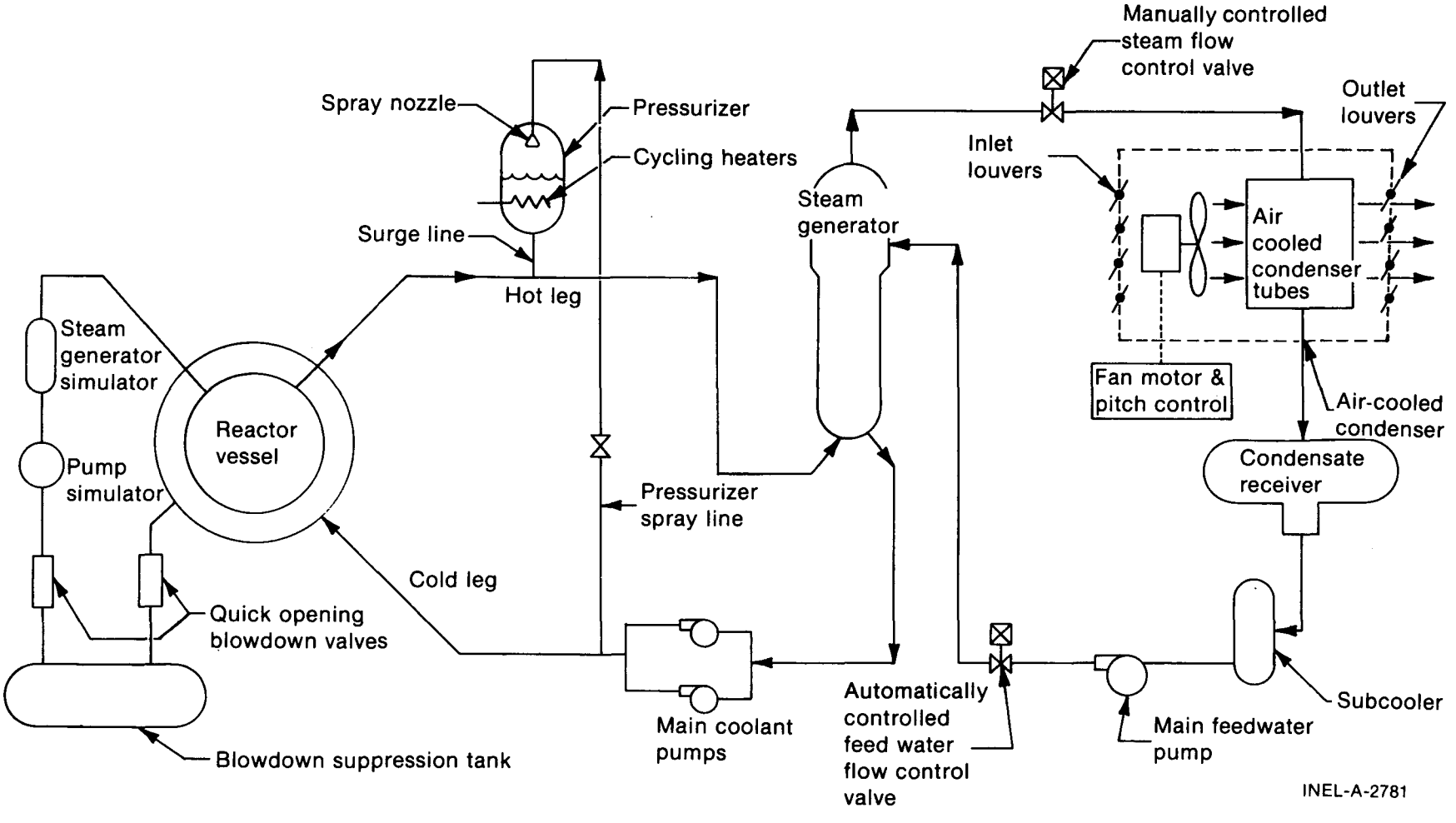

Figure 1. LOFT reactor plant schematic diagram.

THE ADVANCED PLANT PROTECTION SYSTEM

Many variables crucial to the protection of nuclear power plants cannot be measured directly. For example, the primary purpose of a pressurized water reactor protection system is to prevent the melting of the nuclear fuel and its cladding under accident conditions. Unfortunately, the harsh environment of the nuclear core precludes direct, reliable measurement of the fuel and cladding temperatures with present instrumentation. Protection system performance must, therefore, rely on measurement of other variables external to the reactor core. A typical protection system may use neutron flux measurements in the shield tank surrounding the reactor; the temperature, pressure, and flow rate of the coolant in the primary loop; control rod position; and steam flow and steam generator water level in the secondary coolant loop. Continuous comparison of these measurement values to pre-established setpoints is used to determine the need for plant shutdown.

Because of these measurement constraints, an extensive simulation study is required as part of the protection system design to verify that the available measurements and associated trip setpoints are adequate to maintain the integrity of the plant. The simulation study involves developing a detailed mathematical model of the entire power plant, including the proposed protection system, programming the model on a computer, hypothesizing a set of accidents believed credible for the given plant design, and simulating the plant response under these accident conditions. The simulation results are then analyzed to determine whether or not the limiting values of any plant variable have been exceeded. If they have, the protection system design is modified and the accidents are resimulated. This process is repeated until a satisfactory, although probably not optimum, protection system design evolves. The entire process must then be repeated to account for potential changes in, or uncertainty in the knowledge of, plant parameter values, until some compromise in design is reached. Complex as this procedure is, it is further complicated by the fact that it is usually not possible, or even desirable, to simulate the full spectrum of credible accidents with a single computer code.

In practice, then, protection system design becomes an iterative process involving a set of postulated accidents the completeness of which depends on the skill and experience of the analyst, many mathematical plant models and computer codes, and a number of specialists from a variety of disciplines, including reactor physics, thermal-hydraulics, instrumentation, and system analysis. This very complicated process is not only expensive but abounding with opportunities for serious errors and misunderstandings directly affecting reactor safety. Clearly, some improvement in reactor protection system design methods is desirable.

The methods of optimal estimation theory offer a promising new approach to plant protection system design. The advanced plant protection system (PPS), shown in Figure 2, is conceptually quite straightforward. A Kalman filter is used to generate estimates of the current plant state vector, x, based on a set of available noisy, diverse measurements, y. The state vector would include such variables as fuel and cladding temperature, and the values of related variables, such as DNBR (departure from nucleate boiling ratio) and LHGR (linear heat generation rate), can be readily obtained from the estimated state values. The state estimates and values of DNBR and LHGR are then directly compared with limiting setpoints, and appropriate control action is initiated to avoid violating these limits.

This approach offers a number of advantages over current methods. System modeling efforts will concentrate on the development of a suitable model for the estimator, which will lead to a more efficient and organized modeling effort and make model limitations and assumptions more clearly visible. Protective action will be based on a direct comparison of an optimal estimate of a critical variable with its limiting value, not on auxiliary variables whose limits were determined by a complicated analysis involving a myriad of simplifying, often conflicting, assumptions. Changing plant parameter values can be estimated on-line, and the effects of these changes can immediately be accounted for in the estimator.

Measurement diversity, an important element in protection system reliability, is inherent in the advanced system. Reactor plant safety will be independent of an analyst's ability to postulate a complete set of potential reactor accidents. Finally, as seen in Figure 2, it would be relatively simple to add an optimal

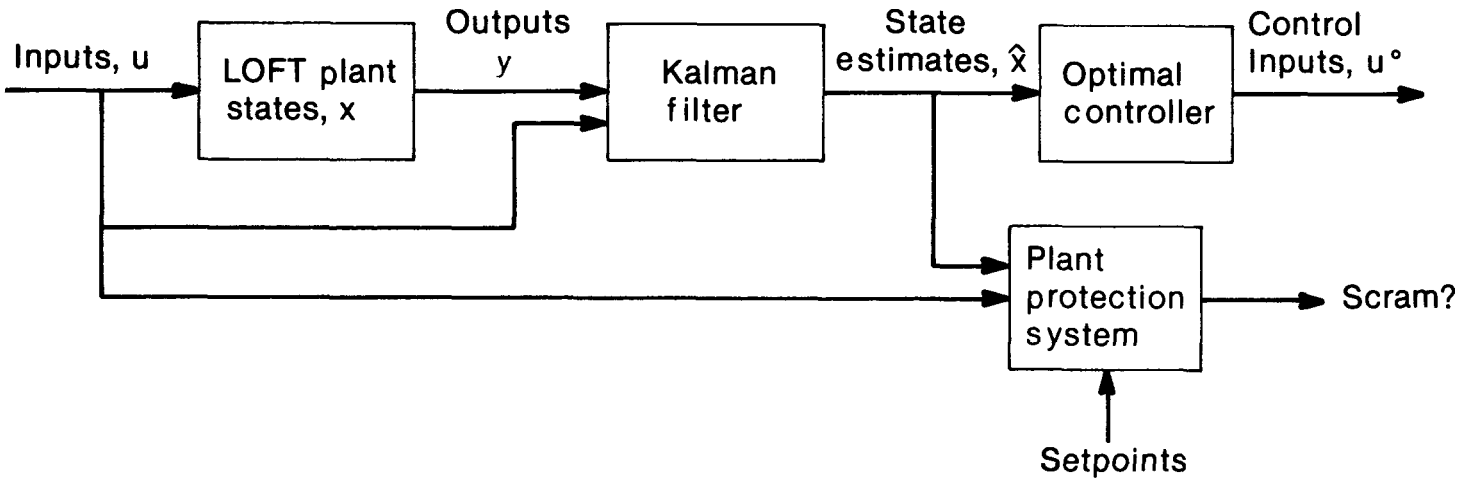

Figure 2. Advanced LOFT plant protection system.

state feedback controller to this system since estimates of the full plant state vector are available. The generated optimal control, u^o, could either be used as suggested control information for the plant operator or it could be used in a closed-loop fashion to provide a complete computer-based advanced plant protection and control system.

KALMAN FILTER ESTIMATOR

As seen in Figure 2, the Kalman filter uses a model of the LOFT plant dynamics to generate optimal estimates of the plant states. It is essentially a least-squares estimator minimizing the error between the actual plant state and the state estimate. No effort is made here to derive the Kalman filter equations; several excellent texts[1,2,3] provide such derivations. Instead, the equations are presented with a brief description of what each one does.

We assume the plant dynamics can be modeled as a linear, time-varying, discrete system of the form[a]

$$x(k+1) = \Phi(k+1,k)x(k) + \Theta(k)u(k) + w(k) \tag{1}$$

where x(k) is the plant state vector at time k, u(k) a deterministic control input, and w(k) a zero-mean, white disturbance vector. Also, $\Phi(k+1,k)$ is the state transition matrix from k to k+1, and $\Theta(k)$ is the input system matrix. Although it is possible to derive a nonlinear form of the Kalman filter (extended Kalman filter), the faster time propagation of the linear formulation dictates the use of the linear Kalman filter in the advanced plant protection system. Also, the discrete filter is used instead of a continuous filter since it is anticipated that the advanced system will be implemented on a digital, rather than analog, computer.

Similarly, a model of the plant measurements is required. This must be a linear model of the form

$$y(k) = C(k)x(k) + D(k)u(k) + v(k) \tag{2}$$

where v(k) is a zero-mean, white measurement noise, uncorrelated with the process noise w(k); and C(k) and D(k) are the required measurement system matrices. Plant model statistics required by the Kalman filter include the covariance of the two white noise processes w(k) and v(k), the initial estimate of the state vector x(O), and the variance of the estimate of x(O).

The basic information flow in the discrete Kalman filter is shown in Figure 3. At time k, a plant measurement y(k) is taken and used to update the current estimate of the plant state using

$$\hat{x}(k|k) = \hat{x}(k|k-1) + K(k)\,[y(k) - C(k)\hat{x}(k|k-1) - D(k)u(k)] \tag{3}$$

where x(k|k-1) is the state estimate at k, based on measurements up to time k-1. The matrix K(k) is the Kalman gain, which simply weights the difference between the actual measurement y(k) and the filter estimate of y(k). K(k) is calculated using

$$K(k) = P(k|k-1)C^T(k)\,[C(k)P(k|k-1)C^T(k) + R(k)]^{-1} \tag{4}$$

where R(k) is the covariance matrix of the measurement noise and P(k|k-1) is the covariance of the error in the estimate of the state prior to the measurement. The error covariance is updated using

$$P(k|k) = [I - K(k)C(k)]\,P(k|k-1). \tag{5}$$

Prior to taking the next measurement at time k+1, both the state estimate and estimate error covariance are propagated ahead in time using the state dynamics equations

$$\hat{x}(k+1|k) = \Phi(k+1,k)\hat{x}(k|k) + \Theta(k)u(k) \tag{6}$$

---

a. All variables and other nomenclature are defined in the NOMENCLATURE section immediately following the CONTENTS.

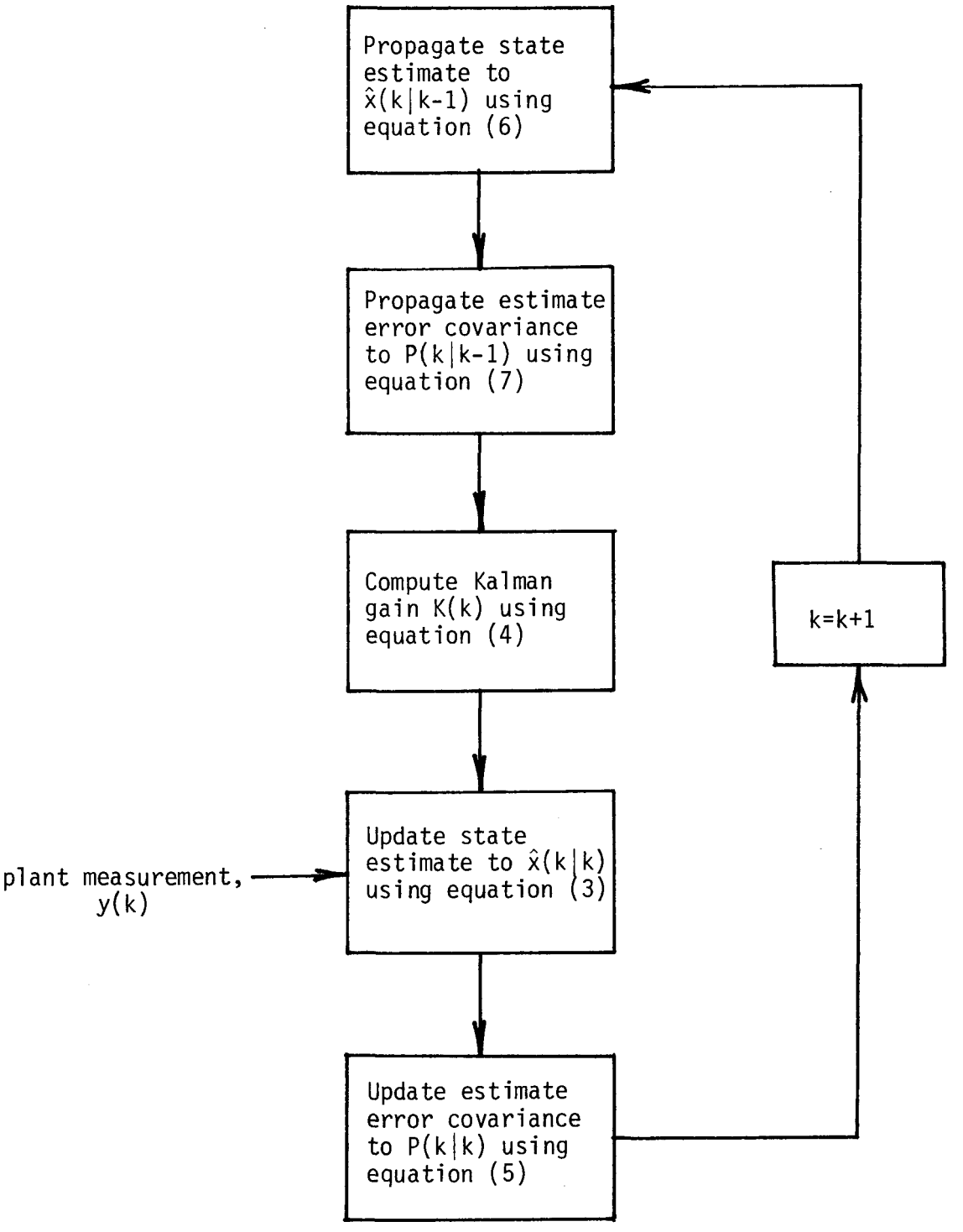

Figure 3. Discrete Kalman filter information flow.

and

$$P(k+1|k) = \Phi(k+1,k)P(k|k)\Phi^{T}(k+1,k) + Q(k) \tag{7}$$

where Q(k) is the covariance matrix for the process noise vector w(k).

Equations (3) through (7) are processed once for each measurement. In the advanced PPS, these equations are solved using routines from Reference 4. These optimal estimation routines, developed at the Idaho National Engineering Laboratory, incorporate the factorization methods of Bierman[5] in performing the estimate updates defined by Equations (3), (4), and (5).

LOFT PLANT MODEL

The primary effort in Kalman filter design is the development of the linear, discrete plant dynamics description in the form of Equations (1) and (2). Unfortunately, the dynamics of a nuclear reactor and its supporting subsystems are highly nonlinear, and direct derivation of the model required by the Kalman filter is difficult. Thus, it is convenient to first derive a nonlinear plant model, numerically linearize it about some operating point, and then discretize the resulting linear model.

In this section, such a nonlinear model of the LOFT plant is described. The model consists of twenty-three first-order differential equations with all major subsystems of both the primary and secondary sides of the plant represented. Also described are the linearization and discretization processes involved in getting the model in the form of Equations (1) and (2).

Nonlinear LOFT Model

The model derived here is based on a model developed in Reference 6, to which you are referred for specific simulation parameters and for details of the model validation using LOFT test data. The plant model is divided into eight subsystems (see Figure 1):

1. Reactor Kinetics
2. Core Thermal
3. Primary Loop
4. Pressurizer
5. Steam Generator
6. Air-Cooled Condenser
7. Condensate Receiver
8. Feedwater.

The modeling of each of these subsystems is now discussed in detail.

Reactor Kinetics. The reactor kinetics simulate the power generation within the nuclear fuel. The standard time-dependent point kinetics,[7] based on neutron conservation, are used:

$$\frac{dP}{dt} = \frac{\beta}{\ell}\left\{(\rho - 1)P + \sum_{i=1}^{N} \lambda_i \Psi_i\right\} \tag{8}$$

and

$$\frac{d\Psi_i}{dt} = f_i P - \lambda_i \Psi_i, \quad i = 1, N \tag{9}$$

where N is the number of delayed neutron groups simulated. For the LOFT model, an algebraic approximation to Equation (8) was made[8] by setting it equal to zero and solving for P, the core power level

$$P = \frac{\sum_{i=1}^{N} \lambda_i \Psi_i}{1 - \rho} . \tag{10}$$

This approximation implies that the power equation has much faster dynamics than the precursor equations. Two delayed neutron groups were used yielding two state equations:

$$\frac{d\Psi_1}{dt} = f_1 P - \lambda_1 \Psi_1 \tag{11}$$

and

$$\frac{d\Psi_2}{dt} = f_2 P - \lambda_2 \Psi_2 . \tag{12}$$

Equations (10) through (12) constitute the reactor kinetics model yielding two state variables, Ψ_1 and Ψ_2. The net reactivity, ρ, is made up of several components. First, reactivity due to control rod motion is input to the model upon scram initiation or can be input as a ramp function to simulate a slow rod withdrawal. Rod worth upon scram is based on rod calibration data and is calculated using the curve fit

$$\rho_{rod} = \begin{cases} 0, & (t - t_s) \leq t_d \\ a[t - (t_s + t_d)]^3, & t_e > (t - t_s) > t_d \\ a(t_e - t_d)^3, & (t - t_s) \geq t_e \end{cases} . \tag{13}$$

Reactivity due to fuel temperature, average core coolant density, and coolant boron concentration variations is calculated using constant coefficient multipliers

$$\rho_f = \alpha_f (T_f - T_{fo}) \tag{14}$$

$$\rho_m = \alpha_m (\bar{\rho}_m - \bar{\rho}_{mo}) \tag{15}$$

and

$$\rho_b = \alpha_b (B_{ave} - B_{aveo}) \tag{16}$$

making the total net reactivity for use in Equation (10)

$$\rho = \rho_{rod} + \rho_f + \rho_m + \rho_b . \tag{17}$$

The generation of decay heat in the core is calculated using the curve in Figure 4 (Reference 9). Constant decay power (6.73% of the initial power level) is assumed as long as a plant scram does not occur. Following a scram, this decay heat fraction is reduced according to Figure 4. The decay heat summed with the power computed in Equation (10) yields the total core power P_T.

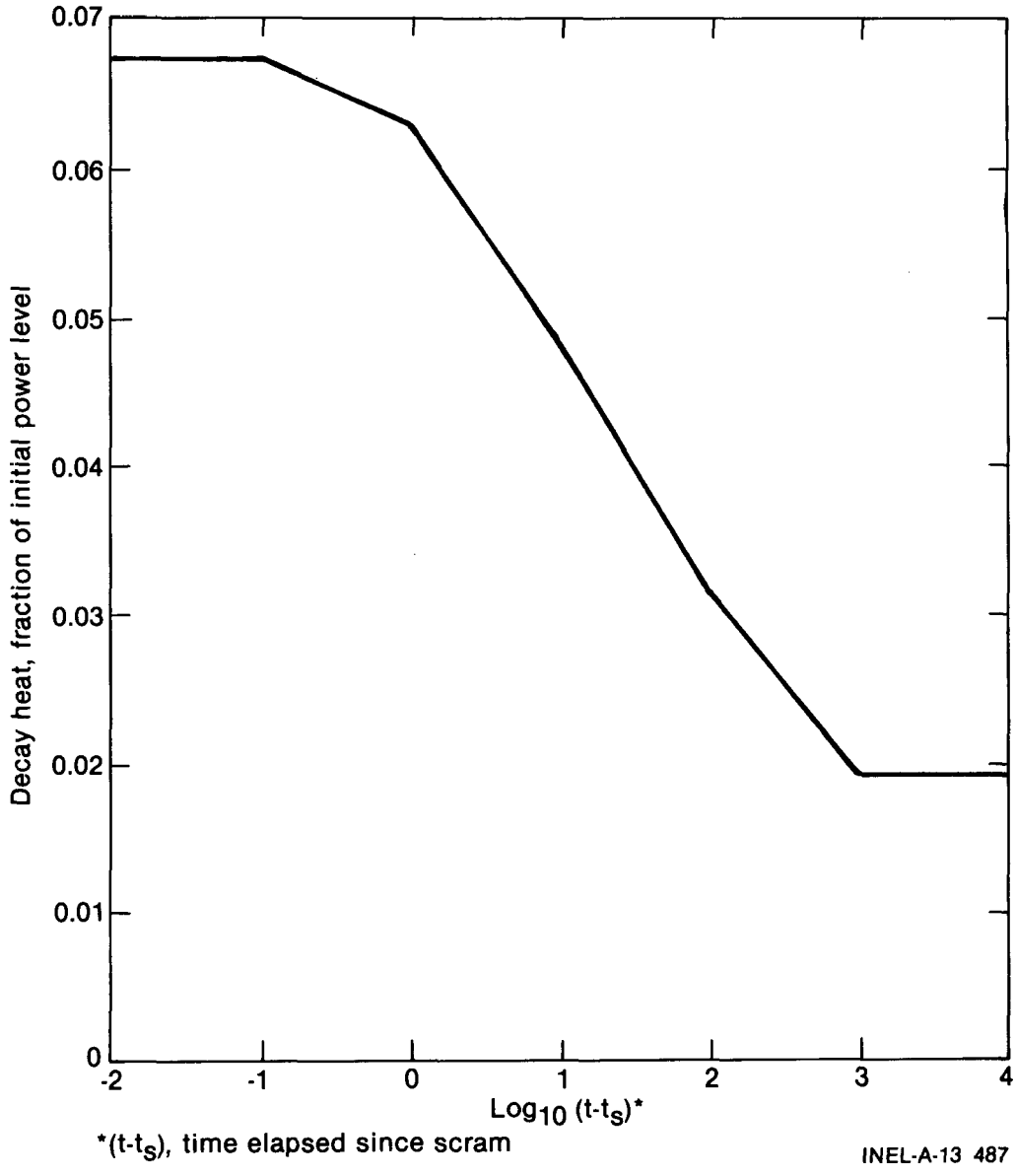

Figure 4. ANS decay heat curve.

Core Thermal. The core thermal model accounts for transfer of heat generated within the fuel, through the fuel, the gas gap, and the cladding, to the core coolant. A single fuel node and a single cladding node separated by a variable width gas gap constitute the model shown in Figure 5. Performing a heat balance on the reactor fuel yields the state equation

$$\frac{dT_f}{dt} = \frac{1}{(Mc_p)_f} [\Psi P_T + U_{fc} (T_c - T_f)] \tag{18}$$

and a similar heat balance on the fuel cladding leads to

$$\frac{dT_c}{dt} = \frac{1}{(Mc_p)_c} U_{fc}[(T_f - T_c) - \frac{Q_{cp}}{\Omega}]. \tag{19}$$

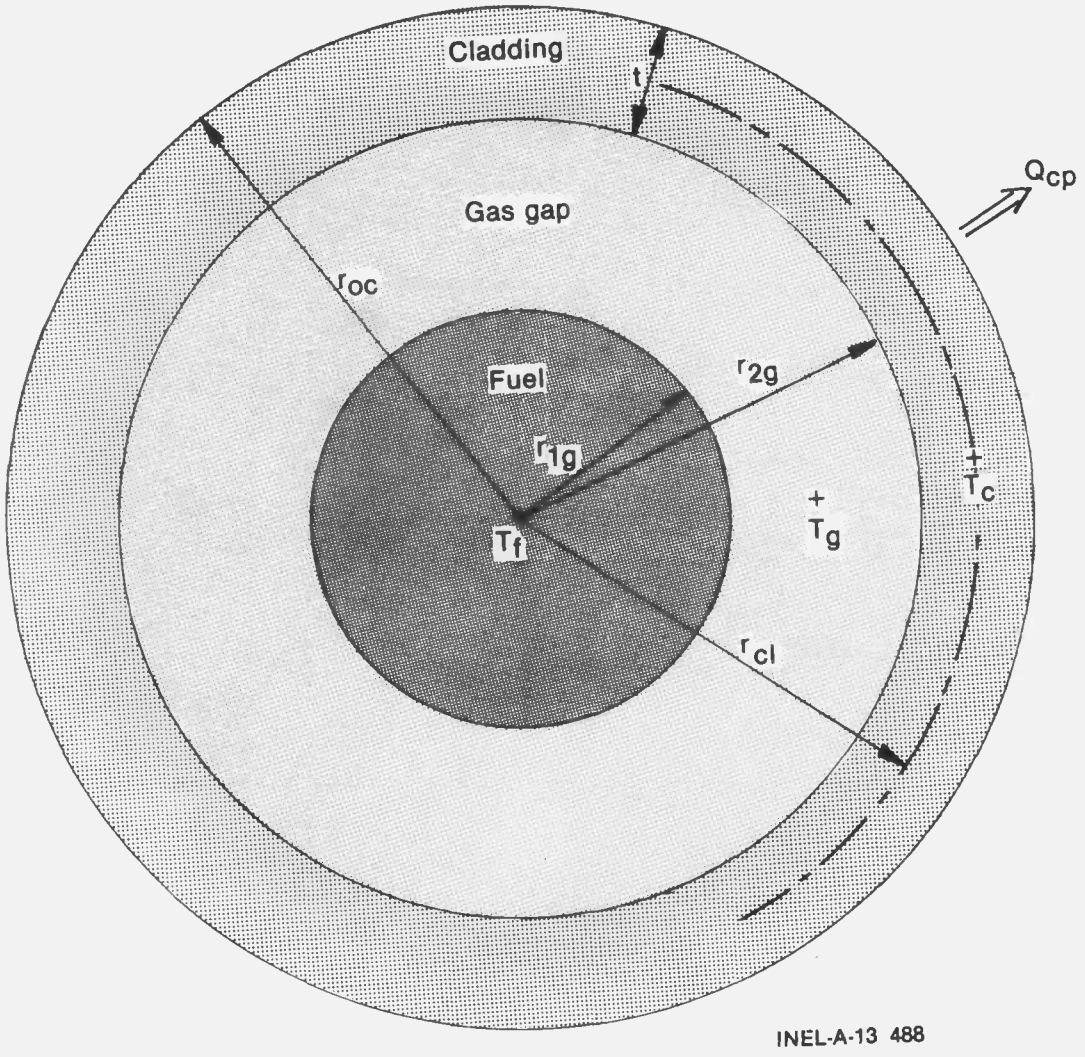

(Note: The gap size is overexaggerated for clarity of notation.)

Figure 5. Core thermal model.

These two equations make up the core thermal model.

The overall heat transfer coefficient, U_{fc}, is made up of the conductance of the fuel, gap, and clad metal:

$$U_{fc} = \frac{1}{(\frac{1}{K_f}) + (\frac{1}{K_g}) + (\frac{1}{K_{cl}})} \tag{20}$$

which individually are

$$K_f = (\frac{A_f}{l_f})\ k_f(T_f) \tag{21}$$

and

$$K_g = \frac{2\pi N_{rod} L_{rod}}{\ln \frac{r_{2g}}{r_{1g}}} k_g(T_g) \tag{22}$$

where

$$T_g = \frac{(T_f + T_c)}{2} \tag{23}$$

and

$$K_{c1} = \frac{2\pi N_{rod} L_{rod}}{\ln \left[\frac{r_{c1}}{r_{2g}}\right]} k_c(T_c) . \tag{24}$$

The temperature-dependent conductivities, k_f, k_g, and k_c, are obtained by curve fitting data from Reference 10. The (A_f/l_f) factor in Equation (21) is selected to yield a correct average fuel temperature at steady state. Finally, expansion of the fuel and cladding is modeled, hence the various radii are given by

$$r_{1g} = r_f\left(1 + \frac{\Delta r_f}{r_f}\right) \tag{25}$$

$$r_{2g} = r_c\left(1 + \frac{\Delta r_c}{r_c}\right) - t \tag{26}$$

and

$$r_{c1} = r_{2g} + \frac{t}{2} \tag{27}$$

where the expansion factors are calculated using relations from Reference 10.

The heat transferred to the core coolant, Q_{cp}, is defined in the primary loop model description below.

Primary Loop. The primary loop model covers the transport of the heat generated within the core into the loop. The loop is divided into five nodes, as shown in Figure 6. A heat balance on each of the nodes yields the following state equations:

$$\frac{dT_{ave}}{dt} = \frac{1}{(Mc_p)_{core}} (Q_{cp} + Q_{dhc} - Q_{core}) \tag{28}$$

$$\frac{dT_{bpa}}{dt} = \frac{1}{(Mc_p)_{bp}} (Q_{dhbp} - Q_{bp}) \tag{29}$$

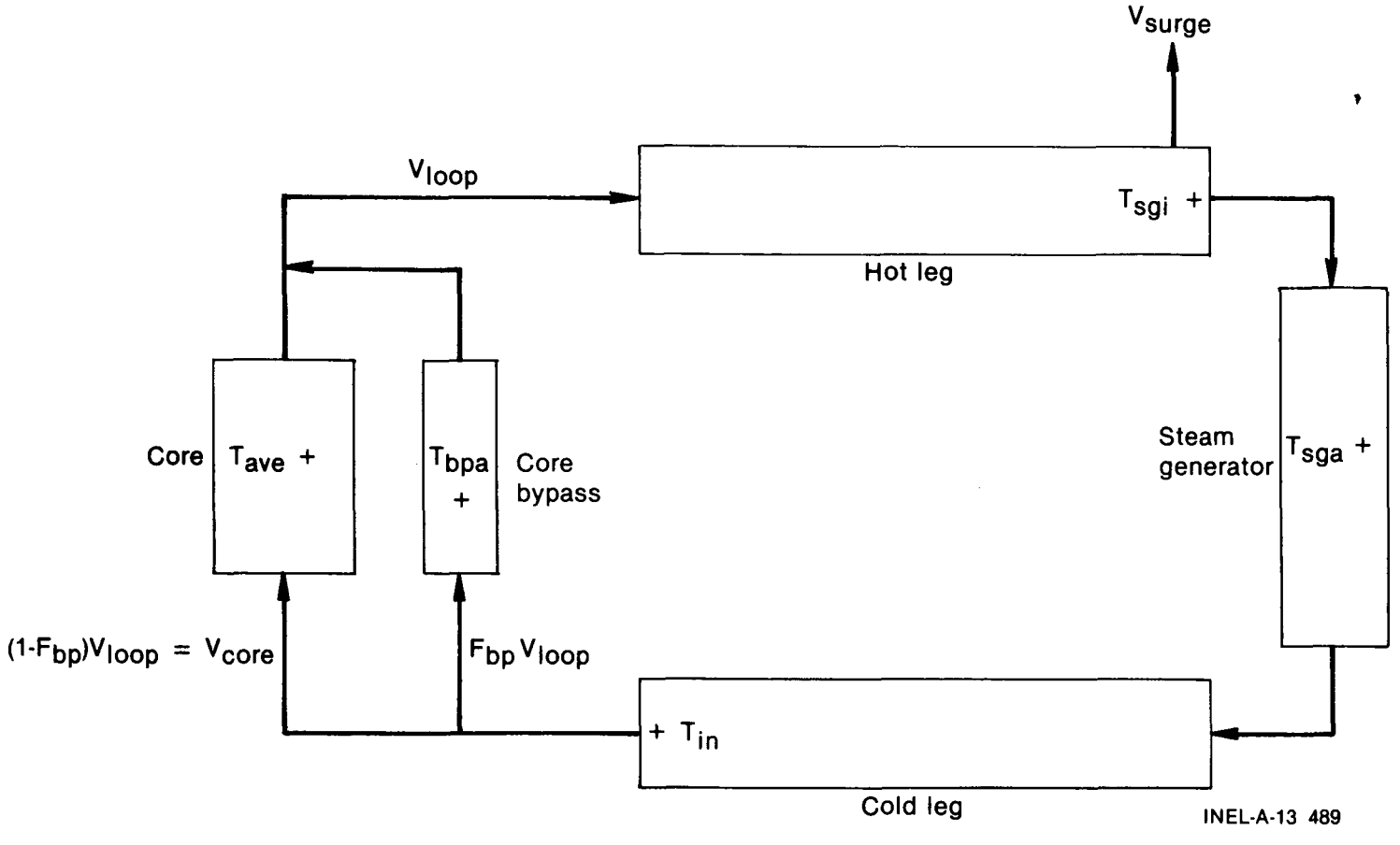

Figure 6. Primary loop nodalization.

$$\frac{dT_{sgi}}{dt} = \frac{V_{loop}}{V_{hl}} (T_{hot} - T_{sgi}) - \frac{V_{surge}}{V_{hl}} (T_{surge} - T_{sgi}) \tag{30}$$

$$\frac{dT_{sga}}{dt} = \frac{1}{(Mc_p)_{sg}} (Q_{sg} - Q_{sgout}) \tag{31}$$

and

$$\frac{dT_{in}}{dt} = \frac{V_{loop}}{V_{cl}} (T_{sgo} - T_{in}). \tag{32}$$

Note that in the nodes without heat addition or removal, perfect fluid mixing is assumed. Note also that constant volumetric flow in the loop is assumed and that structural heating is ignored.

The heat flows to and from the core coolant are given by

$$Q_{cp} = U_{cp}(T_c - T_{ave}) \tag{33}$$

$$Q_{dhc} = f_{dhc} P_T \Omega \tag{34}$$

and

$$Q_{core} = \rho_{core} V_{core} c_{pcore} (T_{out} - T_{in}). \tag{35}$$

The heat transfer coefficient, U_{cp}, combines the fuel cladding conductance and the convective coefficient of the flowing coolant:

$$U_{cp} = \frac{1}{\left(\frac{3600}{h_{clad} A_{clad}}\right) + \left(\frac{1}{\Omega K_{c2}}\right)}. \tag{36}$$

The convective coefficient, h_{clad}, is found using the Dittus-Boelter correlation,[11] or

$$h_{clad} = \frac{0.023 k_{core} (Re)^{0.8}_{core} (Pr)^{0.4}_{core}}{D_{eqcor}} \tag{37}$$

and the clad conductance from the centerline to the outer surface is

$$K_{c2} = \frac{2\pi N_{rod} L_{rod}}{\ln\left[\frac{r_{oc}}{r_{cl}}\right]} k_c(T_c) \tag{38}$$

where

$$r_{oc} = r_c\left(1 + \frac{\Delta r_c}{r_c}\right). \tag{39}$$

The clad surface area is given by

$$A_{clad} = \frac{2\pi r_{oc} L_{rod} N_{rod}}{12} \tag{40}$$

and the equivalent core diameter is

$$D_{eqcor} = \frac{4A_{core} L_{rod}}{A_{clad}}. \tag{41}$$

The core outlet temperature is by definition

$$T_{out} = 2\,T_{ave} - T_{in}. \tag{42}$$

Finally, the properties of the subcooled primary loop coolant, i.e., density, conductivity, specific heat, and viscosity, are all modeled as being temperature dependent, using data from Reference 12.

Similarly, for the core bypass, the heat flows are defined by

$$Q_{dhbp} = f_{dhbp}\, P_T\, \Omega \tag{43}$$

and

$$Q_{bp} = \rho_{bp} F_{bp} V_{loop} c_{pbp} (T_{bpo} - T_{in}) \tag{44}$$

where

$$T_{bpo} = 2\,T_{bpa} - T_{in} \tag{45}$$

and for the steam generator:

$$Q_{sg} = U_{pri} (T_{tsg} - T_{sga}) \tag{46}$$

and

$$Q_{sgout} = \rho_{sg} V_{loop} c_{psg} (T_{sgo} - T_{sgi}) \tag{47}$$

where

$$T_{sgo} = 2T_{sga} - T_{sgi}. \tag{48}$$

The primary side heat transfer coefficient, U_{pri}, is described in the section covering the steam generator model.

The vessel outlet temperature T_{hot} used in Equation (30), is a flow-weighted average of the core and core bypass outlet temperatures:

$$T_{hot} = \frac{\rho_{out}(1 - F_{bp})T_{out} + \rho_{bpo}F_{bp}T_{bpo}}{\rho_{out}(1 - F_{bp}) + \rho_{bpo}F_{bp}} . \quad (49)$$

The flow and temperature due to pressurizer surge, V_{surge} and T_{surge}, are described with the pressurizer model.

Pressurizer. The pressurizer, which maintains pressure within the primary loop, is shown schematically in Figure 7. For this model, the steam and liquid in the pressurizer are assumed to be in a homogeneous, saturated mixture; and applying mass and energy balances to the mixture results in the following two equations:

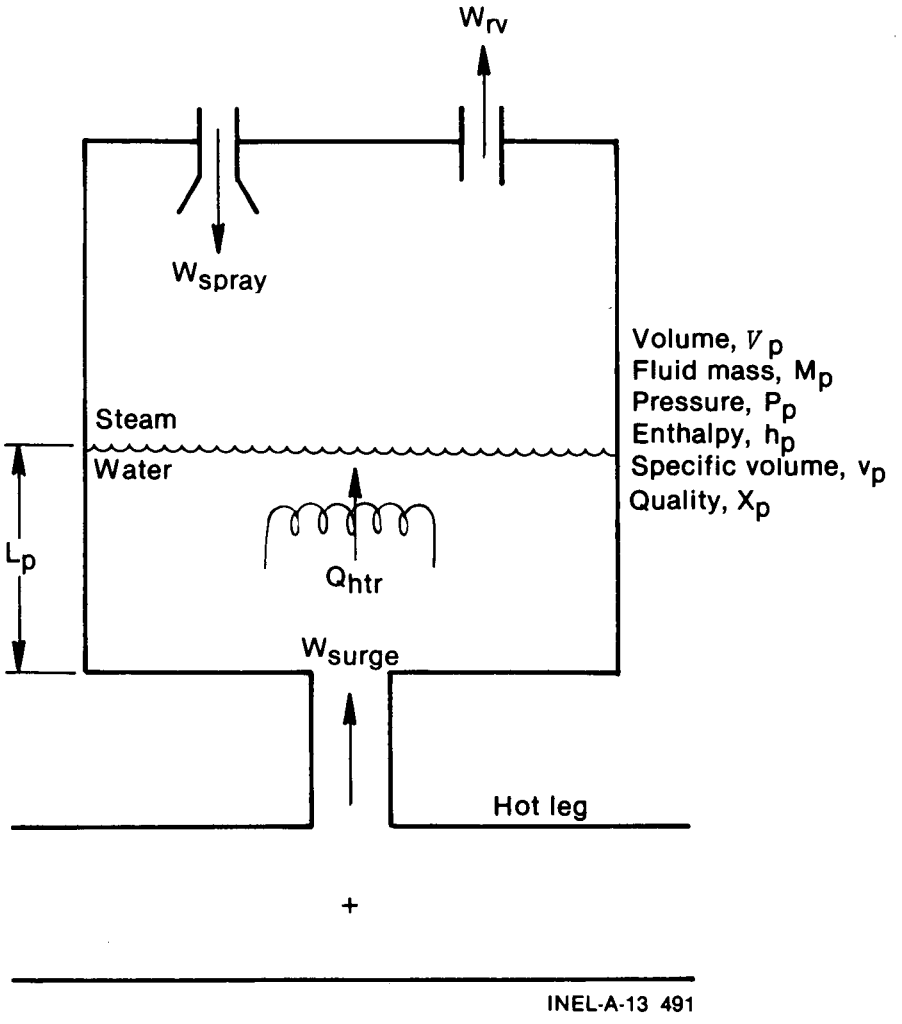

Figure 7. Pressurizer schematic.

$$\frac{dM_p}{dt} = W_{surge} + W_{spray} - W_{rv} \tag{50}$$

and

$$M_p \frac{dh_p}{dt} = \frac{V_p}{J} \frac{dP_p}{dt} + Q_{htr} + W_{surge} (h_{surge} - h_p)$$

$$+ W_{spray} (h_{spray} - h_p) - W_{rv} (h_g - h_p). \tag{51}$$

The desired state variables for the pressurizer are P_P, the pressure, and X_P, the mixture quality. We obtain equations in this form by first noting

$$v_p = \frac{V_p}{M_p} \tag{52}$$

and hence Equation (50) becomes

$$\frac{dv_p}{dt} = - \frac{v_p^2}{V_p} (W_{surge} + W_{spray} - W_{rv}). \tag{53}$$

The mixture properties v_p and h_p are defined by

$$v_p = v_f + X_p (v_g - v_f) \tag{54}$$

and

$$h_p = h_f + X_p (h_g - h_f) \tag{55}$$

which when differentiated yield

$$\frac{dv_p}{dt} = \frac{\partial v_p}{\partial X_p} \frac{dX_p}{dt} + \frac{\partial v_p}{\partial P_p} \frac{dP_p}{dt} \tag{56}$$

and

$$\frac{dh_p}{dt} = \frac{\partial h_p}{\partial X_p} \frac{dX_p}{dt} + \frac{\partial h_p}{\partial P_p} \frac{dP_p}{dt} \tag{57}$$

where note

$$\frac{\partial v_p}{\partial X_p} = v_g - v_f \tag{58}$$

$$\frac{\partial v_p}{\partial P_p} = \frac{dv_f}{dP_p} + X_p\left(\frac{dv_g}{dP_p} - \frac{dv_f}{dP_p}\right) \tag{59}$$

$$\frac{\partial h_p}{\partial X_p} = h_g - h_f \tag{60}$$

and

$$\frac{\partial h_p}{\partial P_p} = \frac{dh_f}{dP_p} + X_p\left(\frac{dh_g}{dP_p} - \frac{dh_f}{dP_p}\right). \tag{61}$$

Now, by substituting Equations (51) and (53) into (56) and (57), we can solve simultaneously for dX_p/dt and dP_p/dt, the desired state equations. This manipulation yields

$$\frac{dX_p}{dt} = \frac{v_p}{V_p\Sigma}\left\{v_p(W_{surge} + W_{spray} - W_{rv})\left(\frac{\partial h_p}{\partial P_p} - \frac{v_p}{J}\right) + \frac{\partial v_p}{\partial P_p}\left[Q_{htr} + W_{surge}(h_{surge} - h_p) + W_{spray}(h_{spray} - h_p) - W_{rv}(h_g - h_p)\right]\right\} \tag{62}$$

and

$$\frac{dP_p}{dt} = \frac{-v_p}{V_p\Sigma}\left\{v_p\frac{\partial h_p}{\partial X_p}(W_{surge} + W_{spray} - W_{rv}) + \frac{\partial v_p}{\partial X_p}\left[Q_{htr} + W_{surge}(h_{surge} - h_p) + W_{spray}(h_{spray} - h_p) - W_{rv}(h_g - h_p)\right]\right\} \tag{63}$$

where

$$\Sigma = \frac{\partial v_p}{\partial P_p}\frac{\partial h_p}{\partial X_p} - \frac{\partial v_p}{\partial X_p}\left(\frac{\partial h_p}{\partial P_p} - \frac{v_p}{J}\right). \tag{64}$$

In the LOFT model, saturation enthalpies and specific volumes are represented as polynomial functions of P_P; hence all of the partial derivatives in Equations (58) through (61) are evaluated exactly.

The surge flow, W_{surge}, is taken to be the negative of the instantaneous change in the mass of the fluid in the primary loop. That is, an increase in primary loop mass is assumed to be due to an outsurge ($W_{surge} < O$) from the pressurizer, while a decrease in mass results in a pressurizer insurge ($W_{surge} > O$). The mass of fluid in the loop at any time is

$$M_{loop} = \rho_{core}V_{core} + \rho_{bp}V_{bp} + \rho_{hl}V_{hl} + \rho_{sg}V_{sgp} + \rho_{cl}V_{cl} \tag{65}$$

The subcooled densities in Equation (65) are assumed to be functions of temperature only; hence, the surge flow can be expressed as

$$W_{surge} = -\frac{dM_{loop}}{dt} = -\left\{ V_{core}\left[\frac{d\rho_{core}}{dT_{ave}}\ \frac{dT_{ave}}{dt}\right] + V_{bp}\ \left[\frac{d\rho_{bp}}{dT_{bpa}}\ \frac{dT_{bpa}}{dt}\right]\right.$$
$$+ V_{hl}\left[\frac{d\rho_{hl}}{dT_{sgi}}\ \frac{dT_{sgi}}{dt}\right] + V_{sgp}\ \left[\frac{d\rho_{sg}}{dT_{sga}}\ \frac{dT_{sga}}{dt}\right]$$
$$\left. + V_{cl}\left[\frac{d\rho_{cl}}{dT_{in}}\ \frac{dT_{in}}{dt}\right]\right\} \tag{66}$$

with the temperature derivatives being available from the primary loop thermal model. The enthalpy of the surge flow is assumed to be equal to the saturated enthalpy of the liquid within the pressurizer. The volumetric surge flow and surge temperature (used in the primary loop model) are given by

$$V_{surge} = \begin{cases} W_{surge} v_f, & W_{surge} < 0 \\ 0, & W_{surge} = 0 \\ W_{surge}/\rho_{hl}, & W_{surge} > 0 \end{cases} \tag{67}$$

and

$$T_{surge} = \begin{cases} T_{lpzr}, & W_{surge} < 0 \\ T_{sgi}, & W_{surge} > 0 \end{cases} . \tag{68}$$

The pressurizer spray, tapped off from the cold leg, is used to prevent an overpressurization of the primary loop. The control logic for this flow is shown in Figure 8. The spray enthalpy is the enthalpy of the subcooled water in the cold leg:

$$h_{spray} = h_{cl} . \tag{69}$$

Two sets of relief valves are modeled, the power-operated relief valve and the safety reliefs. The logic controlling these valves is shown in Figure 9. The relief flow is assumed to be saturated steam at pressure P_P; hence, the relief flow enthalpy is h_g, the steam saturation enthalpy. Two banks of heaters, cycling and backup, are incorporated in the pressurizer model, and their setpoints are displayed in Figure 10.

The pressure in the primary loop is calculated based on the simple equation

$$P_{loop} = P_p + K_{surge}|V_{surge}|V_{surge} \tag{70}$$

and the liquid level in the pressurizer can be shown to equal

$$L_p = A_p(1 - X_p)\frac{V_p}{v_p} v_f . \tag{71}$$

Steam Generator. The LOFT steam generator is a vertical, U-tube, recirculation type similar to those used in most PWR plants. The model used to describe the transfer of heat from the primary loop to the secondary fluid is sketched in Figure 11. It is seen that heat from the primary fluid is transferred through

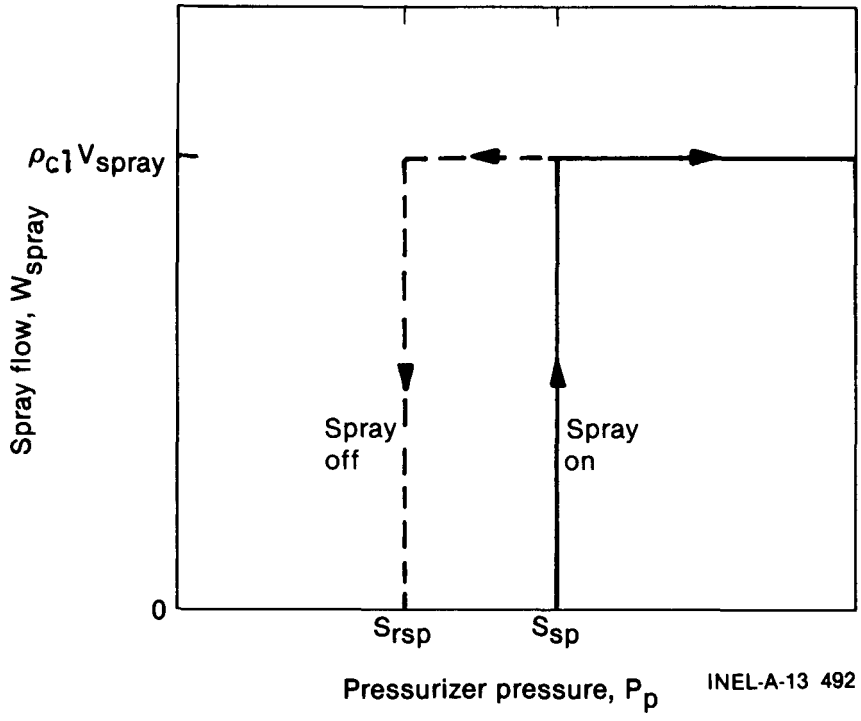

Figure 8. Pressurizer spray logic.

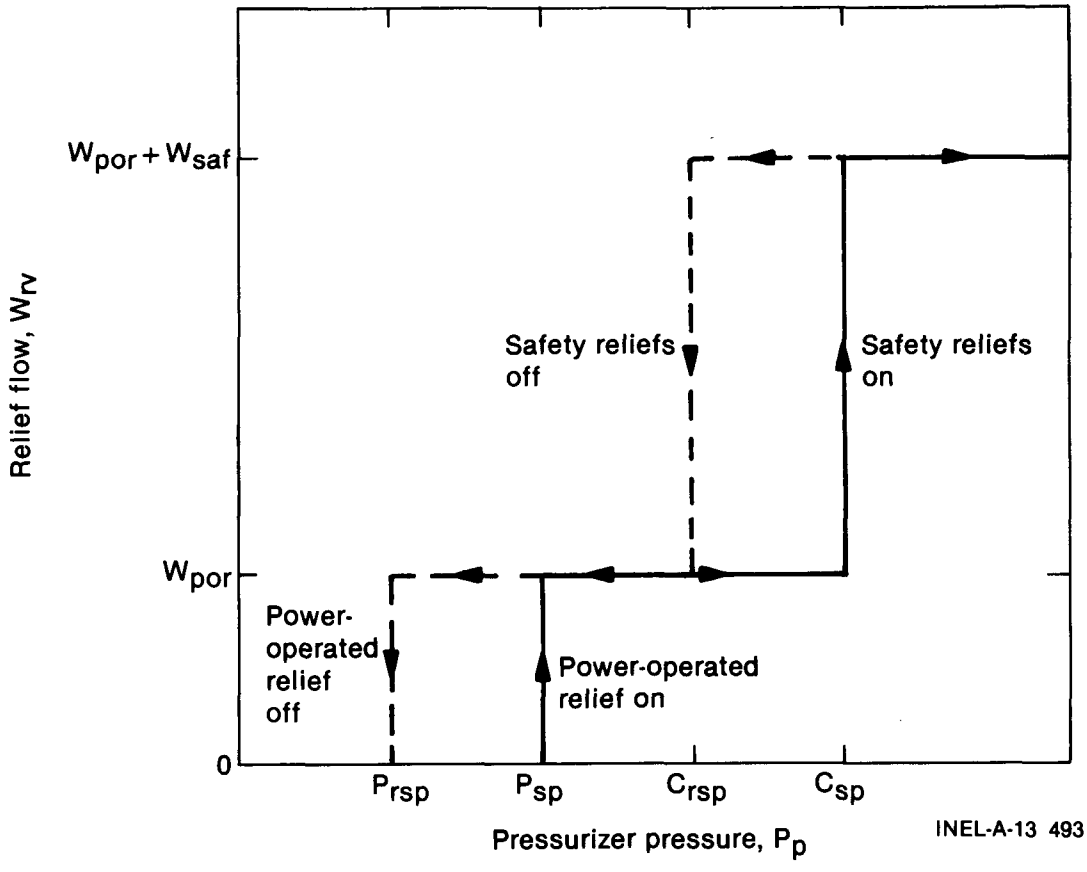

Figure 9. Pressurizer relief valve logic.

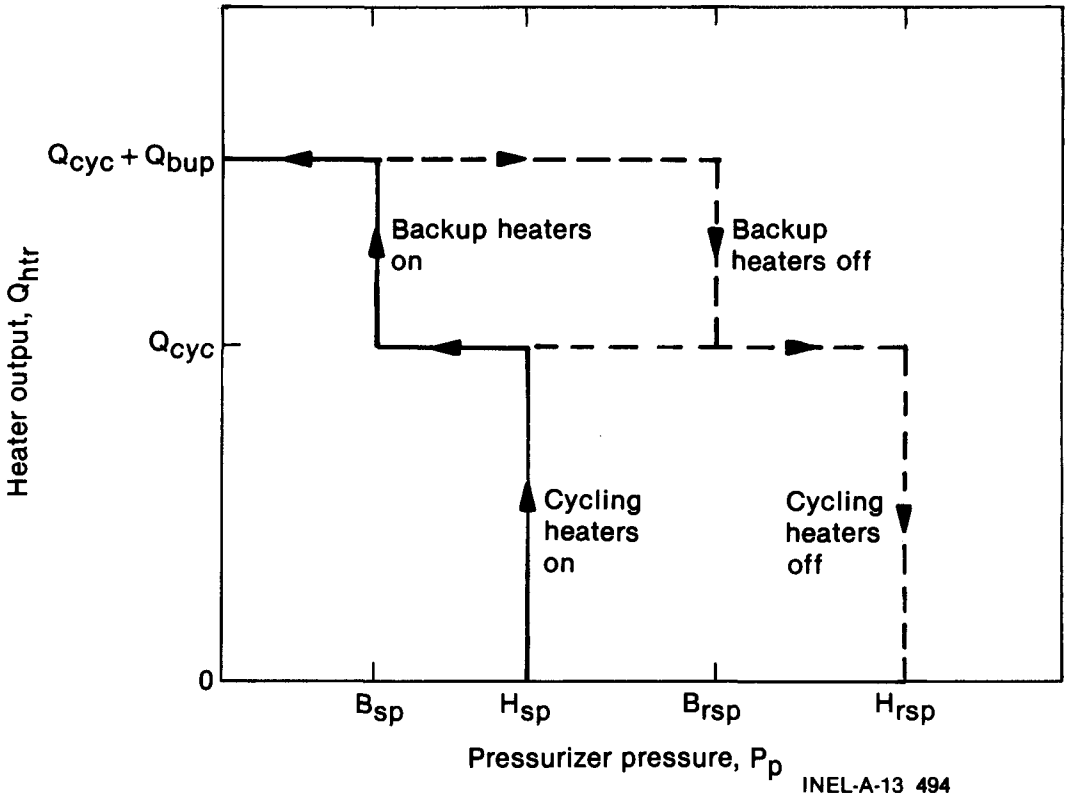

Figure 10. Pressurizer heater logic.

the U-tubes to the water in the shroud drum region. Generated steam then flows through the riser section into the dome region. In the dome are centrifugal steam separators not shown in Figure 11; dry steam (W_{stm}) passes from the dome out of the steam generator to the air-cooled condenser, while separated liquid (W_r) is recirculated to the downcomer region where it combines with the feedwater flow (W_{fw}) to return to the shroud. The first state equation for the steam generator model results from a heat balance on the steam generator tubes:

$$\frac{dT_{tsg}}{dt} = \frac{1}{(Mc_p)_{tsg}} \left(-Q_{sg} - Q_{stm}\right) \tag{72}$$

Note that Q_{sg} is normally a negative quantity.

The remaining state equations result from heat and mass balances on the various fluid regions in the steam generator. For this model, two distinct regions are considered, one being the water in the downcomer region and the other being the water and steam in the dome and shroud, which will be referred to collectively as the secondary fluid. We consider this secondary fluid first. The liquid and steam in the shroud and dome are considered to be in a homogeneous, saturated mixture. A mass and energy balance on this mixture yields

$$\frac{dM_{sgs}}{dt} = W_d - W_r - W_{stm} - W_{sgrv} \tag{73}$$

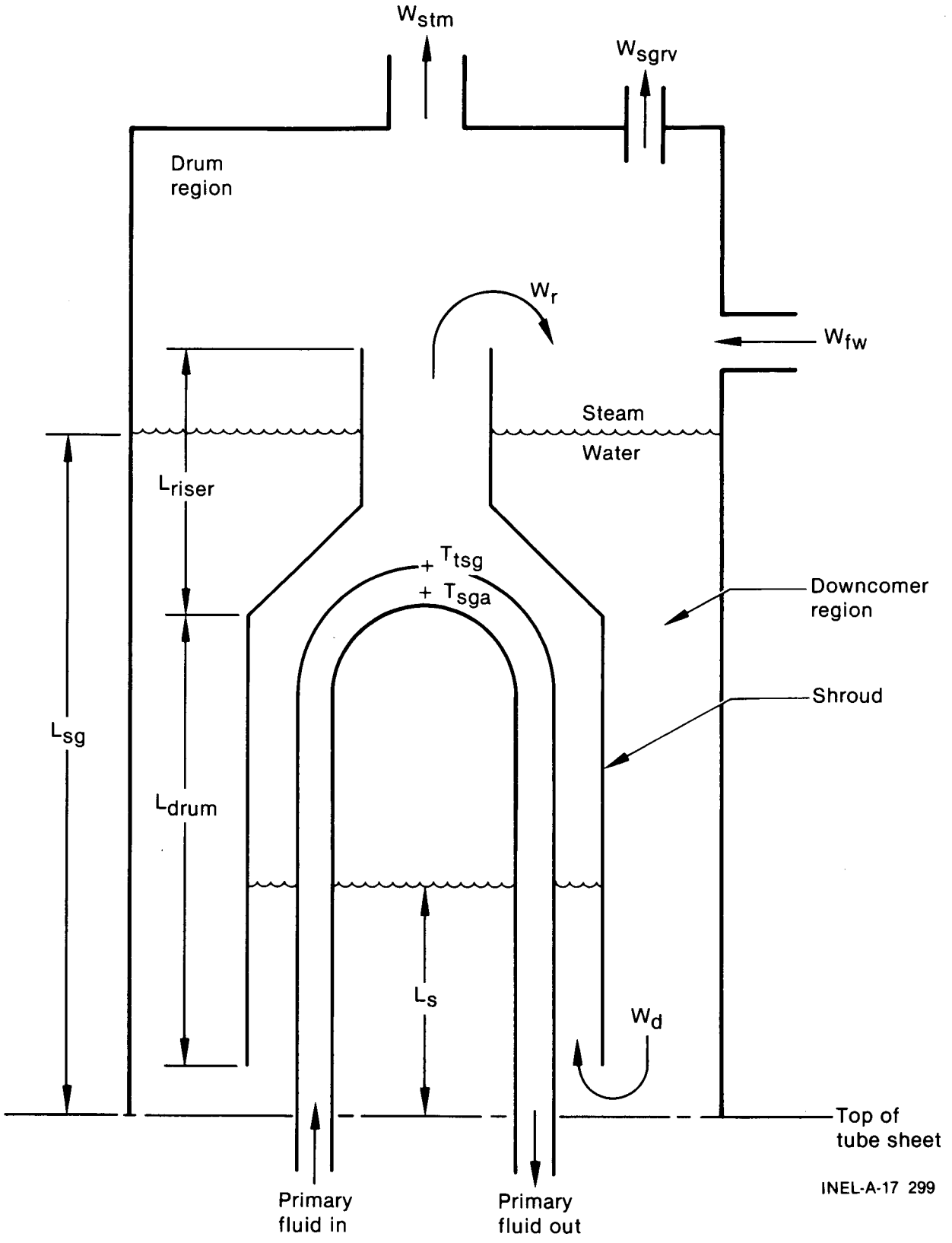

Figure 11. Steam generator model.

and

$$M_{sgs} \frac{dh_{sg}}{dt} = \frac{V_{sgs}}{J} \frac{dP_{sg}}{dt} + Q_{stm} + W_d(h_d-h_{sg}) - W_r(h_f-h_{sg}) - (W_{stm}+W_{sgrv})(h_g-h_{sg}). \quad (74)$$

Using manipulations identical to those explained in the pressurizer model description, Equations (73) and (74) can be cast in a form with P_{sg}, the steam generator pressure, and X_{sg}, the shroud and dome fluid quality, as state variables, or

$$\frac{dP_{sg}}{dt} = - \frac{v_{sg}}{V_{sgs}\Gamma} \left\{ v_{sg} \frac{\partial h_{sg}}{\partial X_{sg}} (W_d-W_r-W_{stm}-W_{sgrv}) + \frac{\partial v_{sg}}{\partial X_{sg}} \left[Q_{stm} + W_d(h_d-h_{sg}) - W_r(h_f-h_{sg}) -(W_{stm}+W_{sgrv})(h_g-h_{sg}) \right] \right\} \quad (75)$$

and

$$\frac{dX_{sg}}{dt} = \frac{v_{sg}}{V_{sgs}\Gamma} \left\{ v_{sg} (W_d-W_r-W_{stm}-W_{sgrv}) \left(\frac{\partial h_{sg}}{\partial P_{sg}} - \frac{v_{sg}}{J} \right) + \frac{\partial v_{sg}}{\partial P_{st}} \left[Q_{stm} + W_d(h_d-h_{sg}) - W_r(h_f-h_{sg}) - (W_{stm}+W_{sgrv})(h_g-h_{sg}) \right] \right\} \quad (76)$$

where

$$\Gamma = \frac{\partial v_{sg}}{\partial P_{sg}} \frac{\partial h_{sg}}{\partial X_{sg}} - \frac{\partial v_{sg}}{\partial X_{sg}} \left(\frac{\partial h_{sg}}{\partial P_{sg}} - \frac{v_{sg}}{J} \right). \quad (77)$$

The mixture properties v_{sg} and h_{sg} are defined by

$$v_{sg} = v_f + X_{sg} (v_g - v_f) \quad (78)$$

and

$$h_{sg} = h_f + X_{sg} (h_g - h_f). \quad (79)$$

For this model, the saturation properties are expressed as polynomial functions of P_{sg}, using Reference 12. Thus, the partial derivatives in Equations (75) through (76) can be exactly evaluated.

The heat from the primary side, Q_{sg}, is defined by

$$Q_{sg} = U_{pri} (T_{tsg} - T_{sga}) \quad (80)$$

where U_{pri} is a combination of the convective properties of the primary loop coolant and the conductance of the steam generator tubes:

$$U_{pri} = \frac{1}{3600 \left\{ \left[\frac{1}{hA}\right]_{pri} + \frac{1}{K_{t1}} \right\}} . \tag{81}$$

The various components of the U_{pri} are computed using

$$h_{pri} = \frac{0.023 k_{sg} (Re)_{pri}^{0.8} (Pr)_{pri}^{0.4}}{D_{eqpri}} \tag{82}$$

$$D_{eqpri} = \frac{d_{itsg}}{12} \tag{83}$$

and

$$K_{t1} = \frac{2\pi L_{tsg} N_{tsg}}{\ln \left[\frac{d_{cltsg}}{d_{itsg}}\right]} k_{tsg}(T_{tsg}). \tag{84}$$

The tube conductivity is obtained using results from Reference 13.

The heat transferred from the tubes to the secondary coolant is described by Q_{stm}:

$$Q_{stm} = U_{sec}(T_{tsg} - T_{stm}) \tag{85}$$

where

$$U_{sec} = \frac{1}{3600 \left\{ \left[\frac{1}{hA}\right]_{sec} + \frac{1}{K_{t2}} \right\}} . \tag{86}$$

The secondary convective coefficient, h_{sec}, is assumed constant in this model, as is A_{sec}. The tube conductance here is given by

$$K_{t2} = \frac{2\pi L_{tsg} N_{tsg}}{\ln \left[\frac{d_{otsg}}{d_{cltsg}}\right]} k_{tsg}(T_{tsg}). \tag{87}$$

The steam temperature T_{stm}, is calculated as a function of P_{sg} only.

The mass and specific heat of the steam generator tubes are calculated using material properties from Reference 13.

The steam flow out of the steam generator, W_{stm}, is described by

$$W_{stm} = C_{vmscv}(X_{mscv}) \left[\overline{P}\Delta P\right]^{\frac{1}{2}} \tag{88}$$

where

$$\overline{P} = \tfrac{1}{2}(P_{sg} + P_{cr}) \tag{89}$$

and

$$\Delta P = P_{sg} - P_{cr} . \tag{90}$$

The loss coefficient, C_{vmscv}, is determined by the stem position of the main steam control valve, X_{mscv}. Under normal conditions, the main steam control valve (MSCV) is manipulated by manual control. In the LOFT model, any motion of the MSCV is defined by the equation

$$\frac{dX_{mscv}}{dt} = \frac{1}{\tau_{mscv}} (X_{mscvd} - X_{mscv}) \tag{91}$$

where X_{mscvd} is the desired steam valve position. Steam valve throttling (i.e., constant speed motion) will automatically occur under two sets of conditions. The first is for overpressurization protection; if the steam generator pressure exceeds a preset value, the valve will begin to open (X_{mscvd} is ramped) until pressure returns to an acceptable range. Similarly, if the steam pressure falls below a certain point, coincident with a plant scram, the valve will close at a constant rate until pressure is back within a predetermined control band. This MSCV throttling logic is shown in Figure 12.

Two relief valves are installed on the LOFT steam generator; their control logic is displayed in Figure 13. The relief flow is normally all steam, hence the assumption of saturation enthalpy for this flow. The calculation of the feedwater properties, W_{fw} and h_{fw}, is covered in the subsection, Feedwater, p.35.

The water level within the downcomer is controlled using the classic three-element controller sketched in Figure 14, yielding another state equation:

$$\frac{dX_{fwv}}{dt} = K_3 \, (X_{fwvd} - K_4 \, X_{fwv}) \tag{92}$$

where the demanded valve stem position is given by

$$X_{fwvd} = K_2 \, (L_o - L_{sg}) + K_1 \, K_2 \, \overline{W}_s . \tag{93}$$

The change in downcomer fluid mass is described by

$$\frac{dM_{dc}}{dt} = W_r + W_{fw} - W_d \tag{94}$$

and the change in the enthalpy of the downcomer water is found using

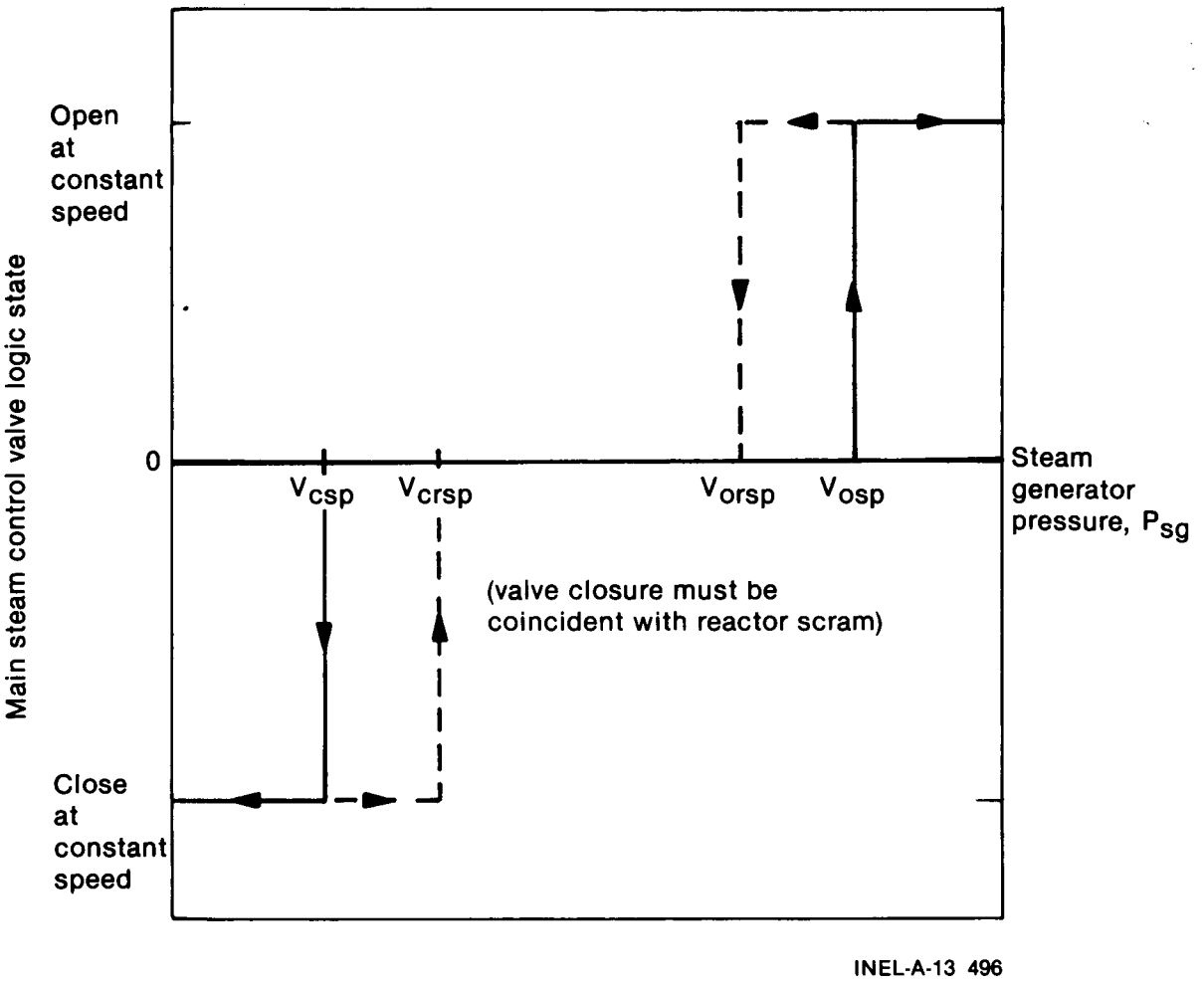

Figure 12. Main steam control valve throttling logic.

$$M_{dc} \frac{dh_{dc}}{dt} = W_r(h_f - h_{dc}) + W_{fw}(h_{fw} - h_{dc}) - W_d(h_d - h_{dc}). \quad (95)$$

Note that the enthalpy associated with the downcomer flow, h_d, depends on the direction of flow:

$$h_d = \begin{cases} h_{dc}, & W_d > 0 \\ h_{sg}, & W_d < 0 \end{cases}. \quad (96)$$

Computation of the internal flows W_r and W_d is a complicated process based primarily on empirical data.[14] The recirculation flow is assumed to be related to the steam flow by

$$W_r = \frac{(1 - X_{riser})}{X_{riser}} W_{stm}. \quad (97)$$

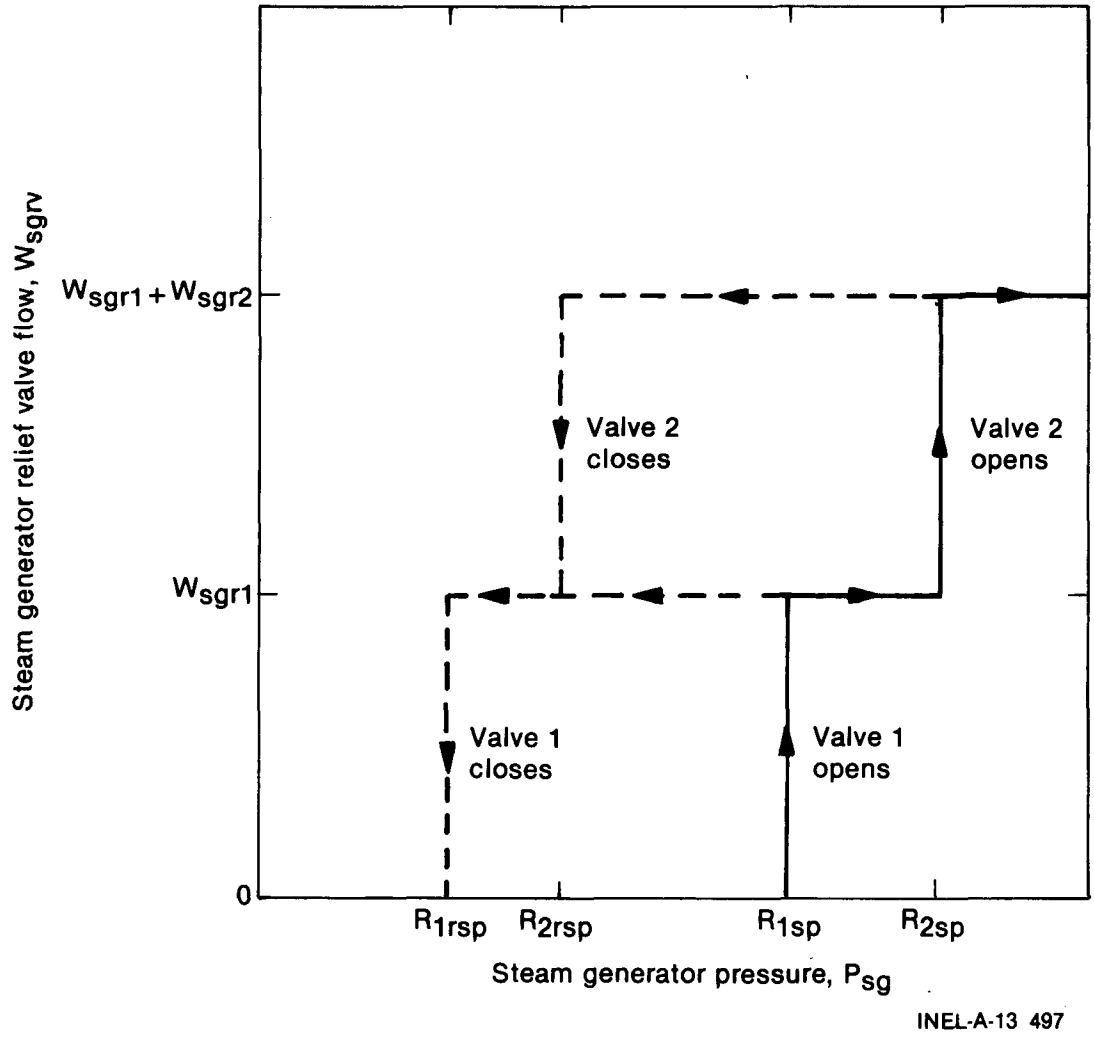

Figure 13. Steam generator relief valve logic.

The riser quality is assumed to be linearly related to the shroud quality:

$$X_{riser} = \alpha X_{shd} \tag{98}$$

where

$$\alpha = 2.8523 + \frac{21974}{Q_{stm}} . \tag{99}$$

Shroud quality is found using the following mass balance equations:

$$V_{dc} = M_{dc} h_f \tag{100}$$

$$V_{sgs} = V_{sg} - V_{dc} \tag{101}$$

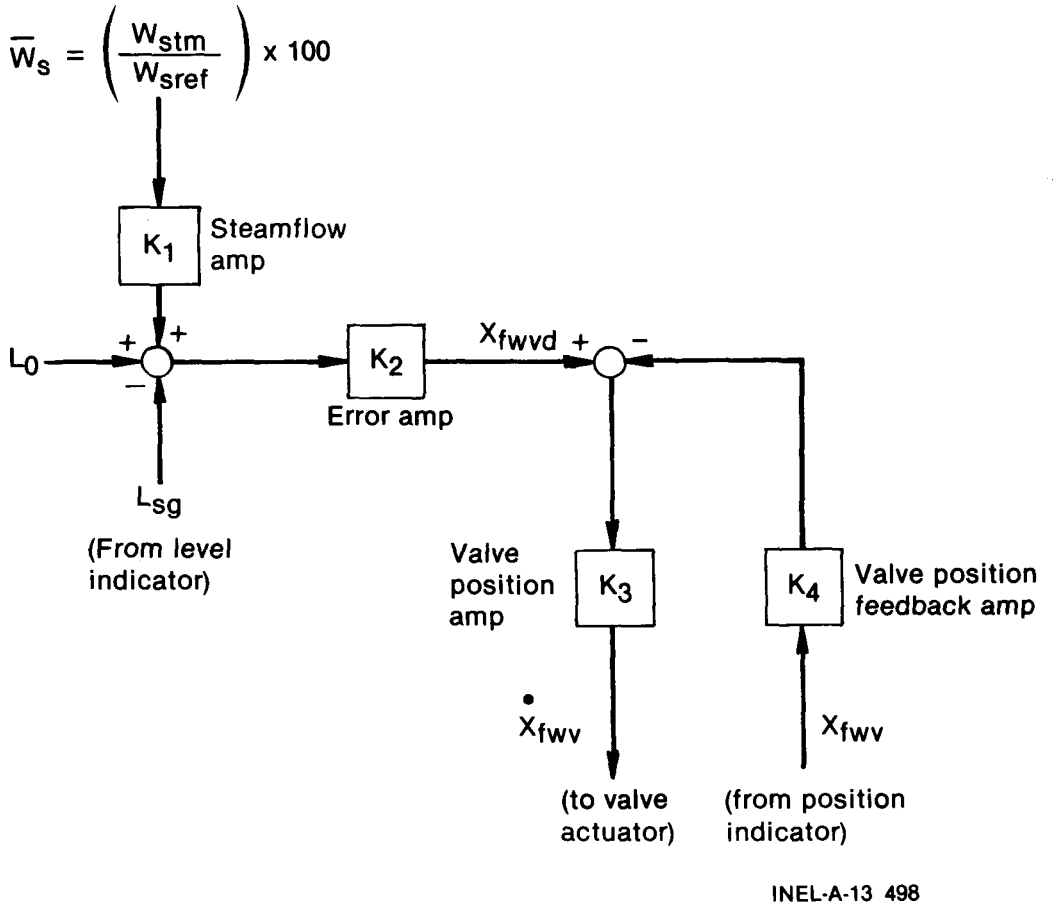

Figure 14. Steam generator water level controller.

$$M_{dome} = (V_{sgs} - V_{shd})/v_g \tag{102}$$

$$M_{shd} = \frac{V_{sgs}}{v_{sg}} - M_{dome} \tag{103}$$

$$v_{shd} = \frac{V_{shd}}{M_{shd}} \tag{104}$$

and

$$X_{shd} = \frac{(v_{shd} - v_f)}{(v_g - v_f)} . \tag{105}$$

The downcomer flow, W_d, depends on the difference in driving heads in the downcomer and shroud. From a momentum balance, we obtain the relation

$$W_d = \left[\frac{(L_{sg}/v_f) - (L_{riser}/v_{riser}) - (L_{drum}/v_{drum}) - 1.3632\ (v_f W_r + v_g W_{stm})^2}{38.0644 v_f^2} \right]^{\frac{1}{2}} \tag{106}$$

where

$$L_{sg} = \begin{cases} 4.8098\ V_{dc}, & V_{dc} < 19.41\ ft^3 \\ 0.9241\ V_{dc} + 75.43, & V_{dc} \geq 19.41\ ft^3 \end{cases} \tag{107}$$

$$v_{riser} = v_f + X_{riser}(v_g - v_f) \tag{108}$$

and

$$v_{drum} = \frac{V_{shd} - V_{riser}}{M_{shd} - (V_{riser}/v_{riser})}. \tag{109}$$

So, Equations (72), (75), (76), (91), (92), (94), and (95) are the seven state equations that constitute the steam generator secondary model.

Air-Cooled Condenser. The steam from the steam generator flows into the tubes of the air-cooled condenser, which is cooled by six variable-pitch fans. The air-cooled condenser model, shown in Figure 15, is a simplified version of the model described in Reference 15. A single state equation based on a heat balance on the finned condenser tubes is used to describe the condensation process:

$$\frac{dT_{tube}}{dt} = \frac{L_t N_t}{3600(Mc_p)_{tube}} (q_{cond} - q_{air}). \tag{110}$$

The fluid within the condenser is assumed to be at uniform saturation pressure P_{cr}, the condensate receiver pressure; i.e., any pressure drop from the condenser to the receiver is neglected.

The heat given off by the condensing fluid is defined by

$$q_{cond} = \frac{(T_{cond} - T_{tube})}{R_{int}}. \tag{111}$$

The internal tube resistance, R_{int}, is based on an empirical correlation developed in Reference 15. The expression used in the model for R_{int} is

$$R_{int} = R_{film} + R_{wall} \tag{112}$$

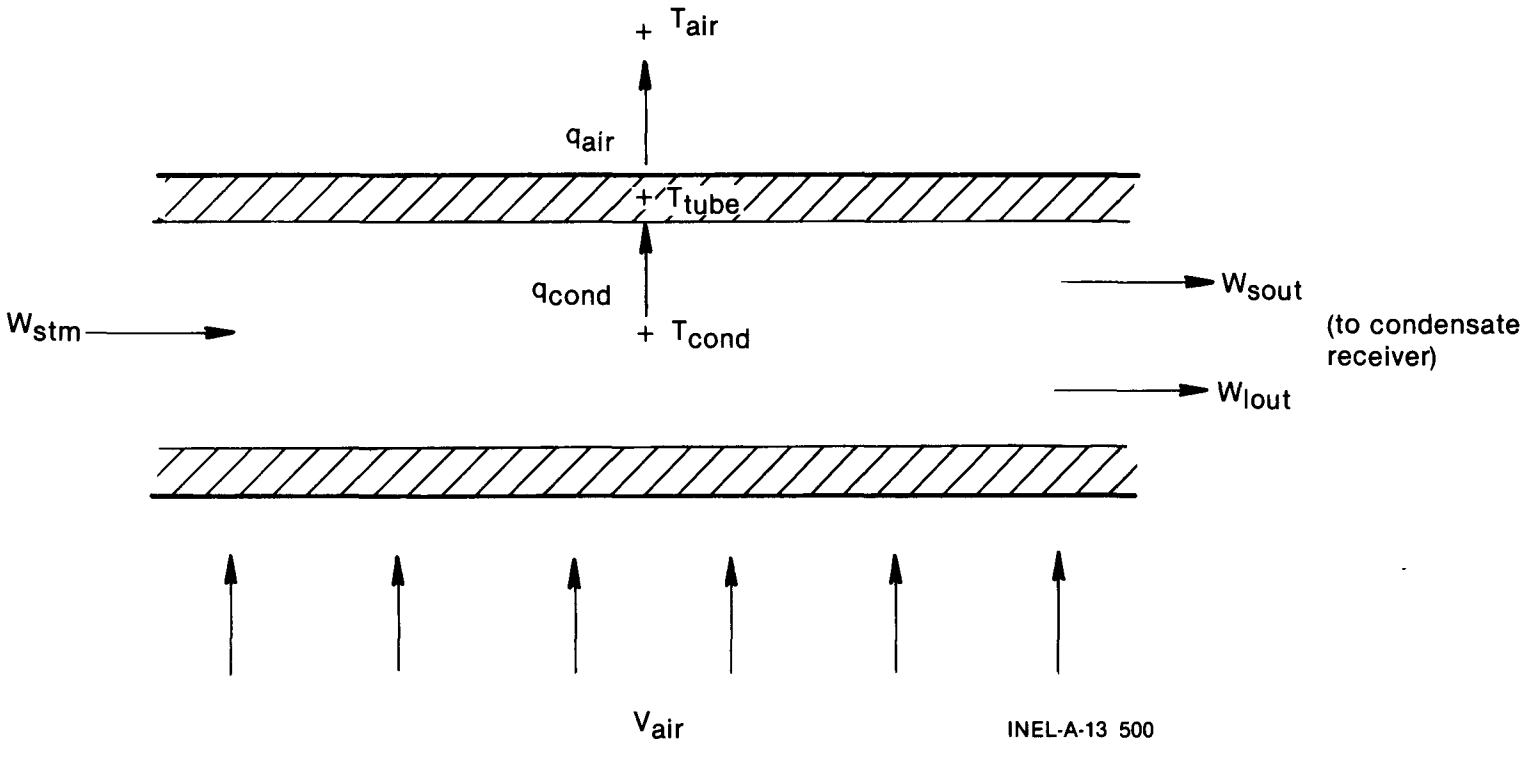

Figure 15. Air-cooled condenser model schematic.

where

$$R_{film} = \frac{1}{\pi d_{in}[5.261\ \Lambda(T_{cond})\ (|W_{stm}W_{lout}v_g|)^{\frac{1}{2}}]} \tag{113}$$

and R_{wall} is a constant tube wall heat resistance. The temperature T_{cond} is the saturation temperature corresponding to P_{cr}, and v_g is the corresponding saturation specific volume of steam.

The heat removed by the six fans is expressed by

$$q_{air} = \frac{(T_{tube} - \bar{T}_{air})}{R_{fin}} \tag{114}$$

where R_{fin} is an empirical heat transfer correlation also presented in Reference 15. R_{fin} is evaluated using the following expressions:

$$R_{fin} = \frac{1}{h_{fin}(\eta_c A_f + A_o)} \tag{115}$$

where

$$h_{fin} = \frac{j_H k_a \left(\frac{c_{pa}\mu_a}{k_a}\right)^{0.3333}}{D_{eq}} \tag{116}$$

$$j_H = \exp\,[0.731(Re)_a - 2.4515] \tag{117}$$

$$Re_a = \frac{D_{eq}\rho_a V_a}{\mu_a A_{fan}} \tag{118}$$

$$\rho_a = \frac{144\ P_{air}}{53.3\ (\bar{T}_{air} + 460)} \tag{119}$$

and

$$\eta_c = 0.99555 - 0.86555F_h + 0.536F_h^2 \tag{120}$$

$$F_h = 0.018275\ h_{fin}\,. \tag{121}$$

In the above expressions, all air properties are found as functions of the average air temperature, $\bar{T}_{air}$, using data from Reference 11. The fan volumetric air flow V_a, which depends on the fan blade pitch angle, is determined from information in Reference 16.

The liquid flow out of the condenser into the condensate receiver is given by

$$W_{lout} = \frac{L_t N_t}{3600}\left(\frac{q_{cond}}{h_{fg}}\right). \tag{122}$$

and hence any steam flow out is

$$W_{sout} = W_{stm} - W_{lout}. \tag{123}$$

Note, to evaluate Equation (122), q_{cond}, which is dependent on W_{lout}, is needed. Thus, in the model, Equations (111) and (122) are solved simultaneously, iterating on W_{lout} until satisfactory convergence is obtained. Finally, the average air temperature surrounding the condenser tubes is found by performing a heat balance on the air, i.e.,

$$q_{air} = \frac{2\rho_a V_a c_{pa}}{L_t N_t}\left(\bar{T}_{air} - T_{amb}\right) \tag{124}$$

Substituting (114) into (124) and solving for $\bar{T}_{air}$ yields

$$\bar{T}_{air} = \frac{\left(T_{tube} + \theta T_{amb}\right)}{1 + \theta} \tag{125}$$

where

$$\theta = \frac{2R_{fin}\rho_a V_a c_{pa}}{L_t N_t}. \tag{126}$$

Solving Equation (125) for $\bar{T}_{air}$ involves an iterative solution since θ is dependent on $\bar{T}_{air}$.

Condensate Receiver. The condensate receiver is simply a large tank used to collect the fluid from the condenser and supply feedwater to the steam generator. The condensate receiver model used here, sketched in Figure 16, is quite similar to the models previously described for the pressurizer and the steam generator secondary fluid. The steam and water are assumed to be a homogeneous, saturated mixture at pressure P_{cr}. By performing a mass and energy balance on this mixture and using as state variables P_{cr} and X_{cr}, the mixture quality, we obtain the two state equations

$$\frac{dX_{cr}}{dt} = \frac{v_{cr}}{V_{cr}\phi}\left\{v_{cr}\left(W_l + W_s - W_{fw} - W_{rcr}\right)\left(\frac{\partial h_{cr}}{\partial P_{cr}} - \frac{v_{cr}}{J}\right) + \frac{\partial v_{cr}}{\partial P_{cr}}\left[W_l(h_f - h_{cr})\right.\right.$$
$$\left.\left. + W_s(h_g - h_{cr}) - W_{fw}(h_f - h_{cr}) - W_{rcr}(h_g - h_{cr})\right]\right\} \tag{127}$$

and

$$\frac{dP_{cr}}{dt} = -\frac{v_{cr}}{V_{cr}\phi}\left\{v_{cr}\frac{\partial h_{cr}}{\partial X_{cr}}\left(W_l + W_s - W_{fw} - W_{rcr}\right) + \frac{\partial v_{cr}}{\partial X_{cr}}\left[W_l(h_f - h_{cr})\right.\right.$$
$$\left.\left. + W_s(h_g - h_{cr}) - W_{fw}(h_f - h_{cr}) - W_{rcr}(h_g - h_{cr})\right]\right\} \tag{128}$$

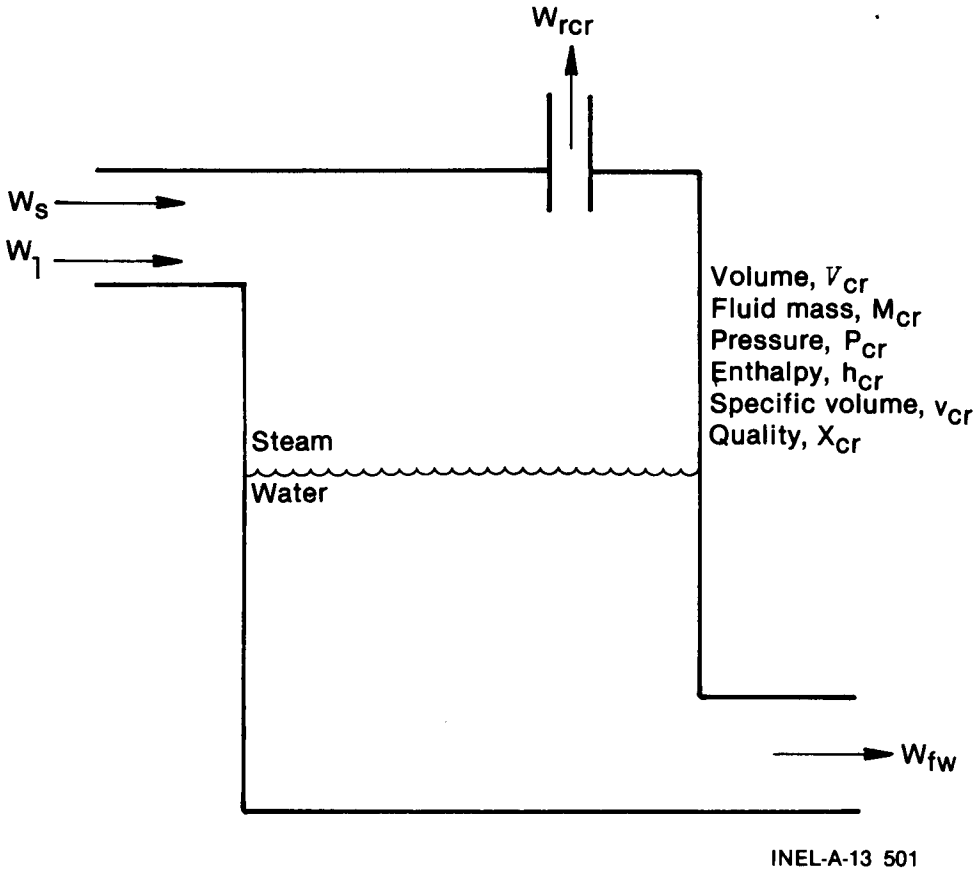

Figure 16. Condensate receiver model.

where

$$\phi = \frac{\partial v_{cr}}{\partial P_{cr}} \frac{\partial h_{cr}}{\partial X_{cr}} - \frac{\partial v_{cr}}{\partial X_{cr}} \left(\frac{\partial h_{cr}}{\partial P_{cr}} - \frac{v_{cr}}{J} \right). \tag{129}$$

The mixture properties in these equations are defined as

$$v_{cr} = v_f + X_{cr} (v_g - v_f) \tag{130}$$

and

$$h_{cr} = h_f + X_{cr} (h_g - h_f) \tag{131}$$

and all saturation properties are functions of the condensate receiver pressure, P_{cr}. Water level in the receiver is given by the empirical relation

$$L_{cr} = 0.1167 \left[\frac{V_{cr} v_f (1-X_{cr})}{v_{cr}} \right] + 50.0. \tag{132}$$

The liquid flow and steam flow into the receiver, W_l and W_s, respectively, are defined in the subsection "Air-Cooled Condenser," p.30, and the feedwater flow, W_{fw}, will be presented in the following subsection, "Feedwater." Note that all flows entering and leaving the condensate receiver are assumed to be at saturation.

The condensate receiver has a single safety relief valve to prevent a system overpressurization. The opening and closing logic for this valve is sketched in Figure 17.

The receiver pressure is automatically controlled by varying the blade pitch of the fans used to cool the air-cooled condenser. The control system used to adjust the blade pitch is shown in Figure 18. This control system adds one state to the LOFT model, namely P_f:

$$\frac{dP_f}{dt} = \frac{1}{\tau_{cr}} \left\{ K_A K_{IP} K_{POS} [K_{PX} X_{mscv} + K_{PA} (P_{cr} - P_{crsp})] - P_f \right\}. \quad (133)$$

Note that P_f is physically limited to a maximum value of 22 degrees.

Equations (127), (128), and (133) constitute the state equations for the condensate receiver.

Feedwater. Prior to entering the steam generator, the temperature of the feed flow from the condensate receiver is decreased in the subcooler. For this model (Figure 19), a constant amount of feedwater subcooling is assumed:

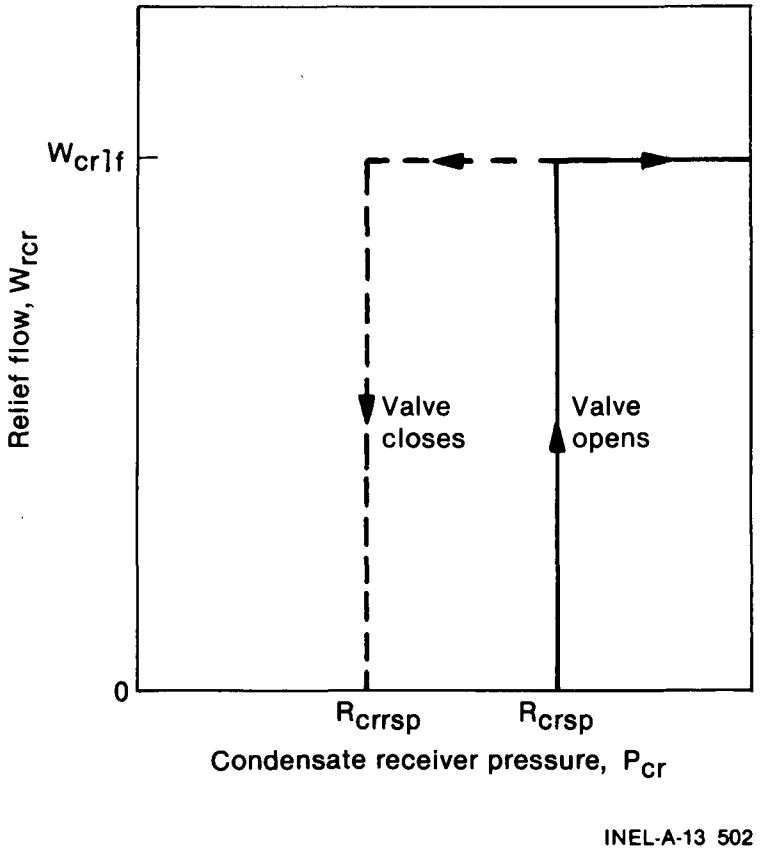

Figure 17. Condensate receiver relief valve logic.

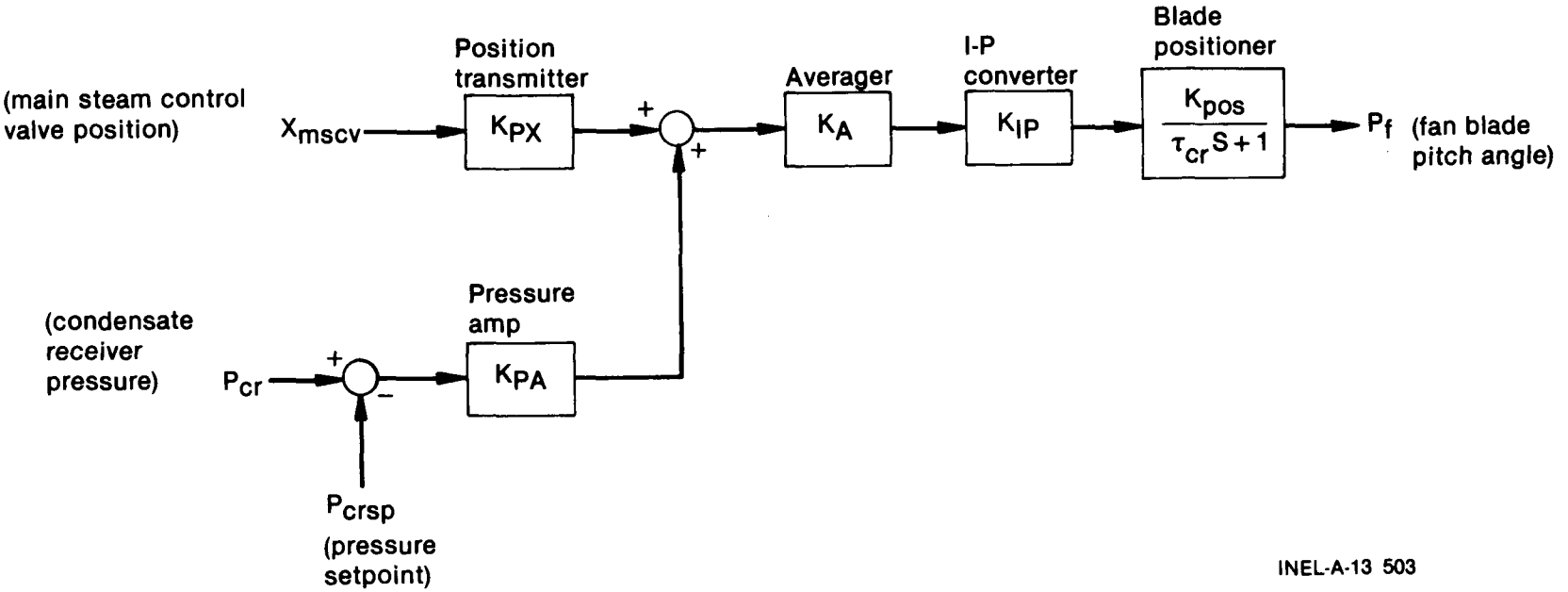

Figure 18. Condensate receiver pressure control system.

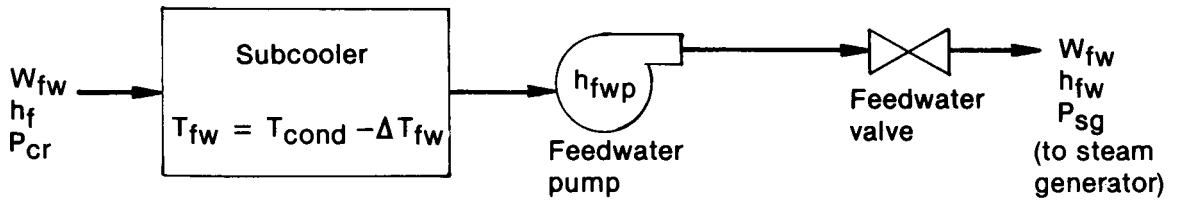

Figure 19. Feedwater system model.

$$T_{fw} = T_{cond} - \Delta T_{fw} \tag{134}$$

where T_{cond} is still the saturation temperature based on P_{cr}. A value of $\Delta T_{fw} = 10°F$ is usually used. The feedwater enthalpy is then calculated based on T_{fw}, using subcooled data from Reference 12.

The feedwater flow rate is dependent on the feedwater valve position:

$$W_{fw} = C_{vfwv}(X_{fwv})[\rho_{fw}\Delta P_{fw}]^{\frac{1}{2}} \tag{135}$$

where the characteristic C_{vfwv} is obtained from the valve specifications. The pressure drop across the feed valve is defined by

$$\Delta P_{fw} = (P_{cr} + h_{fwp}) - P_{sg}. \tag{136}$$

A constant pump head, h_{fwp}, is assumed. The feedwater density is modeled as being temperature-dependent, again using Reference 12.

Sensor Dynamics. Any measurement device has certain dynamics associated with it, e.g., time constants, natural frequencies, and damping ratios. In this model, first-order sensor dynamics are assumed; hence, a measurement is characterized by a single time constant, as shown in Figure 20. Furthermore, the only measurement with a significant time constant (i.e., greater than 0.5 seconds) is the measurement of hot leg temperature. So one final state equation in the LOFT model is

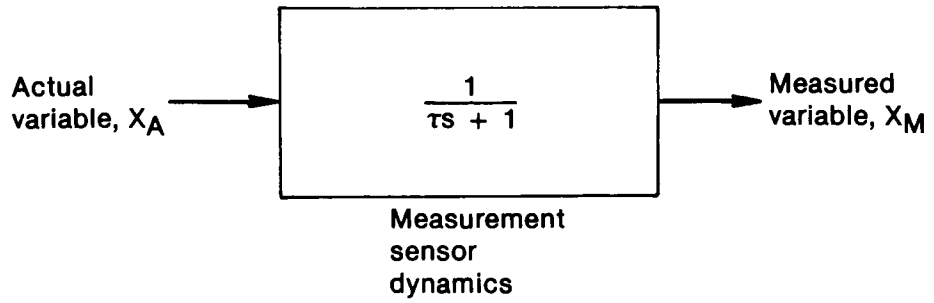

Figure 20. Sensor model.

$$\frac{dT_{hlm}}{dt} = \frac{1}{\tau_{hl}} (T_{hla} - T_{hlm}) \tag{137}$$

where

$$T_{hla} = \frac{1}{2} (T_{hot} + T_{sgi}). \tag{138}$$

Model Linearization and Discretization

As mentioned, to get the plant model in the form required by the Kalman filter, the continuous nonlinear LOFT model must first be linearized about some nominal operating point, then discretized. In functional form, the LOFT model differential equations of the subsection "Nonlinear LOFT Model," p.9, can be written as

$$\dot{x} = f(x,u) \tag{139}$$

$$y = g(x,u) \tag{140}$$

where x is the vector of system state variables, u a vector of system inputs, and y a vector of available outputs. Equations in this form can be linearized by expanding each equation in a Taylor series about some steady-state operating point (x,u) and neglecting terms higher than first-order to yield

$$(\dot{x} - \dot{\bar{x}}) = A(x - \bar{x}) + B(u - \bar{u}) \tag{141}$$

$$(y - \bar{y}) = C(x - \bar{x}) + D(u - \bar{u}) \tag{142}$$

where

$$\dot{\bar{x}} = f(\bar{x},\bar{u}) \tag{143}$$

$$\bar{y} = g(\bar{x},\bar{u}) \tag{144}$$

and the system matrices A, B, C, and D are defined by

$$A = \frac{\partial f}{\partial x}\bigg|_{\substack{x=\bar{x} \\ u=\bar{u}}} \tag{145}$$

$$B = \frac{\partial f}{\partial u}\bigg|_{\substack{x=\bar{x} \\ u=\bar{u}}} \tag{146}$$

$$C = \frac{\partial g}{\partial x}\bigg|_{\substack{x=\bar{x} \\ u=\bar{u}}} \tag{147}$$

and

$$D = \left.\frac{\partial g}{\partial u}\right|_{\substack{x=\bar{x} \\ u=\bar{u}}} . \tag{148}$$

The difficult part in obtaining linear equations in the form of (141) and (142) is in determining the matrices A, B, C, and D. One obvious method would be to analytically find the required partial derivatives of each nonlinear state equation and evaluate the matrices directly. For the highly nonlinear LOFT model developed, this would be quite a laborious task. The approach taken here was to simply approximate each derivative by a first-order gradient. For example, the derivative of the ith state equation with respect to the jth state variable is expressed as

$$A_{ij} = \left.\frac{\partial f_i}{\partial x_j}\right|_{\substack{x=\bar{x} \\ u=\bar{u}}} \simeq \frac{\left\{f_i \,\middle|\, \substack{x=\bar{x};\ x_j=\bar{x}_j+\Delta x_j \\ u=\bar{u}}\right\} - \left\{f_i \,\middle|\, \substack{x=\bar{x};\ x_j=\bar{x}_j-\Delta x_j \\ u=\bar{u}}\right\}}{2\Delta x_j} . \tag{149}$$

So, to numerically evaluate this term, we perturb state x_j by an amount Δx_j and evaluate f_i, then perturb x_j by $-\Delta x_j$ and evaluate f_i, subtract the two values, and divide by twice the perturbation. Similarly, other matrix elements are approximated by

$$B_{ik} = \left.\frac{\partial f_i}{\partial u_j}\right|_{\substack{x=\bar{x} \\ u=\bar{u}}} \simeq \frac{\left\{f_i \,\middle|\, \substack{x=\bar{x} \\ u=\bar{u};\ u_k=\bar{u}_k+\Delta u_k}\right\} - \left\{f_i \,\middle|\, \substack{x=\bar{x} \\ u=\bar{u};\ u_k=\bar{u}_k-\Delta u_k}\right\}}{2\Delta u_k} \tag{150}$$

$$C_{ij} = \left.\frac{\partial g_i}{\partial x_j}\right|_{\substack{x=\bar{x} \\ u=\bar{u}}} \simeq \frac{\left\{g_i \,\middle|\, \substack{x=\bar{x};\ x_j=\bar{x}_j+\Delta x_j \\ u=\bar{u}}\right\} - \left\{g_i \,\middle|\, \substack{x=\bar{x};\ x_j=\bar{x}_j-\Delta x_j \\ u=\bar{u}}\right\}}{2\Delta x_j} \tag{151}$$

and

$$D_{ik} = \left.\frac{\partial g_i}{\partial u_i}\right|_{\substack{x=\bar{x} \\ u=\bar{u}}} \simeq \frac{\left\{g_i \,\middle|\, \substack{x=\bar{x} \\ u=\bar{u};\ u_k=\bar{u}_k+\Delta u_k}\right\} - \left\{g_i \,\middle|\, \substack{x=\bar{x} \\ u=\bar{u};\ u_k=\bar{u}_k+\Delta u_k}\right\}}{2\Delta u_k} . \tag{152}$$

So, by sequentially perturbing each state and then each input, we can obtain the elements of A, B, C, and D, using Equations (145) through (152) in a simple straightforward manner and hence develop a linear system model in the form of Equations (141) and (142).

Once the continuous linear model has been derived, the discrete form of the model is found using standard discretization techniques,[17] to be

$$x[(k+1)T] - \bar{x} = \Phi(T)[x(kT) - \bar{x}] + \Theta(T)[u(kT) - \bar{u}] \tag{153}$$

and

$$y(kT) - \bar{y} = C\,[x(kT) - \bar{x}] + D[u(kT) - \bar{u}] \tag{154}$$

where $\Phi(T)$ is the system state transition matrix and $\Theta(T)$ the discrete system input matrix, both dependent on the sample time step T.

$$\Phi(T) = e^{AT} = I + AT + \frac{A^2T^2}{2!} + \ldots \tag{155}$$

$$\Theta(T) = \left(\int_0^T \Phi(T-\tau)d\tau\right)B\,. \tag{156}$$

Equations (153) and (154) are the form required by the Kalman filter. Note that the matrices Φ, Θ, C, and D are shift-invariant for a fixed operating point (x,u) and fixed time step T.

Obviously, the values of Φ, Θ, C, and D are dependent on the choice of operating point and time step, and no attempt is made here to present numerical values for these matrices. In the advanced PPS, computer routines from Reference 4 perform the discretization, using a sample time step of one second. The state vector x used for the linear LOFT model is given in Table 1. Six inputs (Table 2) and 17 outputs (Table 3) were selected to describe the linear plant dynamics. Note that with 23 states, 6 inputs, and 17 measurements, the linear system vectors and matrices are of the following dimensions: x (23 x 1), u (6 x 1), y (17 x 1), Φ (23 x 23), Θ (23 x 6), C (17 x 23), and D (17 x 6).

The values of P (23 x 23), Q (23 x 23), and R (17 x 17), the different covariance matrices required by the Kalman filter, were determined based on studies of the noise characteristics of the LOFT process variables and instrumentation.

Table 1. Linear LOFT model state vector

Element Number, i	State Variable Description, x_i
1	First precursor group concentration (MW-sec)
2	Second precursor group concentration (MW-sec)
3	Average fuel temperature (°F)
4	Average clad temperature (°F)
5	Average core coolant temperature (°F)
6	Average bypass coolant temperature (°F)
7	Steam generator primary inlet temperature (°F)
8	Steam generator primary average temperature (°F)
9	Reactor vessel inlet temperature (°F)
10	Pressurizer quality

Table 1. (continued)

Element Number, i	State Variable Description, x_i
11	Pressurizer pressure (psia)
12	Steam generator tube temperature (°F)
13	Steam generator secondary pressure (psia)
14	Steam generator secondary quality
15	Condenser tube bank temperature (°F)
16	Fan blade pitch angle (degrees)
17	Condensate receiver quality
18	Condensate receiver pressure (psia)
19	Feedwater valve position
20	Main steam control valve position
21	Steam generator downcomer fluid mass (lbm)
22	Steam generator downcomer fluid enthalpy (Btu/lbm)
23	Measured hot leg temperature (°F)

Table 2. Linear LOFT model input vector

Element Number, j	Input Description, u_j
1	Control rod reactivity ($)
2	Volumetric primary loop flow (ft^3/sec)
3	Demanded main steam valve position
4	Demanded feedwater valve position
5	Demanded condenser fan blade pitch (°)
6	Average core coolant boron concentration (ppm)

Table 3. Linear LOFT model output vector

Element Number, k	Output Description, y_k
1	Reactor power (MW)
2	Control rod reactivity ($)
3	Primary loop flow (lbm/hr)
4	Primary loop pressure (psia)
5	Hot leg temperature (°F)
6	Pressurizer pressure (psia)
7	Pressurizer level (inches)
8	Steam generator pressure (psia)
9	Condensate receiver pressure (psia)
10	Fan blade pitch angle (degrees)
11	Secondary steam flow (lbm/sec)
12	Main steam valve position
13	Feedwater flow (lbm/sec)
14	Feedwater valve position
15	Steam generator water level (inches)
16	Condensate receiver water level (inches)
17	Average core coolant boron concentration (ppm)

THE DNBR AND LHGR CALCULATION

Examining the LOFT model state vector in Table 1, it is noted that using the Kalman filter we now have the capability to make optimal estimates of many variables directly related to the integrity of the plant. Of particular interest are the fuel and cladding temperatures that provide a clear indication of the status of the core fuel rods. Two parameters that are used in commercial PWR operation as indicators of fuel rod status are the minimum DNBR (departure from nucleate boiling ratio) and the maximum LHGR (linear heat generation rate). In this section, methods for computing DNBR and LHGR for the LOFT plant are developed, using the optimal state vector estimate. It is felt that using these optimal estimates of DNBR and LHGR, in conjunction with fuel and clad temperature estimates, will result in more useful information regarding fuel integrity than is presently available.

The minimum DNBR is defined as the critical heat flux computed as a function of distance along the hottest fuel channel divided by the actual surface heat flux at the same position along this channel[18]:

$$DNBR = \frac{q_{dnb}}{q_{hot}} . \tag{157}$$

In this model, the maximum heat flux at the hot channel is computed using the expression for total heat flow through the clad, Q_{cp}, given by Equation (33), the clad surface area, and an appropriate peaking factor:

$$q_{hot} = \gamma_{peak} \frac{3600 Q_{cp}}{A_{clad}} \tag{158}$$

where recall

$$Q_{cp} = U_{cp}(T_c - T_{ave}) . \tag{33}$$

To compute Q_{cp} and A_{clad}, we use the estimated states from the Kalman filter; hence we can rewrite (158) and (33) as

$$\hat{q}_{hot} = \gamma_{peak} \frac{3600\ \hat{Q}_{cp}}{\hat{A}_{clad}} \tag{159}$$

$$\hat{Q}_{cp} = \hat{U}_{cp}\ (\hat{T}_c - \hat{T}_{ave}) \tag{160}$$

where the carets denote optimally estimated values. A peaking factor of $\gamma_{peak} = 2.939$ was developed using sensitivity study results from an elaborate core thermal-hydraulics code.[19]

The critical heat flux is computed using a data correlation described in detail in Reference 20. This correlation is

$$q_{dnb} = 0.11585\ G + 800\ P_{loop} - 0.27442\ P_{loop}^2 - 1.4383\ G\ X_{local} + 0.000256\ G\ P_{loop}\ X_{local} \tag{161}$$

where

G = core mass flux (lbm/hr-ft^2)

P_{loop} = primary loop pressure (psia)

X_{local} = local equilibrium fluid quality.

Again, using the optimal state vector estimates, we can evaluate Equation (161). The mass flux estimate, G, is

$$\hat{G} = \frac{\hat{W}_{loop}\ (1 - F_{bp})}{A_{core}} \tag{162}$$

and P_{loop} is found using Equation (70). The local equilibrium quality X_{local} depends on the total heat transfer to the core coolant at the hot channel and is computed using

$$\hat{X}_{local} = \frac{\hat{h}_{local} - \hat{h}_f}{\hat{h}_g - \hat{h}_f} \tag{163}$$

where

$$\hat{h}_{local} = \gamma_{local}\ \frac{(\hat{Q}_{cp} + \hat{P}_T f_{dhc} \Omega)\ 3600}{\hat{W}_{loop}\ (1-F_{bp})} \tag{164}$$

and h_f and h_g are saturation enthalpies based on P_{loop}. The local peaking factor used is $\gamma_{local} = 1.112$. Thus, using Equation (162), (163), and P_{loop} in (161) will yield q_{dnb}, which when used with (157) will give us an optimal estimate of DNBR.

The maximum value of LHGR (units of kW/ft) is then found using the estimate of hot channel heat flux q_{hot}:

$$\text{maximum LHGR} = \frac{1000\ \hat{q}_{hot} \hat{A}_{clad}}{3600\ N_{rod} L_{rod} \Omega}\ . \tag{165}$$

These estimates of DNBR and LHGR, along with the estimated values of fuel and cladding temperatures, will be the primary outputs of the advanced LOFT plant protection system.

SIMULATION RESULTS

To study the performance of the advanced PPS, the Kalman filter estimator algorithms with the linear LOFT model were implemented on a CYBER-176 computer system. Simulated plant transient data were obtained using the nonlinear LOFT model described in the section "LOFT PLANT MODEL." The results of three such transient studies are presented here. In these transients, no scrams based on estimates from the advanced plant protection system were implemented. The development of appropriate scram logics would be valuable to the future of the advanced PPS project.

The first transient considered was a simulated rod withdrawal accident where reactivity was increased at a rate of $0.005/second for 10 seconds. The response of the estimator during this transient is compared to the simulated measurements in Figures 21 through 28. An uncontrolled rod withdrawal when the reactor is operating could be caused by an equipment failure in the rod control system. This type of accident would cause an increase in reactor power, pressure, and temperature that normally would be detected and terminated by the operator. If, however, the operator fails to take action, the PPS should initiate a reactor scram before excess fuel temperatures or DNB is attained. In this simulation, and the others described here, it was assumed that the LOFT plant was initially at full power conditions [50 MW(t)].

Figures 21 and 22 show the power increase resulting from the withdrawn rod and the accompanying increase in primary coolant temperature. The estimator is seen to follow the plant measurements quite well. Figures 23 through 28 show the response of the rest of the plant to the transient. The increased primary fluid temperature results in an insurge into the pressurizer, yielding an increase in pressure and water level. The higher primary temperatures cause higher secondary temperatures, increasing the secondary pressure and flows slightly. Figures 29 through 32 display the corresponding estimates of fuel and

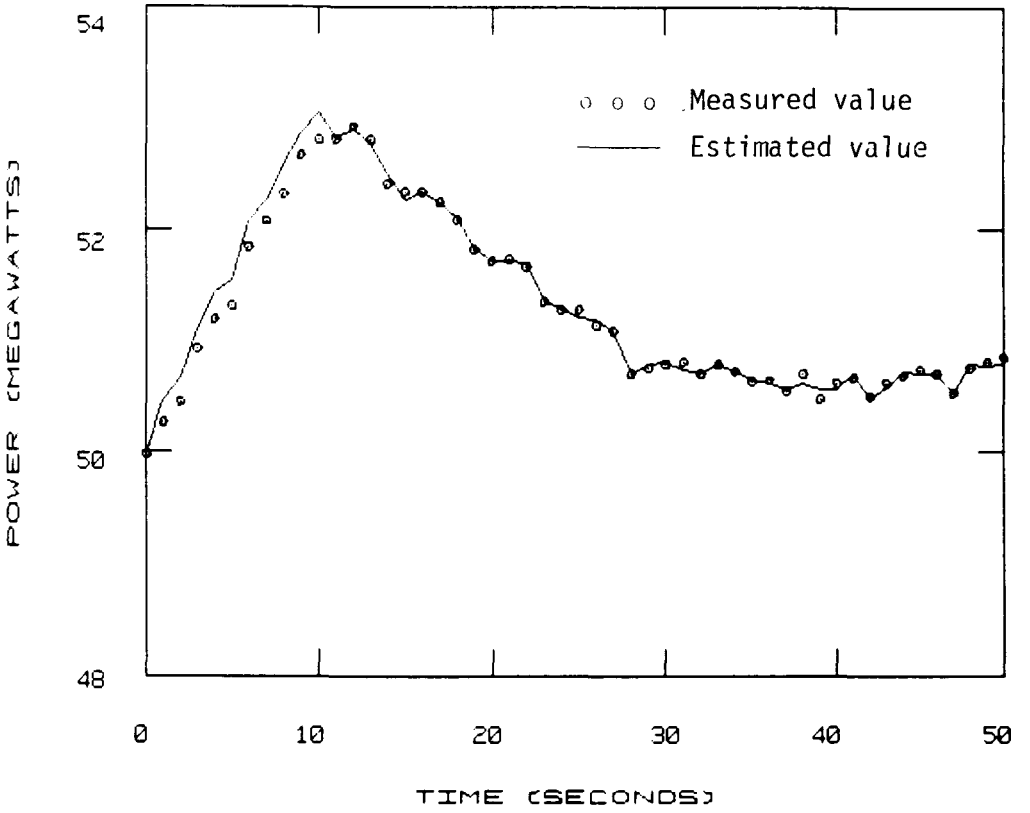

Figure 21. Rod withdrawal accident, core power response.

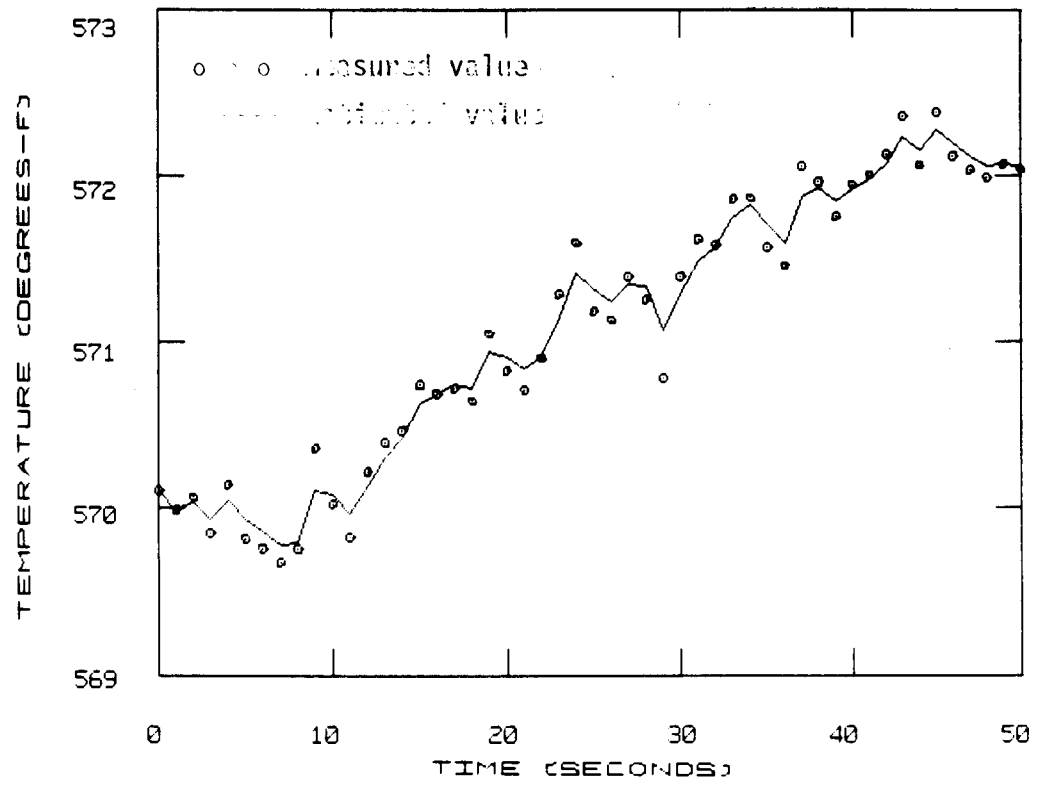

Figure 22. Rod withdrawal accident, hot leg temperature response.

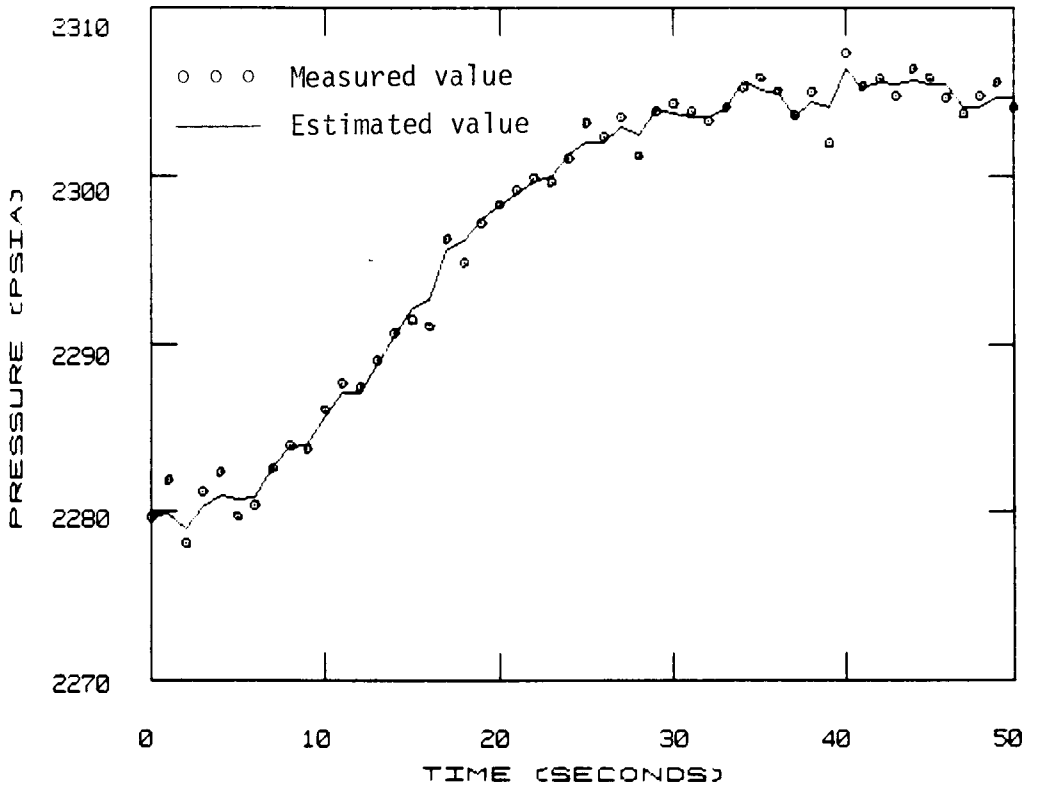

Figure 23. Rod withdrawal accident, pressurizer pressure response.

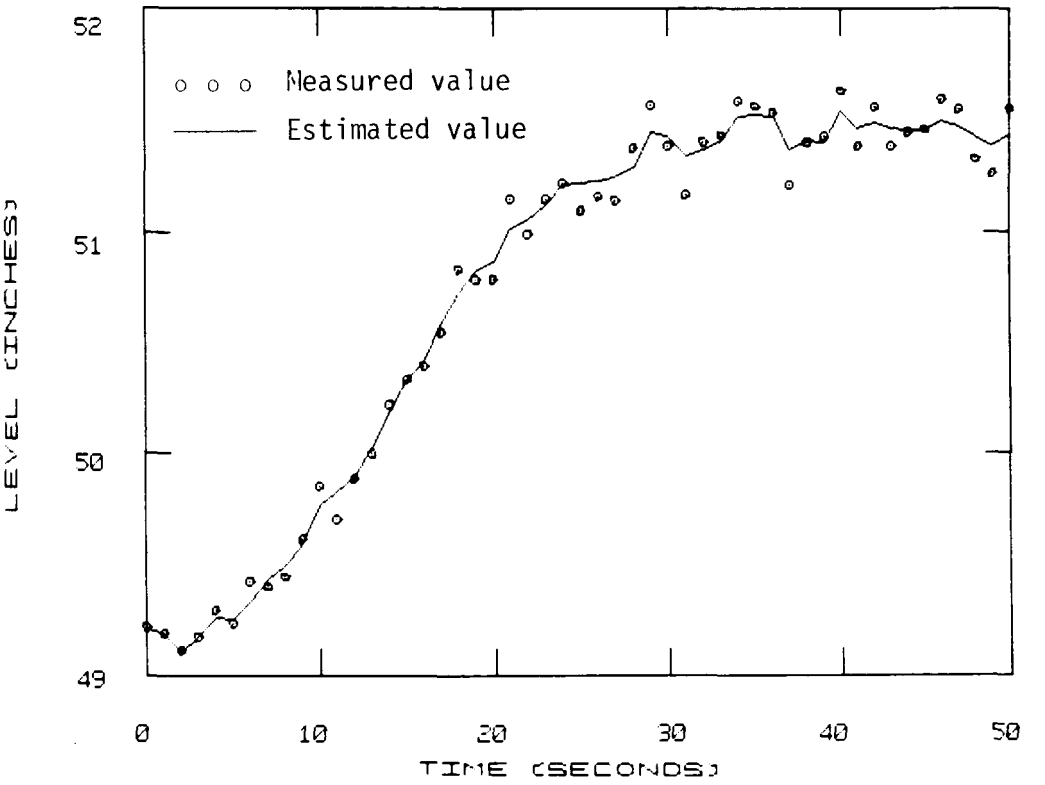

Figure 24. Rod withdrawal accident, pressurizer level response.

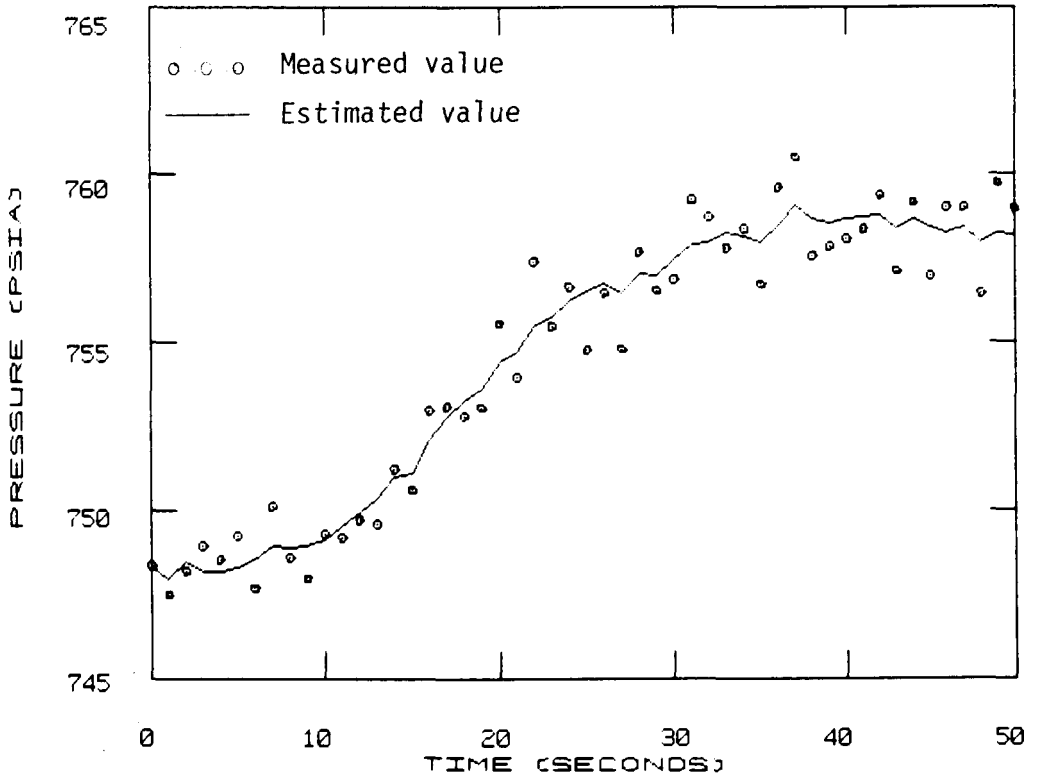

Figure 25. Rod withdrawal accident, secondary pressure response.

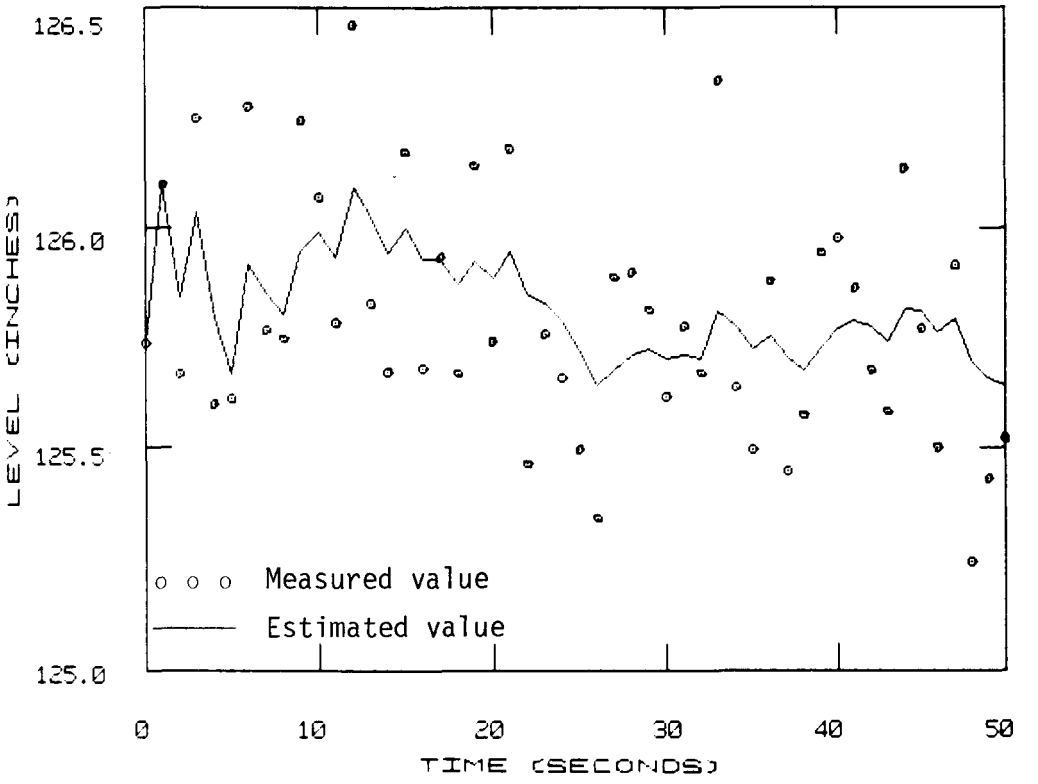

Figure 26. Rod withdrawal accident, steam generator level response.

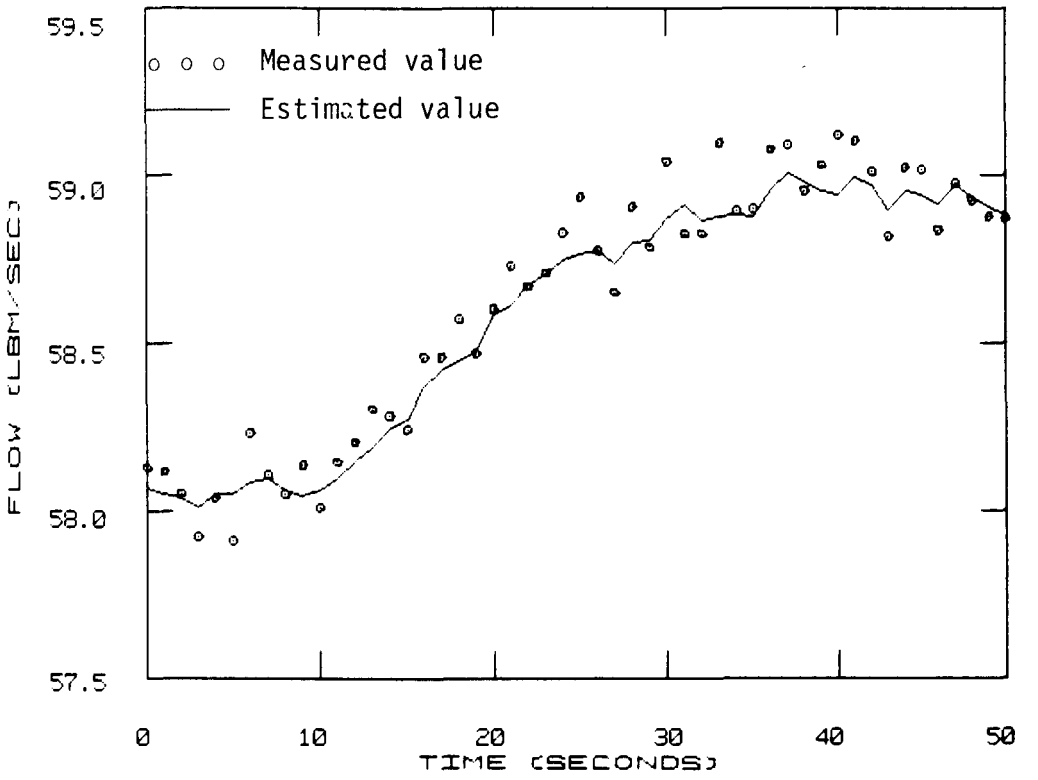

Figure 27. Rod withdrawal accident, steam flow response.

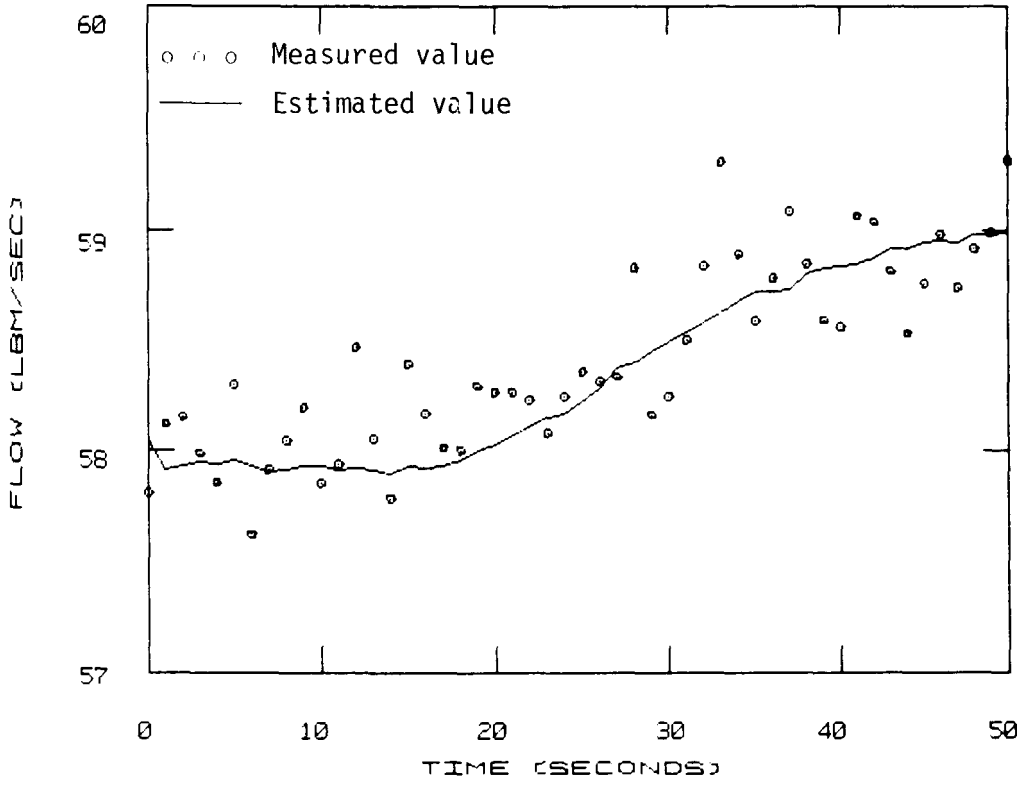

Figure 28. Rod withdrawal accident, feed flow response.

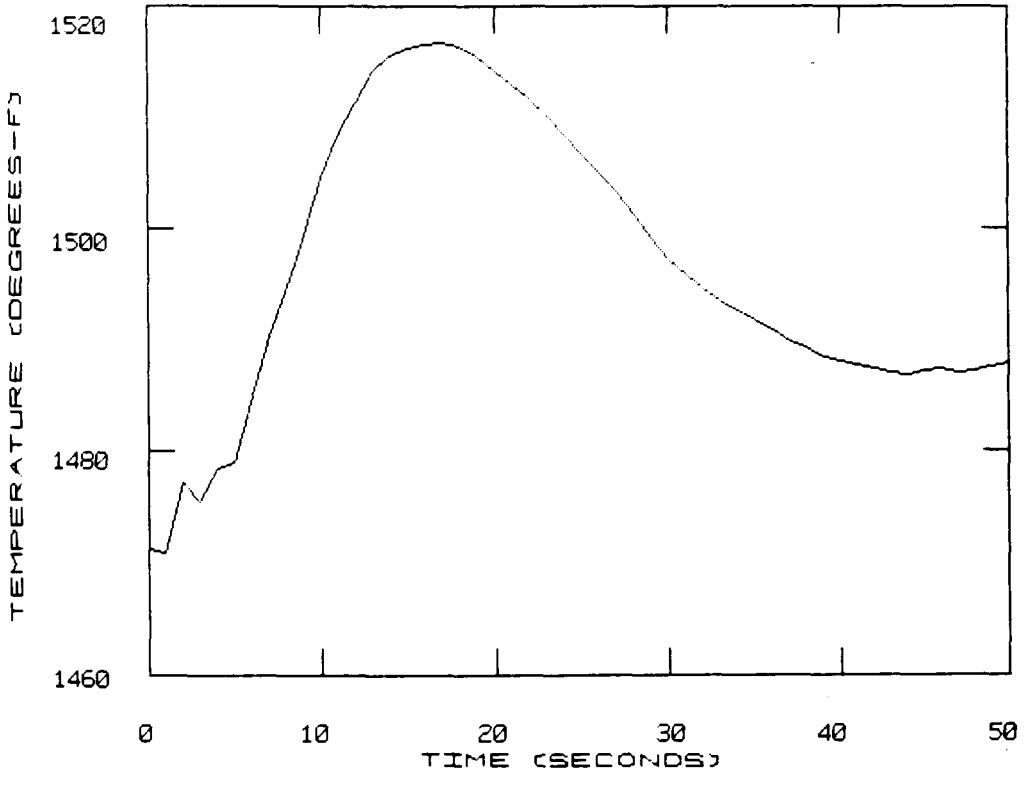

Figure 29. Rod withdrawal accident, fuel temperature estimate.

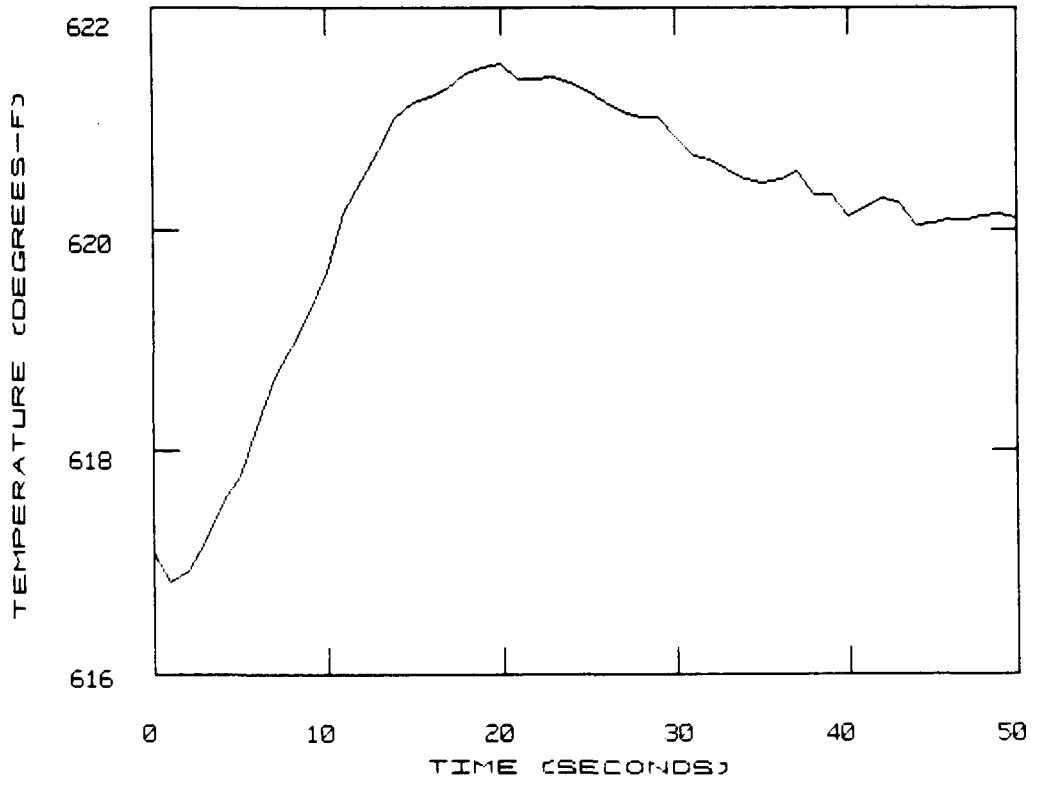

Figure 30. Rod withdrawal accident, clad temperature estimate.

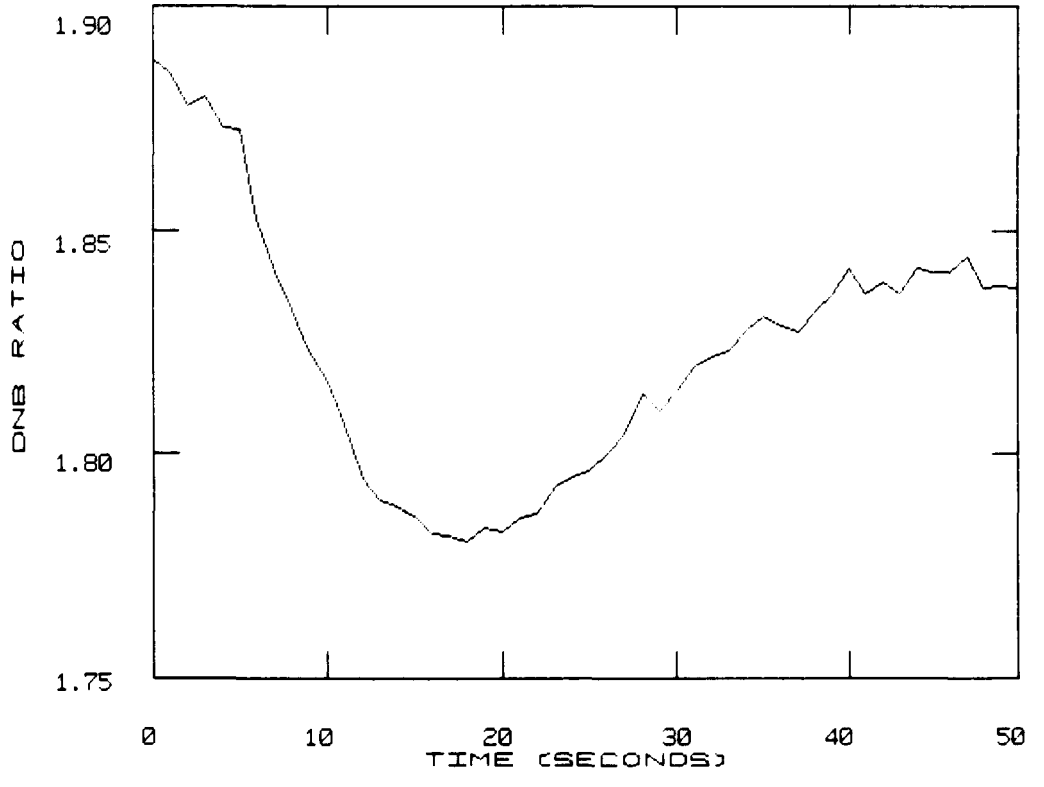

Figure 31. Rod withdrawal accident, minimum DNBR estimate.

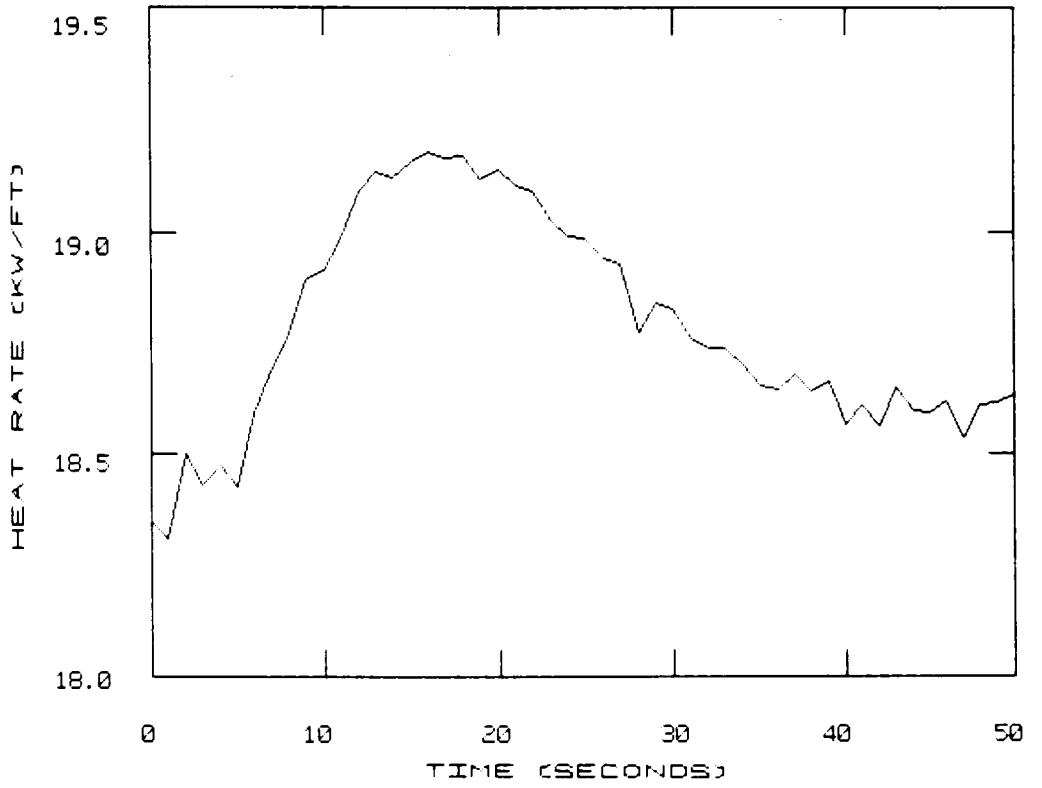

Figure 32. Rod withdrawal accident, maximum LHGR estimate.

cladding temperatures, DNBR, and LHGR. Obviously, the fuel and clad temperatures increase due to the increased power production. This increased power increases the heat flux through the clad and hence LHGR rises, resulting in a corresponding decrease in DNBR.

Under the existing LOFT plant protection systm design, a scram would have occurred when reactor power exceeded 52.5 MW. Perhaps with the advanced plant protection system, a scram could be avoided if the estimates of fuel and clad temperatures, DNBR, and LHGR remain within accepted limits. Again, what these limits should be was never decided. The important point to make is that scram decisions in the advanced PPS would be made on optimal estimates directly related to reactor integrity, whereas the existing protection system relies on noisy measurements of auxiliary variables.

The response of the advanced PPS to two other transients is presented here with a minimum of discussion. Figures 33 through 40 show the response to a simulated 40 percent reduction in the LOFT plant primary loop flow in 10 seconds. Such a reduction would occur if one of the two primary coolant pumps was lost due to some failure. The estimator is seen to track the plant response excellently. The corresponding estimates of fuel and clad temperatures, DNBR, and LHGR are displayed in Figures 41 through 44.

The final transient presented is a ten percent increase in the stem position of the main steam control valve (MSCV) in the secondary side of the LOFT plant. An inadvertent opening of the MSCV causes a power mismatch between the reactor core power and the steam generator load demand. Unless terminated by manual or automatic action, system overpower will result, which could lead to DNB in the core. Figures 45 through 56 show that this valve opening has a fairly severe effect on the plant, increasing reactor power to 58 MW and increasing fuel temperature by over 150°F. Still, the linear estimator follows the plant response excellently throughout the transient, though the plant has moved away from the operating point upon which the estimator model is based.

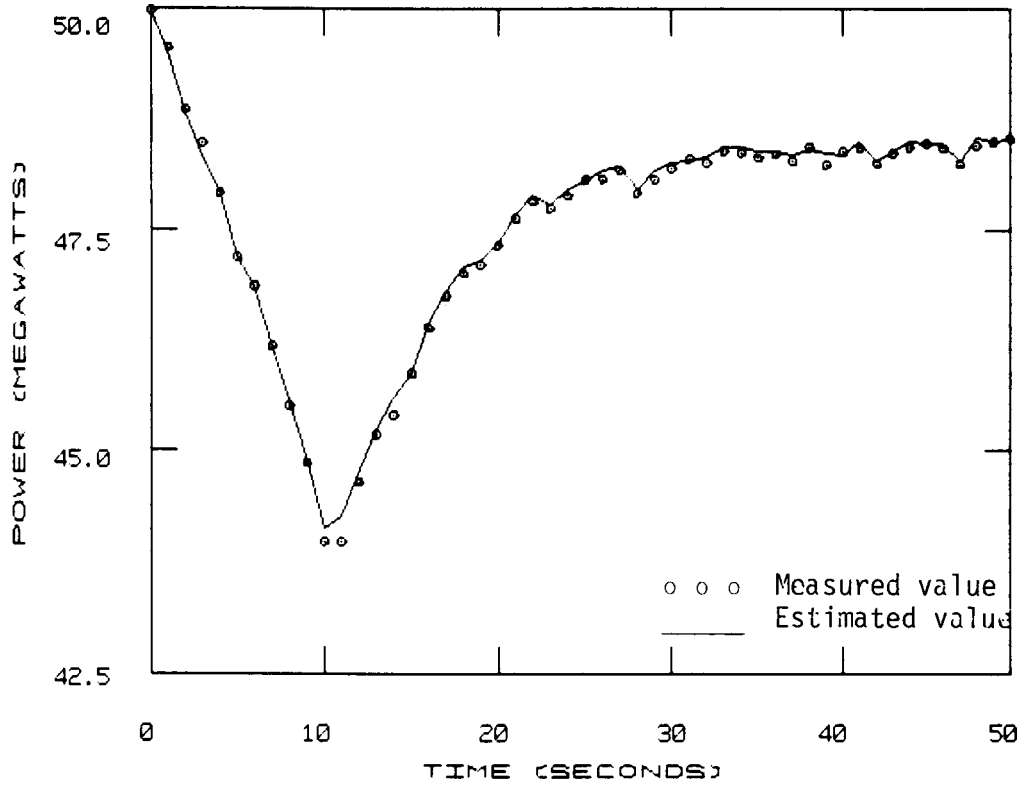

Figure 33. Primary flow reduction, core power response.

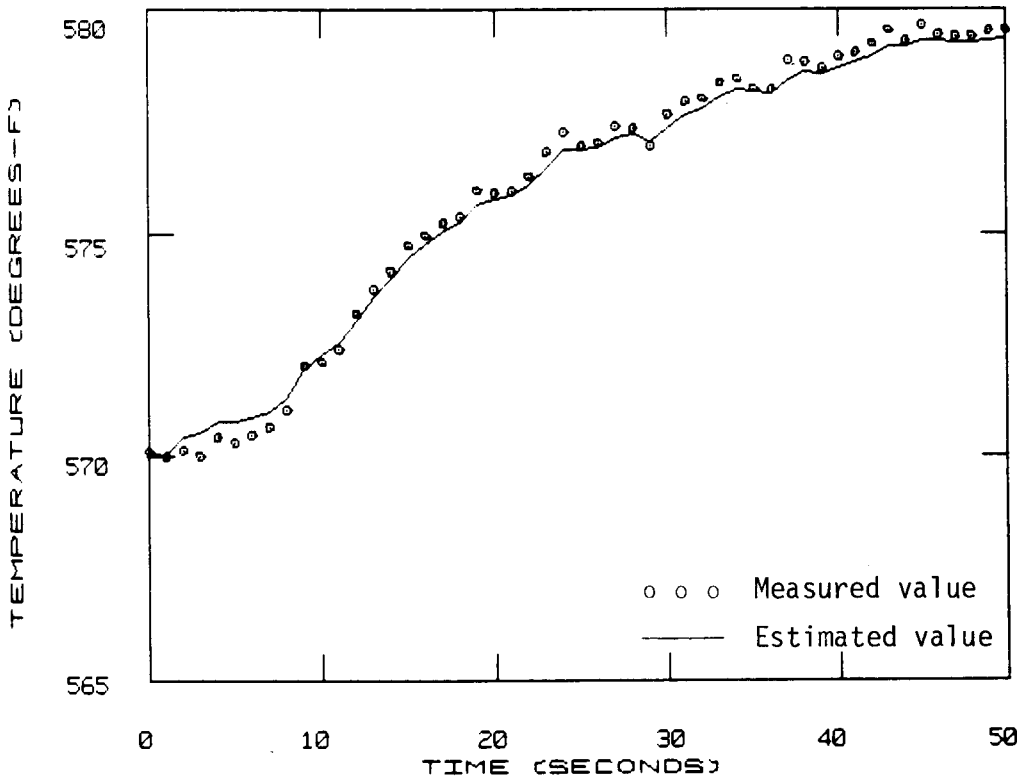

Figure 34. Primary flow reduction, hot leg temperature response.

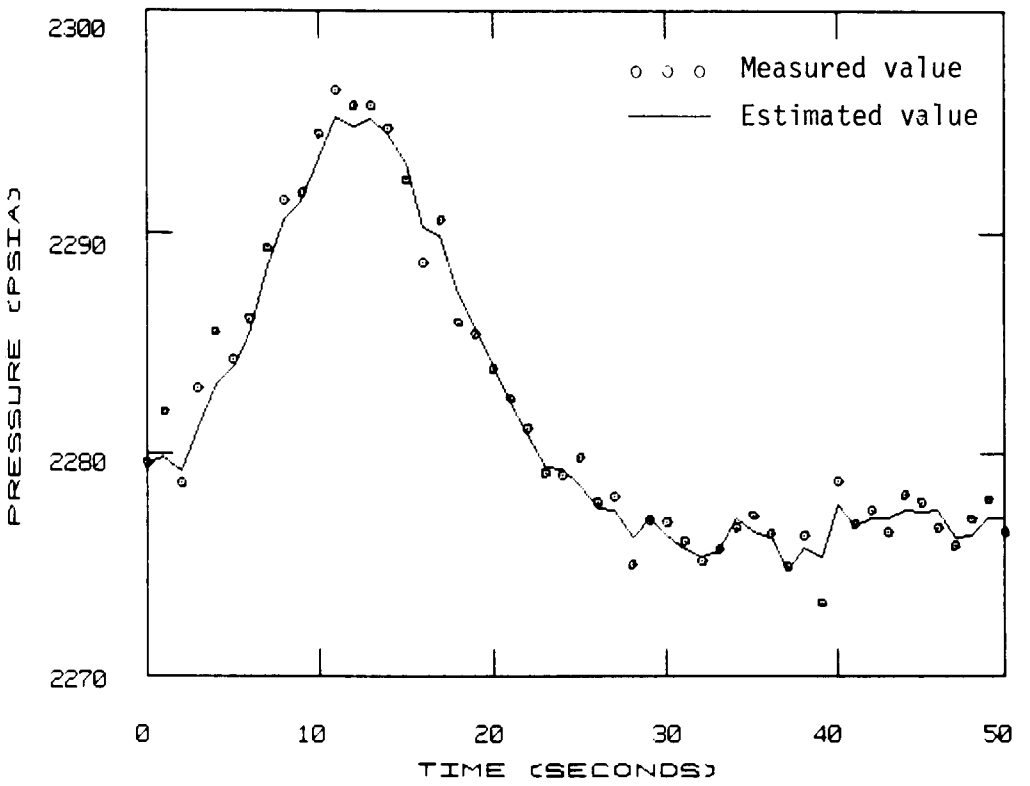

Figure 35. Primary flow reduction, pressurizer pressure response.

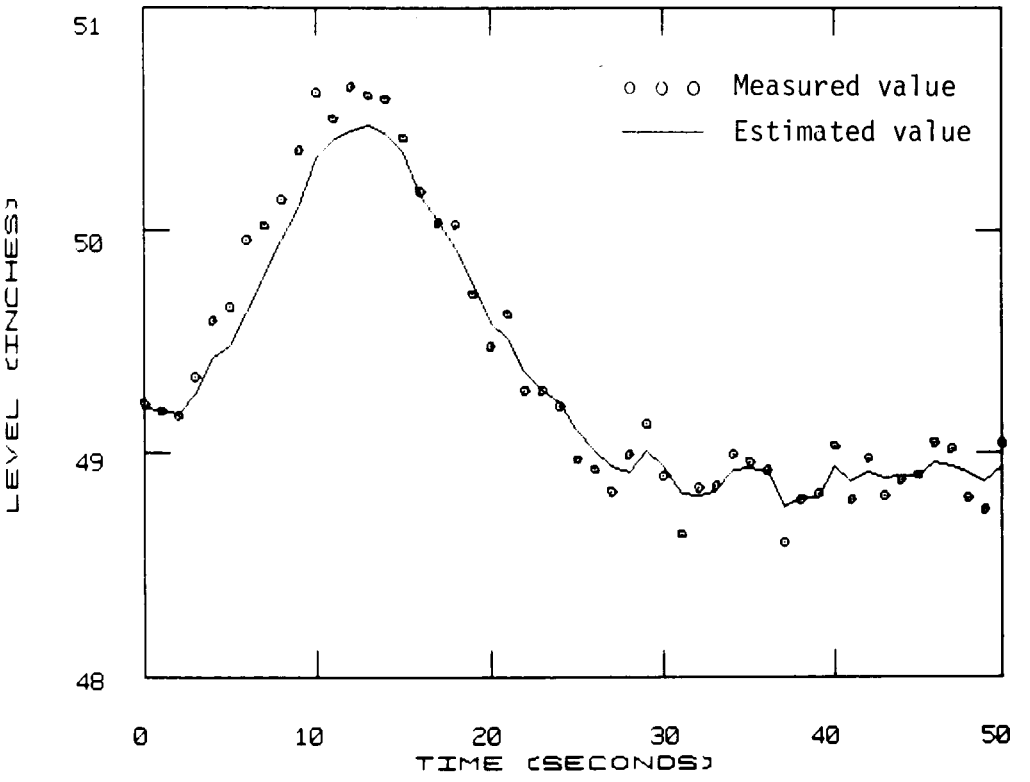

Figure 36. Primary flow reduction, pressurizer level response.

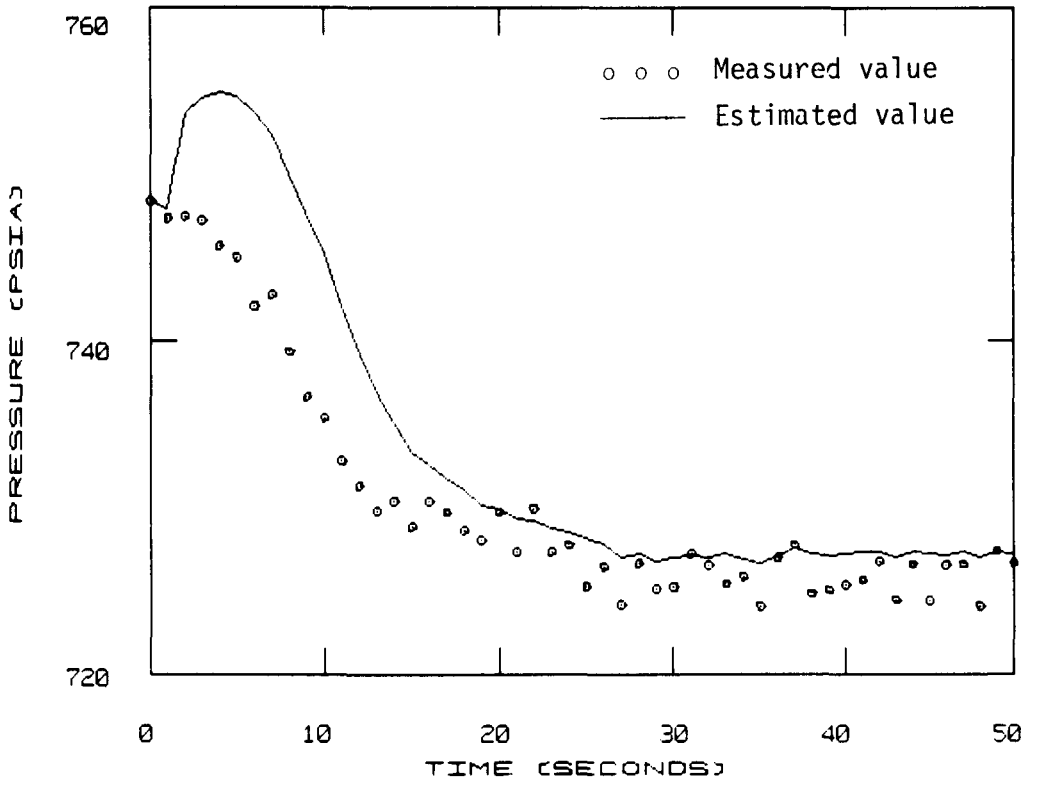

Figure 37. Primary flow reduction, secondary pressure response.

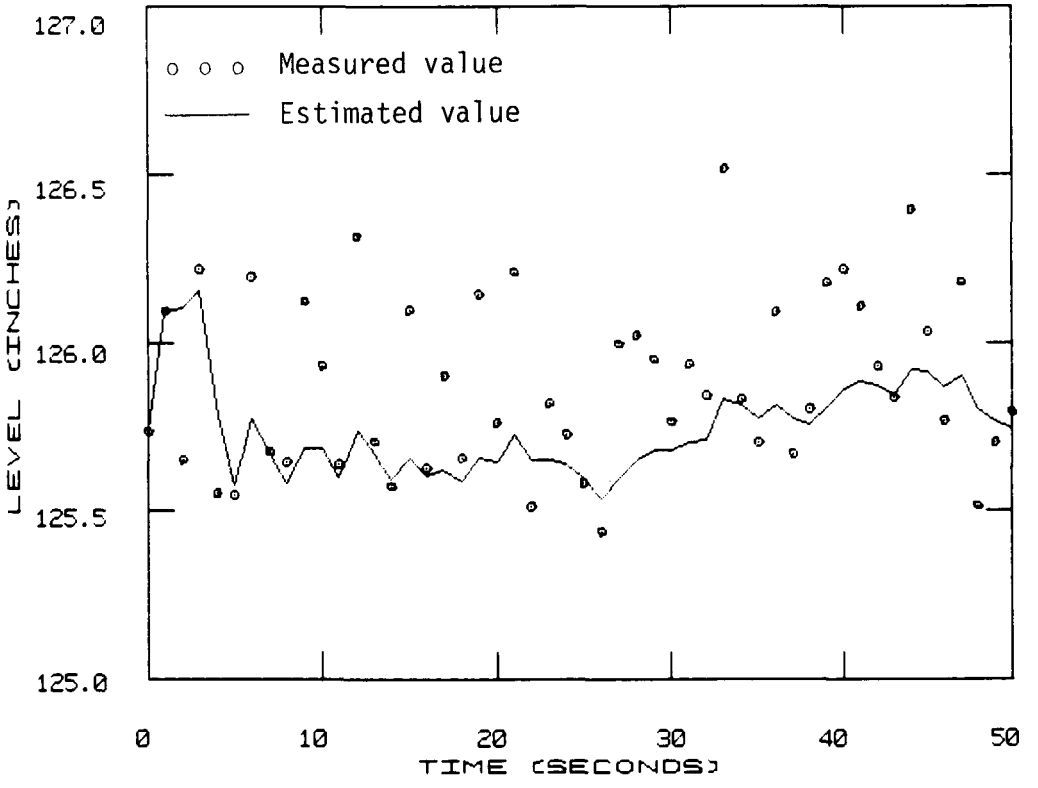

Figure 38. Primary flow reduction, steam generator level response.

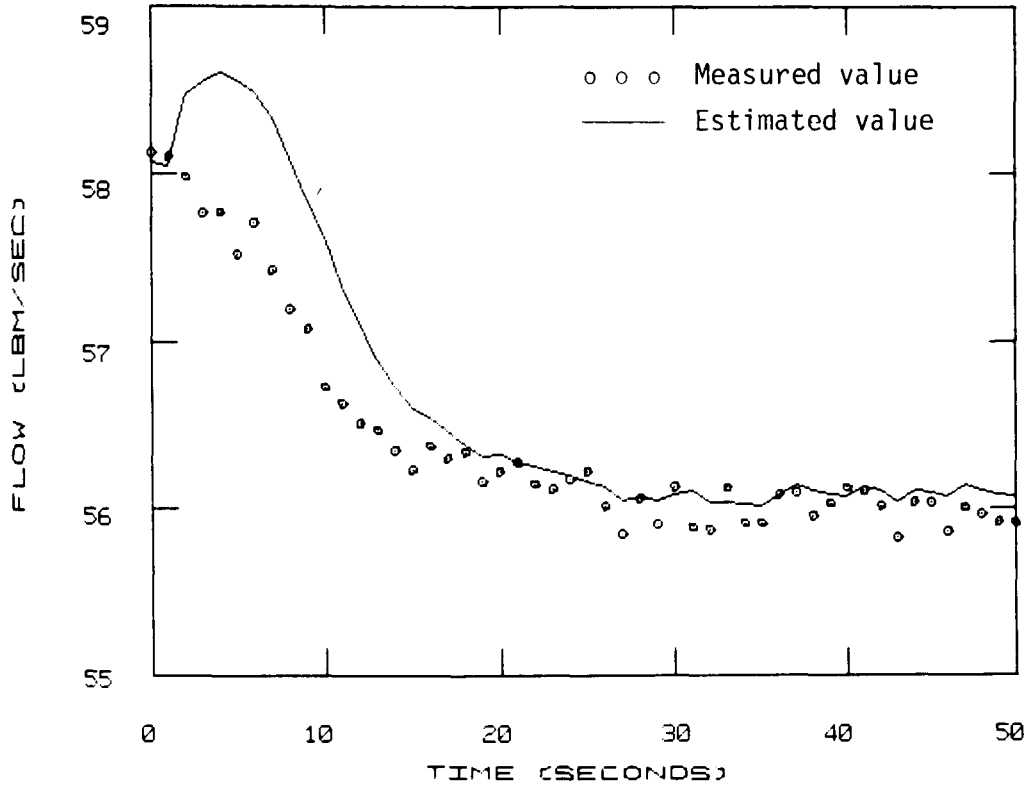

Figure 39. Primary flow reduction, steam flow response.

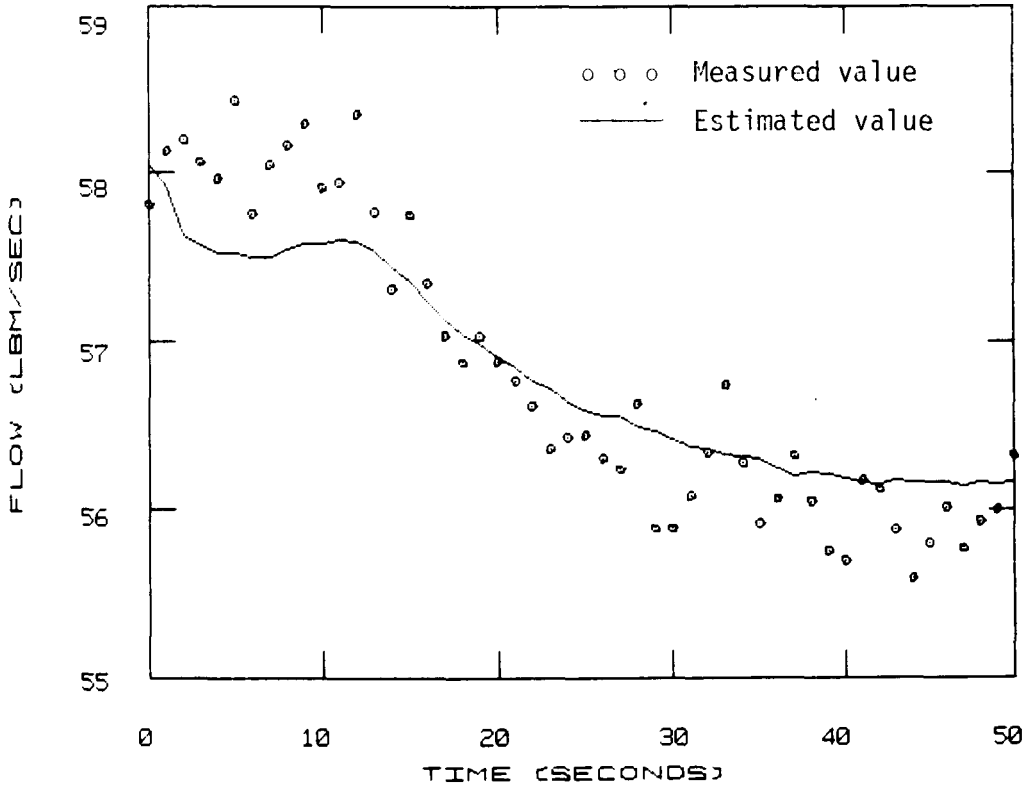

Figure 40. Primary flow reduction, feed flow response.

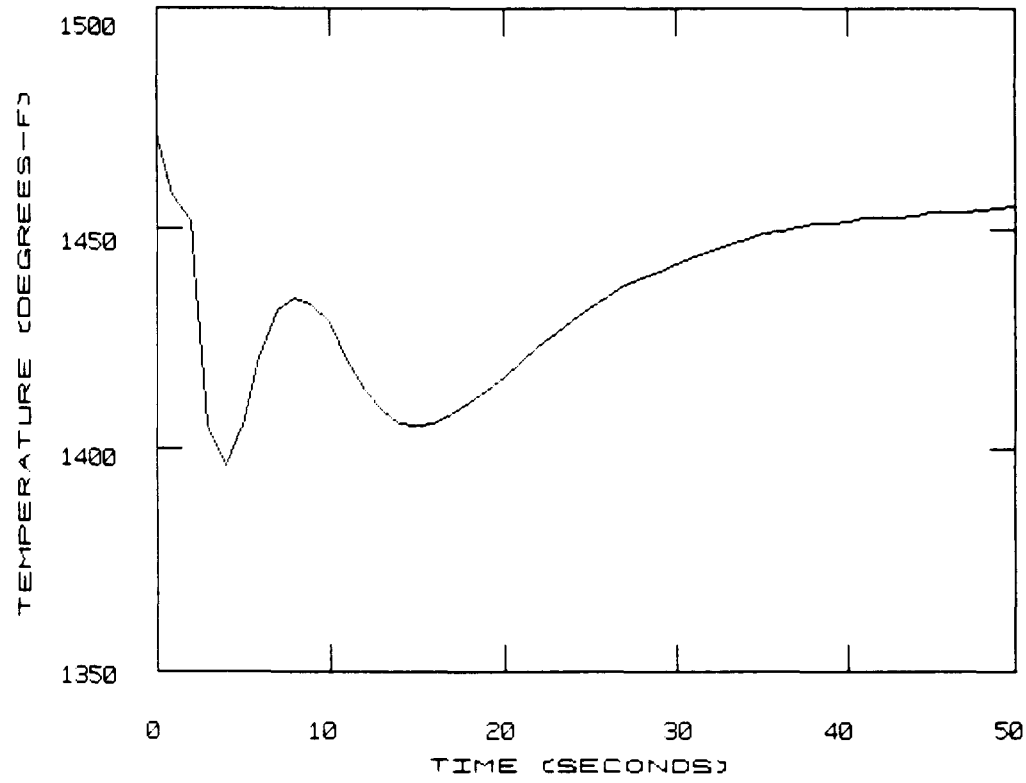

Figure 41. Primary flow reduction, fuel temperature estimate.

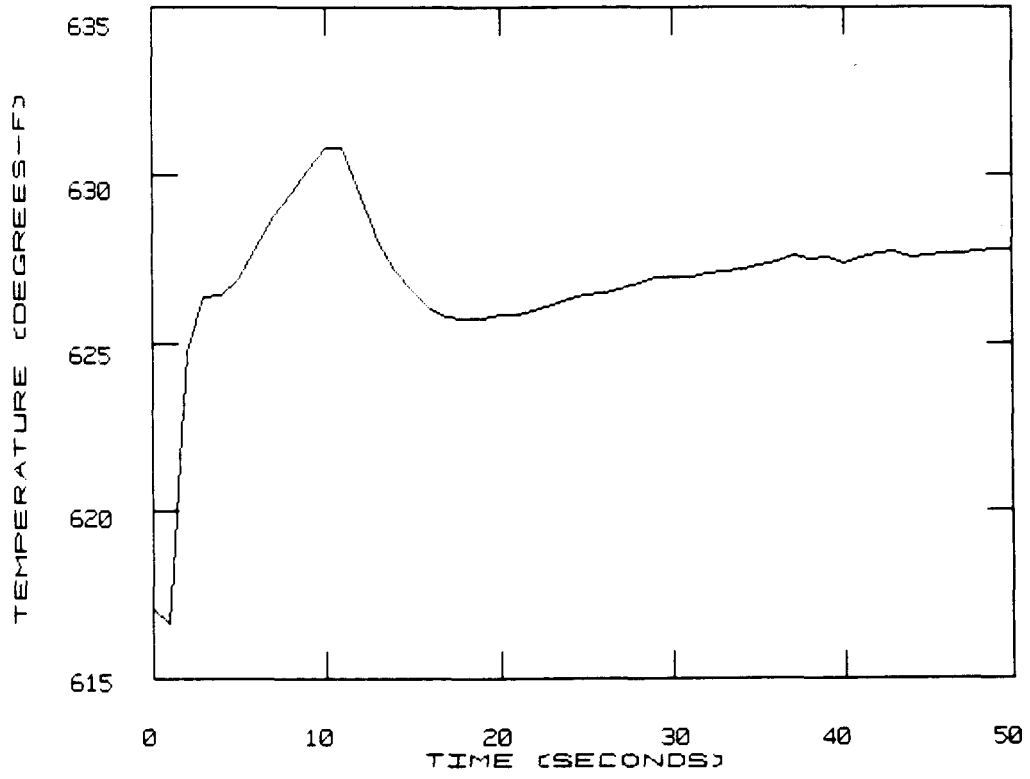

Figure 42. Primary flow reduction, clad temperature estimate.

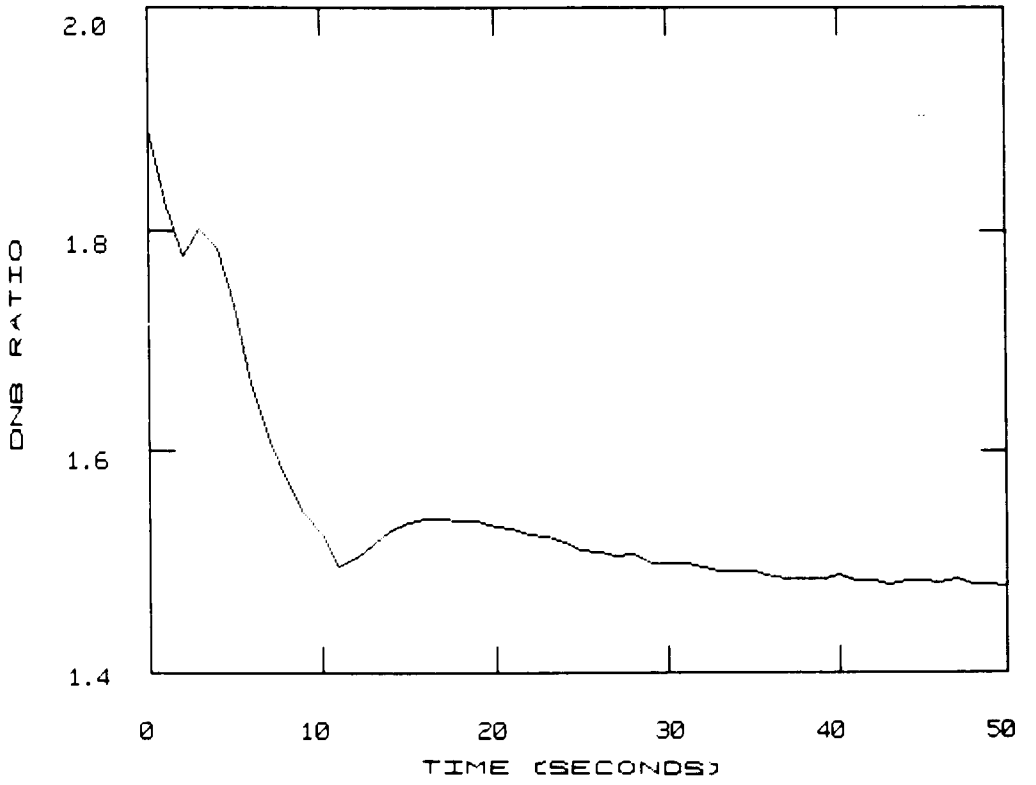

Figure 43. Primary flow reduction, minimum DNBR estimate.

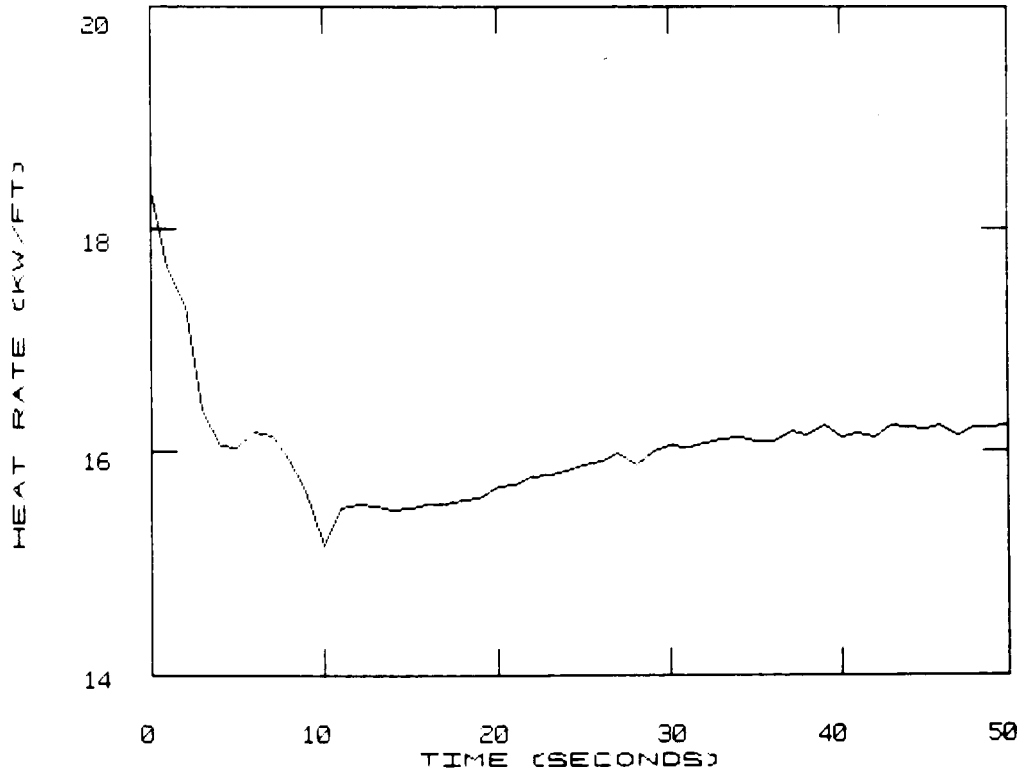

Figure 44. Primary flow reduction, maximum LHGR estimate.

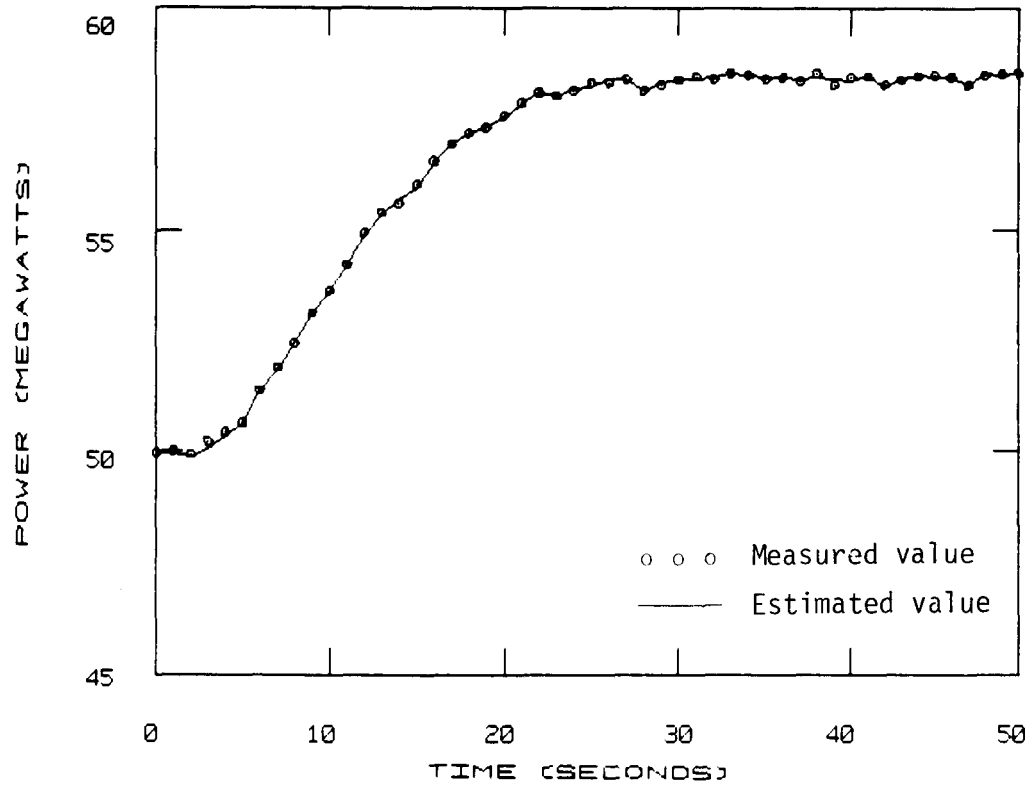

Figure 45. MSCV opening, core power response.

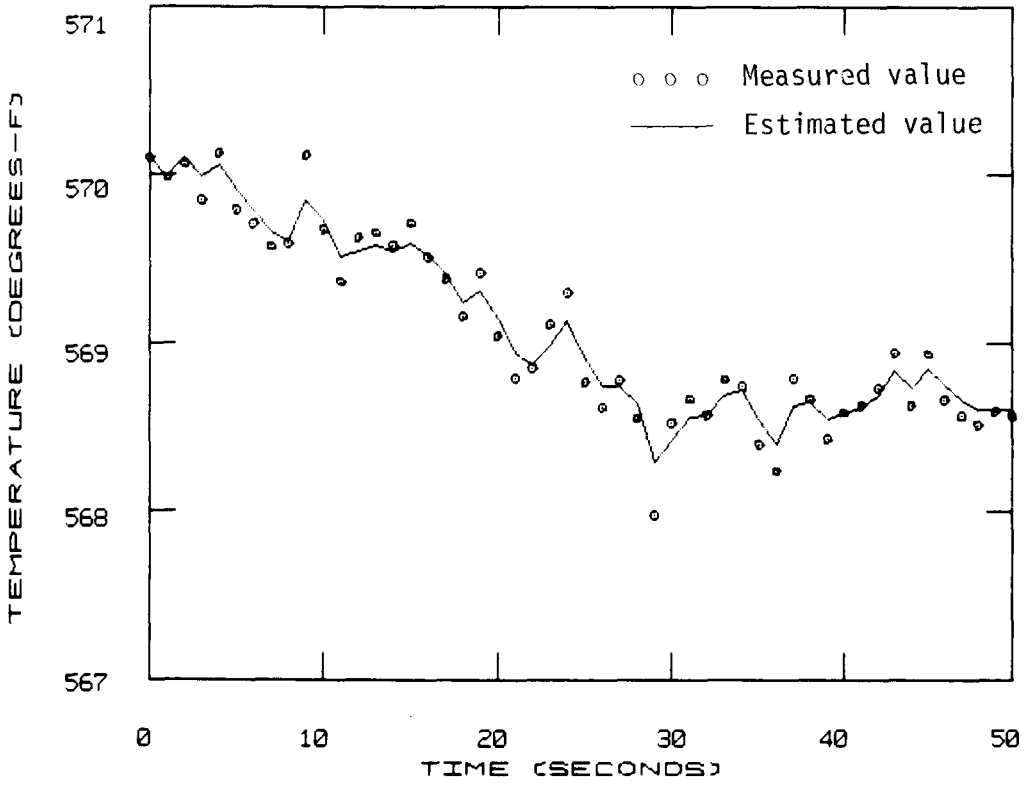

Figure 46. MSCV opening, hot leg temperature response.

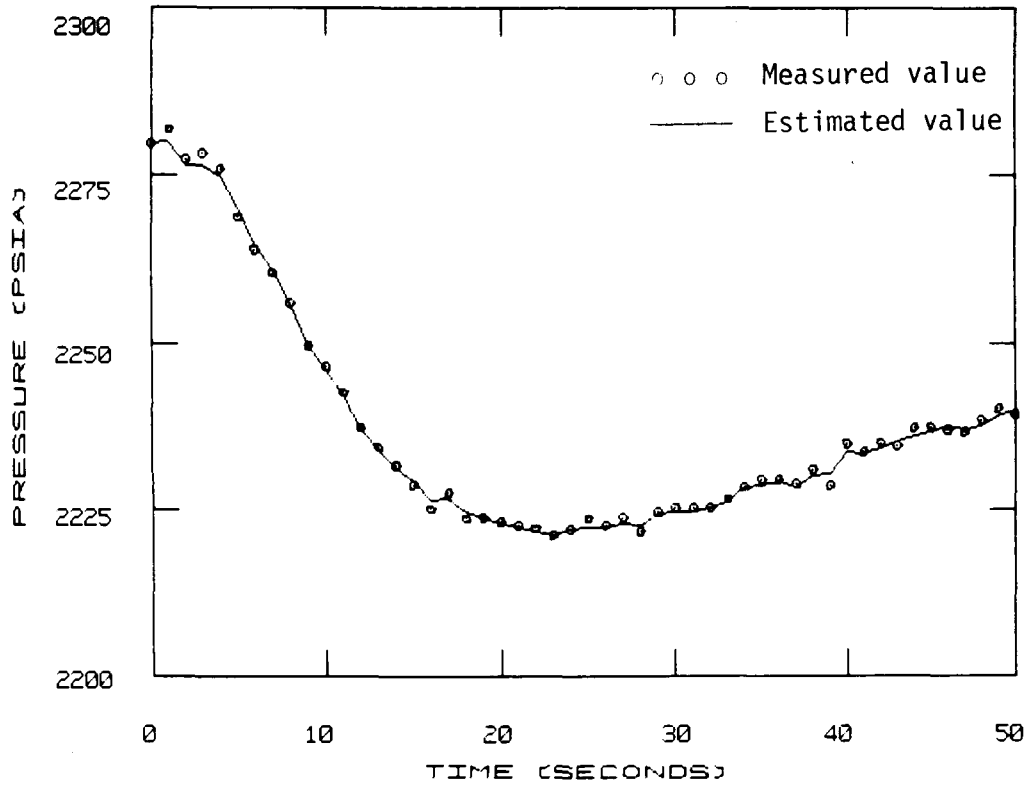

Figure 47. MSCV opening, pressurizer pressure response.

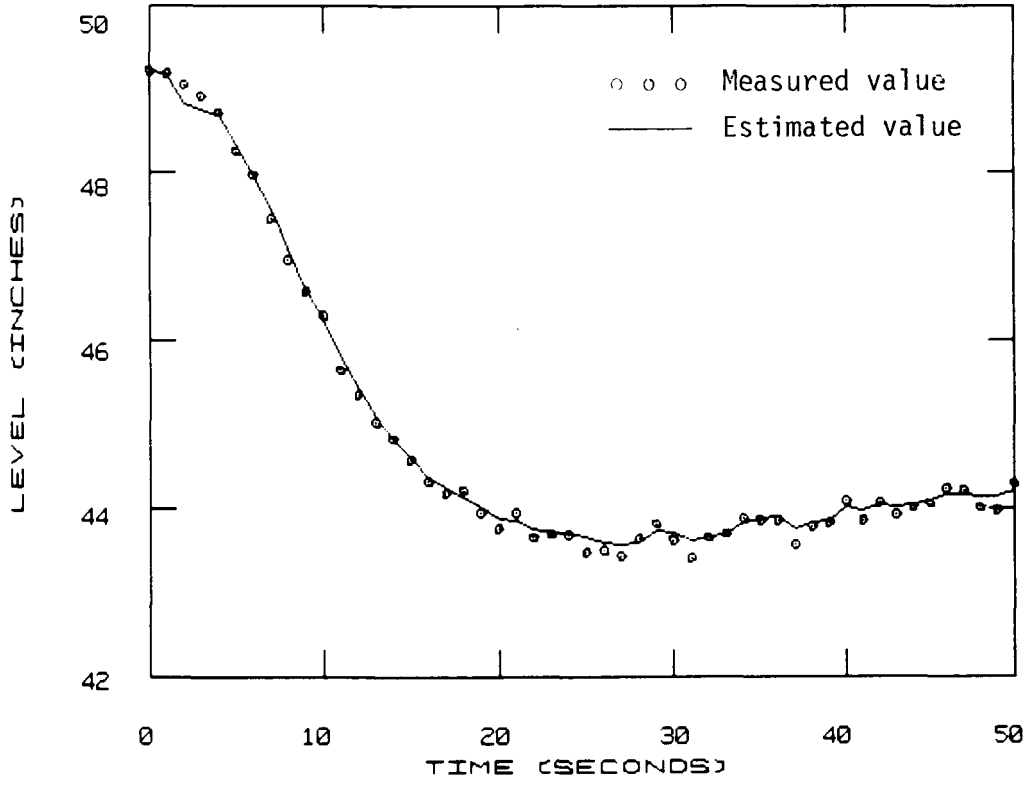

Figure 48. MSCV opening, pressurizer level response.

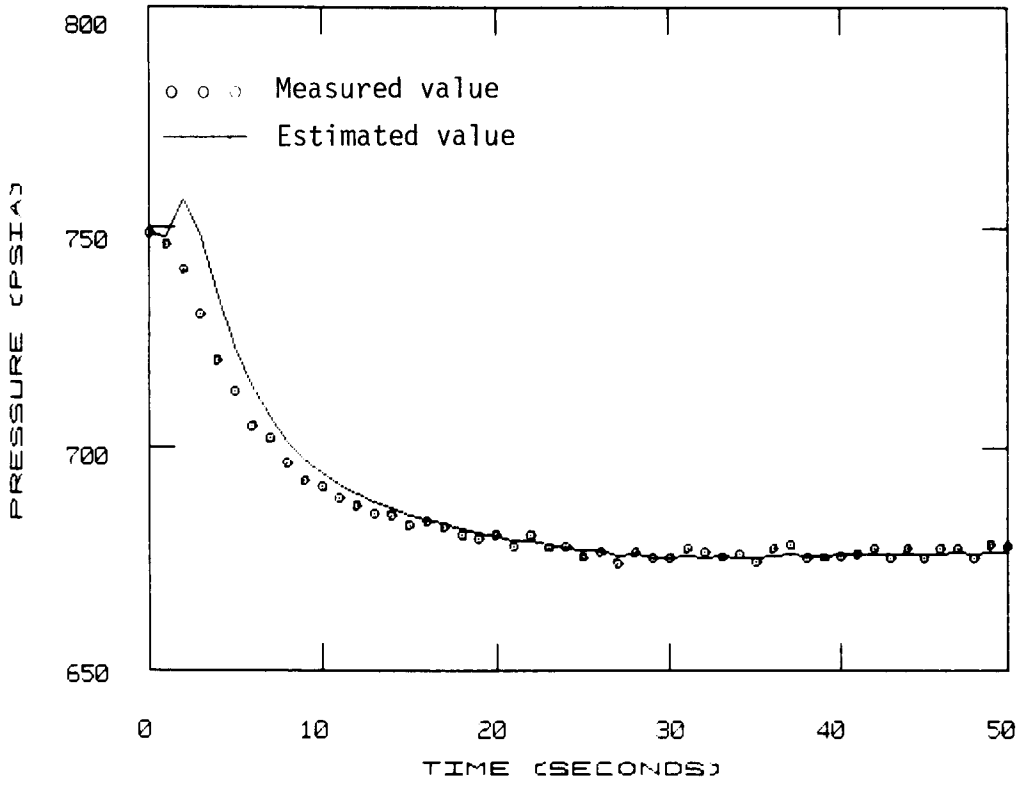

Figure 49. MSCV opening, secondary pressure response.

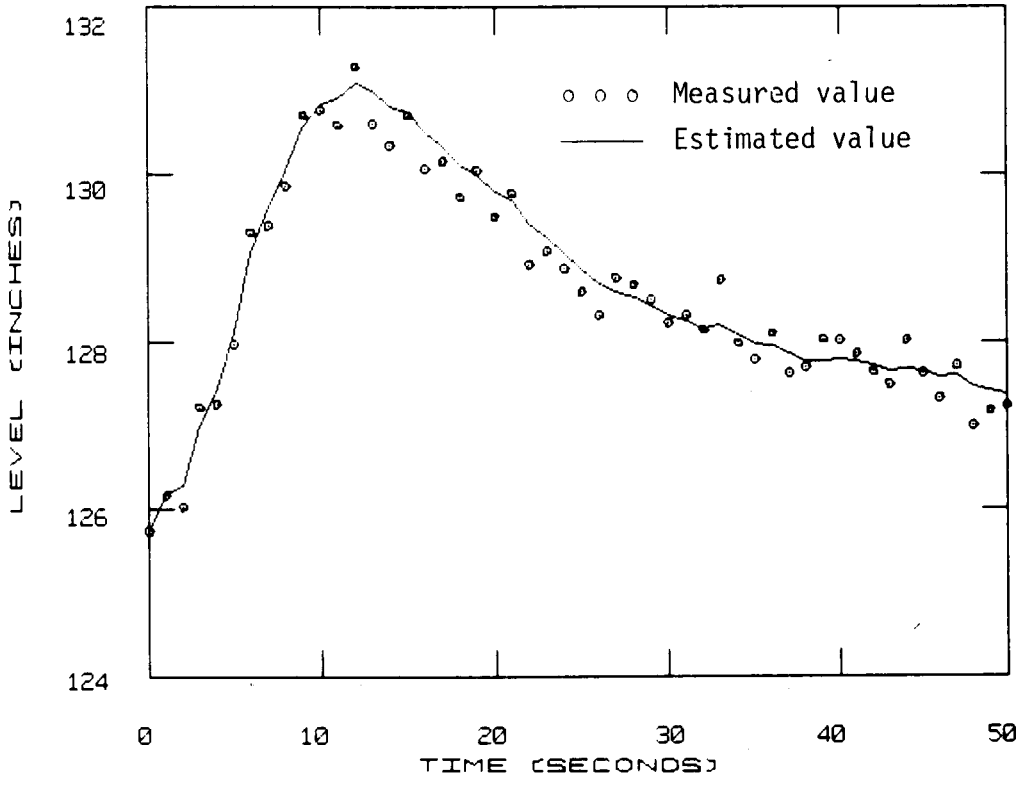

Figure 50. MSCV opening, steam generator level response.

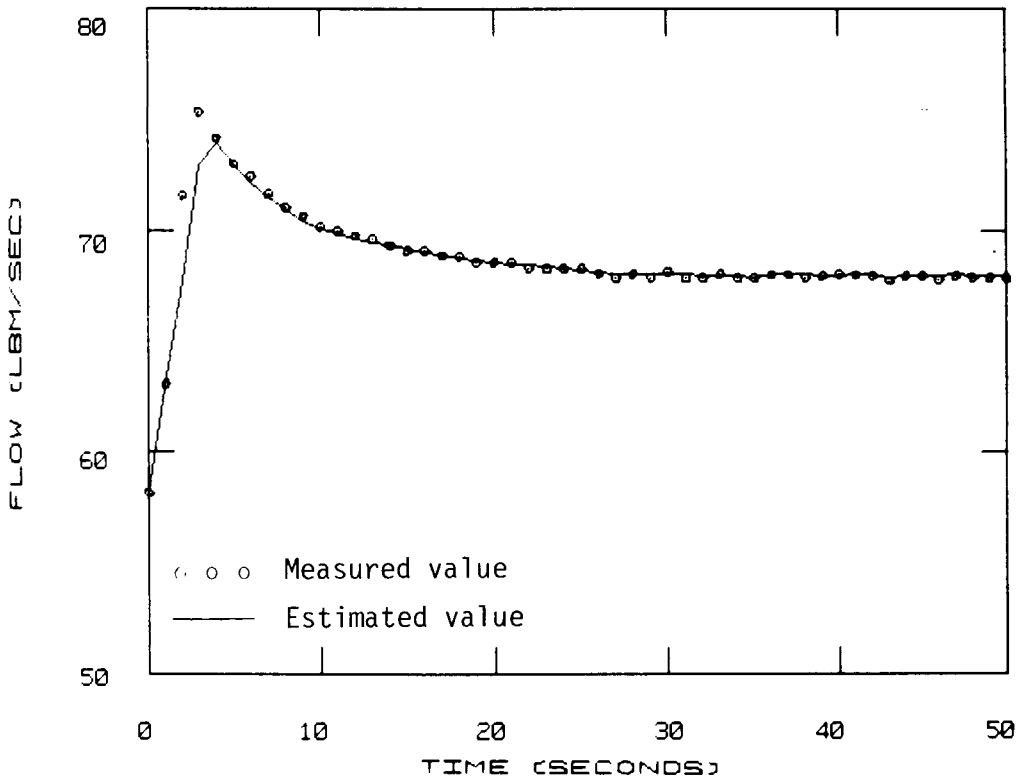

Figure 51. MSCV opening, steam flow response.

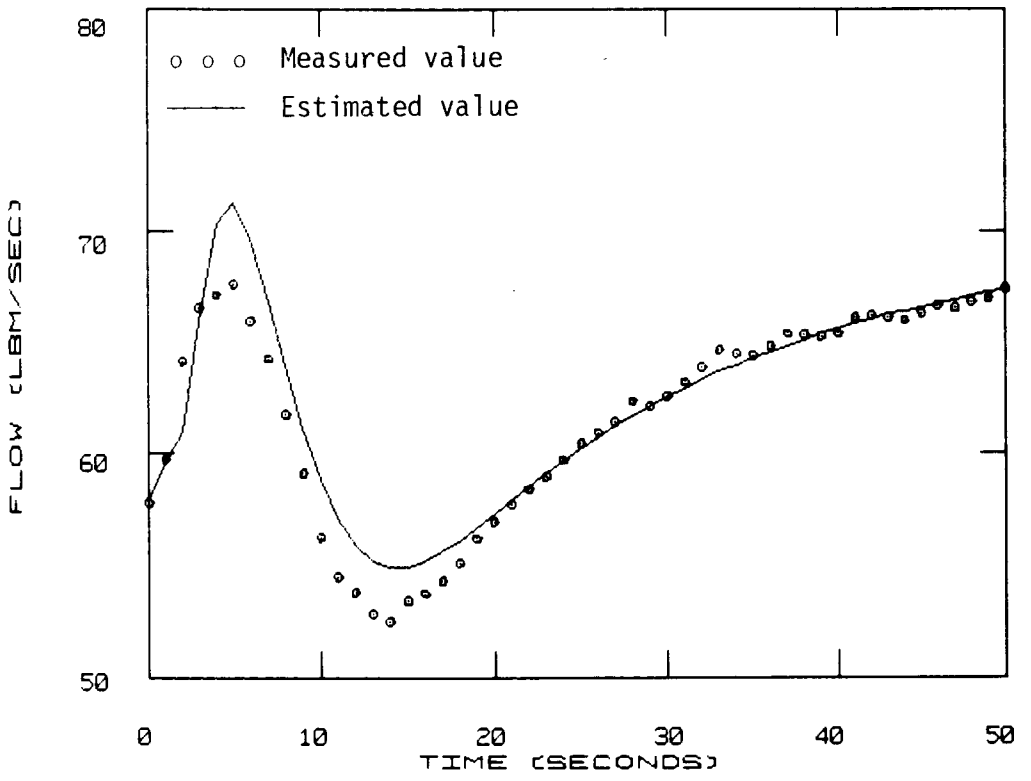

Figure 52. MSCV opening feed flow response.

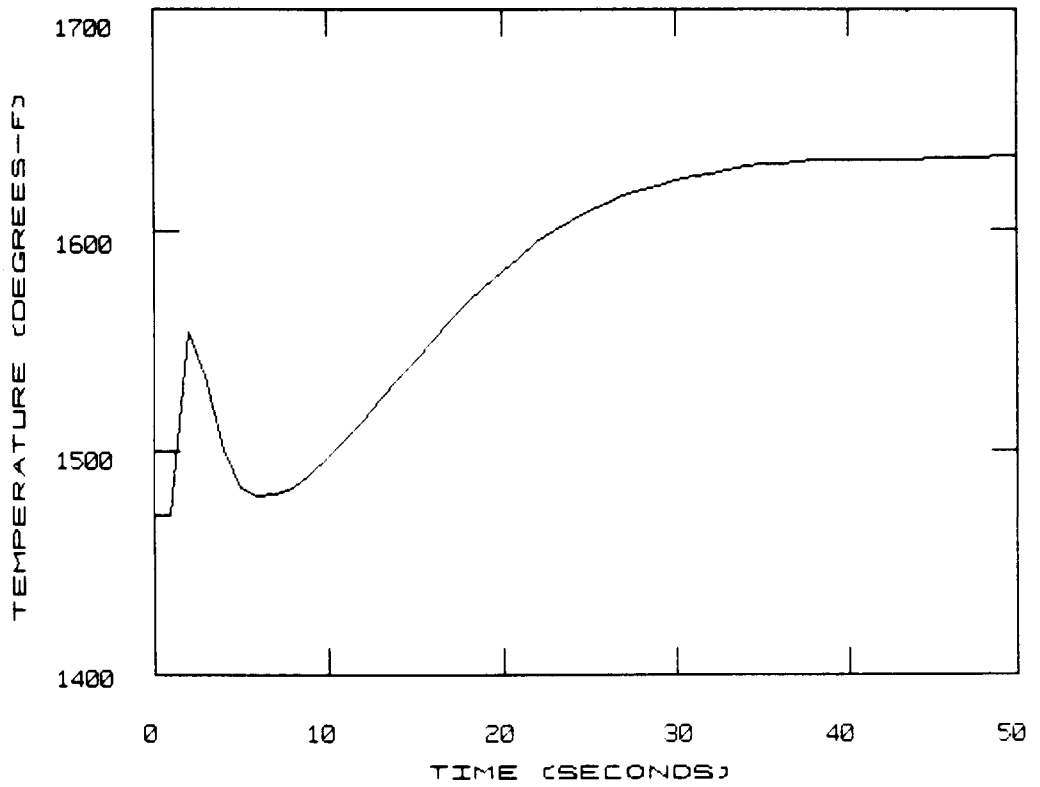

Figure 53. MSCV opening, fuel temperature estimate.

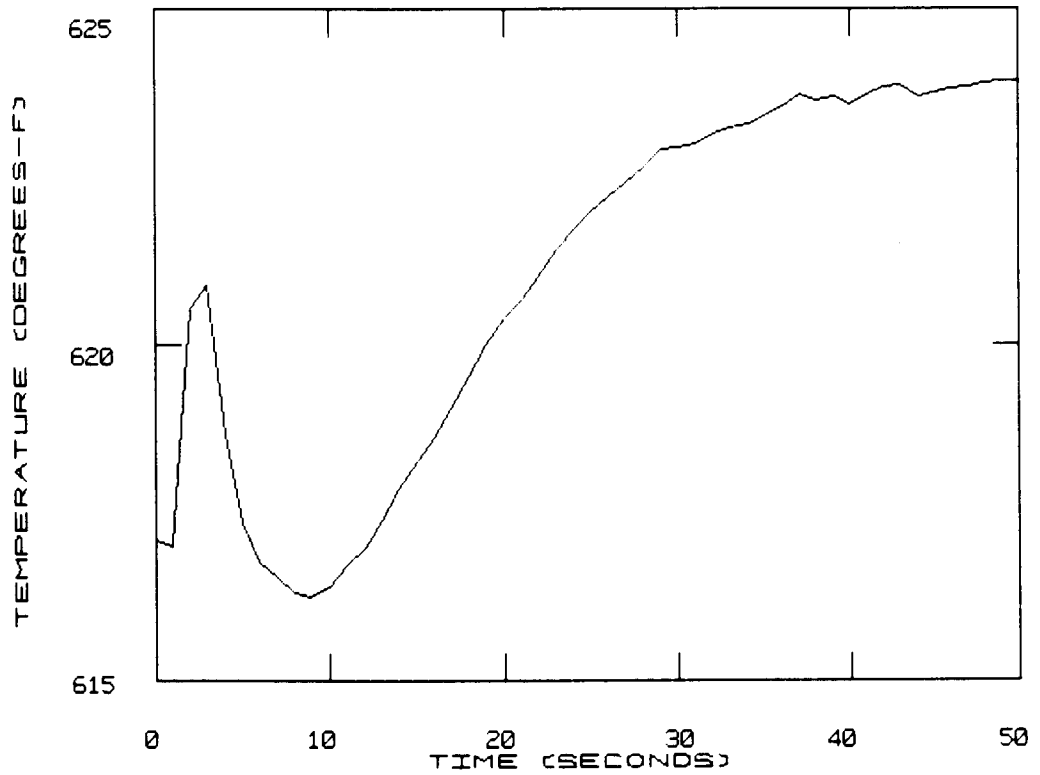

Figure 54. MSCV opening, clad temperature estimate.

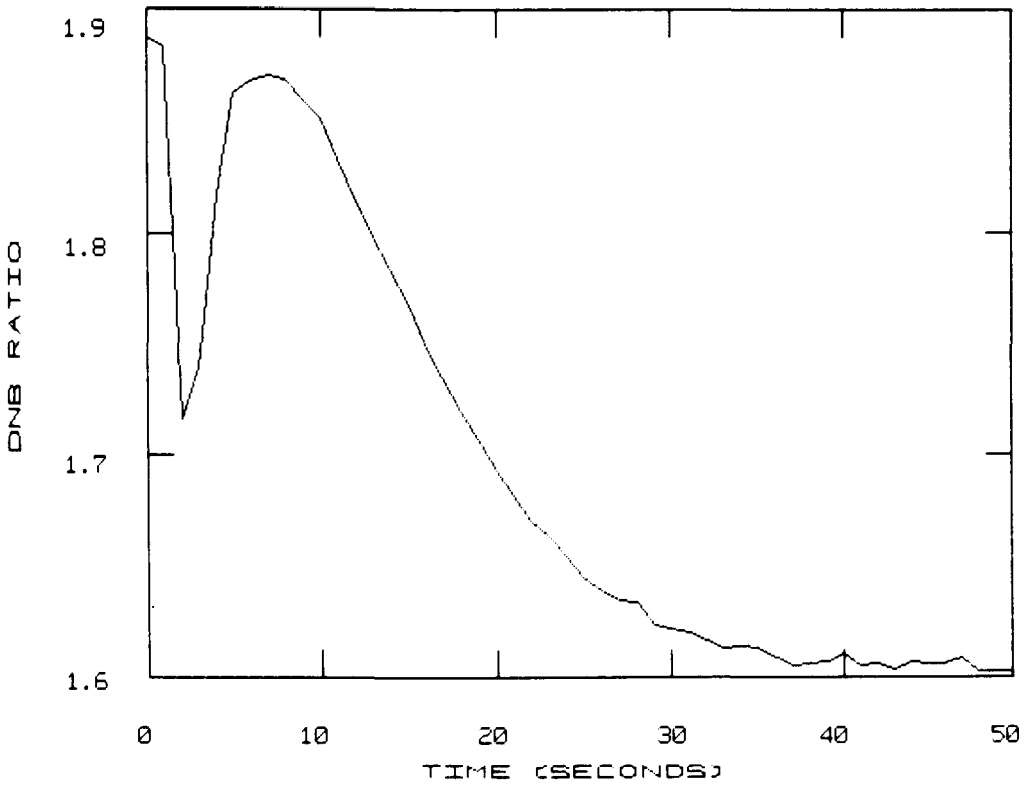

Figure 55. MSCV opening, minimum DNBR estimate.

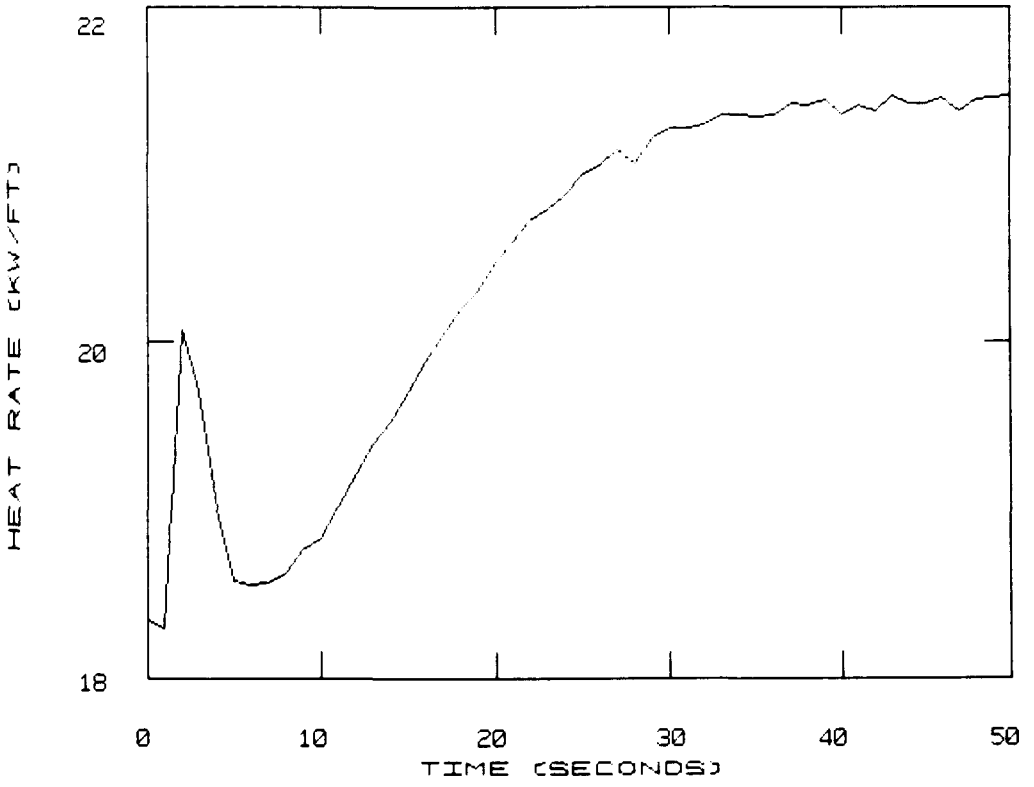

Figure 56. MSCV opening, maximum LHGR estimate.

CONCLUSIONS

The potential capabilities of the advanced system have been demonstrated. And though the simulation studies in the "SIMULATION RESULTS" section were performed using a large mainframe computer, preliminary work using a PDP 11/55 minicomputer showed that the advanced PPS worked equally well in a real-time environment. Implementing the advanced PPS on a small computer has the advantage of transportability, i.e., once the system is proved in simulation studies, it could easily be moved to the plant for testing there.

Other than checking for scrams, several other capabilities were to be added to the advanced plant protection system. These included allowing on-line trend predictions based on the current estimated plant state, the ability to run the LOFT model in the Kalman filter faster than real-time to allow operator inquiries regarding the consequences of proposed control actions, and the implementation of an optimal feedback controller.

The successful application of optimal estimation theory to the advanced LOFT plant protection system provided impetus to several projects currently underway or that have been completed at the Idaho National Engineering Laboratory. A companion project[21] demonstrated that the optimal control of a U-tube steam generator was far superior to the conventional three-element controller, particularly at low power levels. The use of Kalman filtering in detecting and identifying failures in pressurizer instrumentation[22,23] and in providing predicted plant information to the operator[24] are extremely promising areas of current research. The use of linear PWR models in advanced plant diagnostics systems[25] and the uses of Kalman filtering in identifying plant models[26] are also being studied.

REFERENCES

1. A. Gelb (ed.), *Applied Optimal Estimation*, Cambridge, Massachusetts: The M.I.T. Press, 1974.

2. A. P. Sage and J. L. Melsa, *Estimation Theory with Applications to Communications and Control*, Huntington, New York: Robert E. Krieger Publishing Company, 1979.

3. B. D. O. Anderson and J. B. Moore, *Optimal Filtering*, Englewood Cliffs, New Jersey: Prentice-Hall, Inc., 1979.

4. A. N. Anderson, *OPEC, A FORTRAN Library for Optimal Estimation and Control*, Idaho National Engineering Laboratory, unpublished.

5. G. J. Bierman, *Factorization Methods for Discrete Sequential Estimation*, New York: Academic Press, 1977.

6. J. L. Tylee, *Low-Order Model of the Loss-of-Fluid Test (LOFT) Reactor Plant for Use in Kalman Filter-Based Optimal Estimators*, EGG-2006, January 1980.

7. D. L. Hetrick, *Dynamics of Nuclear Reactors*, Chicago: University of Chicago Press, 1971.

8. R. F. Jimenez and R. D. Benham, "Advanced Nuclear Reactor Simulation Techniques," *Simulation*, March 1975.

9. Proposed ANS Standard ANS-5.1, "Decay Energy Release Rates Following Shutdown of Uranium-Fueled Thermal Reactors," ANS Standards Committee, October 1971.

10. P. E. MacDonald and L. B. Thompson, (eds.), *MATPRO-Version 09: A Handbook of Materials Properties for Use in the Analysis of Light Water Reactor Fuel Rod Behavior*, TREE/NUREG-1005, December 1976.

11. A. J. Chapman, *Heat Transfer*, London: MacMillan Company, 1970.

12. *ASME Steam Tables: Thermodynamic and Transport Properties of Steam*, American Society of Mechanical Engineers, New York, 1977.

13. *Material Properties Handbook, Volume IV Heat Resisting Alloys*, Engineering Scientific Data Unit, Royal Aeronautical Society, London, 1966.

14. F. K. Hyer and C. D. Clayton, *Hybrid Computer Simulation of the LOFT Primary and Secondary System*, LTR 10-2C, December 1980.

15. E. C. Lemmon and D. B. MacKay, *LOFCON-LOFT Condenser Program*, LTR 115-28, May 11, 1978.

16. J. J. Feeley, *LOFT Air-Cooled Condenser Air Flow Test*, LTR 115-25, June 1977.

17. B. C. Kuo, *Digital Control Systems*, Champaign, Illinois: SRL Publishing Company, 1977.

18. J. R. Lamarsh, *Introduction to Nuclear Engineering*, Reading Massachusetts: Addison-Wesley Publishing Company, 1975.

19. D. S. Rowe, *COBRA-IIIC: A Digital Computer Program for Steady-State and Transient Thermal-Hydraulic Analysis of Rod Bundle Nuclear Fuel Elements*, BNWL-1695, March 1973.

20. S. A. Eide and R. C. Gottula, *Evaluation and Results of LOFT Steady State Departure from Nucleate Boiling Tests*, TREE/NUREG-1043, April 1977.

21. J. J. Feeley, "Optimal Digital Estimation and Control of a Natural Circulation Steam Generator," Ph. D. Thesis, University of Idaho, November 1980.

22. B. Campbell, "Instrument Failure Detection Using Functional Redundancy Applied to a Nuclear Pressurizer," M. S. Thesis, University of Washington, December 1980.

23. J. L. Tylee, "Bias Identification in PWR Pressurizer Instrumentation Using the Generalized Likelihood Ratio Technique," *Proceedings of the 1981 Joint Automatic Controls Conference, Charlottesville, Virginia, June 1981.*

24. J. J. Feeley, "Janus Displays for Improved Reactor Plant Operation and Control," *Transactions of the American Nuclear Society Summer Annual Meeting, Miami Beach, Florida, June 1981.*

25. J. L. Tylee, "The Utility of Low-Order Linear Nuclear Power Plant Models in Plant Diagnostics and Control," *Proceedings of the 1981 Summer Computer Simulation Conference, Washington, D. C., July 1981.*

26. J. M. Griffith, M. A. Bray, J. J. Feeley, "Optimal Calibration of Nuclear Instrumentation," *Transactions of the American Nuclear Society Summer Annual Meeting, Miami Beach, Florida, June 1981.*